The Asynchronous Graz Brain Switch

Teodoro Solís Escalante

Dissertation

Institute for Knowledge Discovery
Laboratory of Brain-Computer Interfaces
Graz University of Technology

Supervisor: Univ.-Prof.i.R. Dipl.-Ing. Dr.techn. Gert Pfurtscheller

October 2012

Deutsche Fassung:
Beschluss der Curricula-Kommission für Bachelor-, Master- und Diplomstudien vom 10.11.2008
Genehmigung des Senates am 1.12.2008

EIDESSTATTLICHE ERKLÄRUNG

Ich erkläre an Eides statt, dass ich die vorliegende Arbeit selbstständig verfasst, andere als die angegebenen Quellen/Hilfsmittel nicht benutzt, und die den benutzten Quellen wörtlich und inhaltlich entnommene Stellen als solche kenntlich gemacht habe.

Graz, am ……. ……..
(Unterschrift)

Englische Fassung:

STATUTORY DECLARATION

I declare that I have authored this thesis independently, that I have not used other than the declared sources / resources, and that I have explicitly marked all material which has been quoted either literally or by content from the used sources.

……. ……..
date (signature)

Abstract

This dissertation presents the asynchronous Graz Brain Switch, a non-invasive brain-computer interface (BCI) based on the beta rebound after overt and covert foot movements. The first part of this thesis provides an overview on the beta rebound, a burst of beta activity (15 to 35 Hz) that follows somatosensory stimulation or motor behavior, assumed to reflect a process of deactivation/inhibition of cortical networks. This part also presents a novel comparison of the beta rebound between execution and withholding of physical movement, and a novel comparison of the beta rebound between withholding of executed and imagined movement. Across these conditions, the beta rebound appears in the same frequency band and at the same electrode position, with differences in magnitude and breadth: (i) larger beta rebound after execution as compared to during withholding of physical movement, and (ii) larger and broader beta rebound during withholding of motor execution as compared to withholding of motor imagery.

The second part of this work presents an overview on current brain switch designs and evaluation methods. The majority of brain switch designs rely on the detection of motor related phenomena, i.e. motor-related potentials and event-related (de)synchronization. Performance is usually evaluated offline in terms of true and false activations, but comparisons between different approaches are difficult because false activations are considered differently, and class probabilities are unbalanced. A good way to evaluate the rejection of non-target brain patterns is to estimate the number of false activations per minute. Current brain switch designs attempt to provide near-zero false activations, prioritizing reliability over responsiveness.

The third part of this work demonstrates that the beta rebound is suitable for realizing an asynchronous brain switch. After one run of cue-paced motor execution or motor imagery, a support vector machine is trained with spectral features to classify the beta rebound against other brain patterns. For the sake of practicality, the electroencephalogram (EEG) from a single Laplacian derivation at the vertex is used. Offline simulations of an asynchronous BCI show that the detection of overt and covert foot movement, based on the beta rebound, achieves an average true positive rate (TPR) of 0.74 and 0.59, respectively. In both cases, the false positive rate (FPR) is limited to 0.10. Exploiting the similarity of the beta rebound after overt and covert foot movement, EEG data recorded during movement is used to set up the Graz Brain Switch. After a short calibration phase, the brain switch can be used to detect the beta rebound after motor imagery. Since movement execution is required for setting up a classifier, this scheme represents a brain switch

for able-bodied users. An offline simulation of this scheme shows an average TPR of 0.46 (FPR = 0.11) for the detection of imagined movements.

The fourth part of this work describes the online evaluation of the Graz Brain Switch, and the successful implementation of a hybrid BCI. The hybrid BCI is obtained from the combination of the Graz Brain Switch and a BCI based on the classification of steady state visual evoked potentials. A well-defined paradigm with specific timing serves as a benchmark application for the online evaluation. Six participants completed the evaluation with an average of 7.5 true activations and 3.5 false activations per run (a perfect run would have five true activations and zero false activations). The average positive predictive value (PPV) was 0.74, meaning that 74% of all activations were intended, and the number of false positives per minute (FP/min) was 0.47. For comparison, other brain switch designs have achieved 0.7 FP/min in offline analyses and 1.4 FP/min in online experiments.

Zusammenfassung

Diese Doktorarbeit präsentiert den Graz Brain Switch, ein nicht-invasives asynchrones Brain-Computer Interface (BCI), das eine Schalterfunktion bietet. Ein BCI wandelt bestimmte Aktivitätsmuster des Gehirns in Steuersignale um. Der Graz Brain Switch verwendet den Beta Rebound nach einer kurzen Fußbewegung oder Fußbewegungsvorstellung als Gehirnmuster. Im ersten Teil dieser Doktorarbeit wurde ein Überblick über die aktuelle Literatur gegeben. Der Beta Rebound ist eine kurze Zunahme von Spektralkomponenten des Elektroenzephalogramms (EEG) im Beta Frequenzbereich (15 - 35 Hz), der einer somatosensorischen Stimulation oder einer motorischen Aufgabe folgt. Man nimmt an, dass der Beta Rebound mit einer Inhibition kortikaler Neurone zusammenhängt. Weiters wurde der Beta Rebound nach Durchführung von Bewegung und nach Hemmung von Bewegung bzw. Bewegungsvorstellung verglichen. Der Beta Rebound tritt in jeder dieser Bedingungen im gleichen Frequenzbereich und auf der gleichen Elektrodenposition auf. Unterschiede zeigen sich nur in der Amplitude und Verteilung: (i) stärkerer Beta Rebound nach Bewegungsdurchführung als nach Hemmung der Bewegung, und (ii) stärkere und breitere Verteilung des Beta Reboundes nach Hemmung von Bewegung als nach Hemmung von Bewegungsvorstellung.

Im zweiten Teil dieser Doktorarbeit wurde ein Überblick über aktuelle Arten des Brain Switches und Evaluierungsmethoden gegeben. Die aktuellen Brain Switches basieren auf motorischen Gehirnmustern, bzw. motorischen Potentialen und ereignisbezogener Desynchronisation (ERD) und Synchronisation (ERS). Die Evaluierung wird normalerweise offline durchgeführt, mittels True Positive Rate (TPR) und False Positive Rate (FPR). Der Vergleich von verschiedenen Arten des Brain Switches ist jedoch kompliziert, weil falsche Aktivierung unterschiedlich definiert wird. Hilfreich ist der Vergleich zwischen falschen Aktivierungen pro Minute (FP/min), zur Evaluierung der korrekten Zurückweisung von Gehirnmustern, die nicht dem Zielmuster entsprechen. Aktuelle Arten des Brain Switches geben der FPR eine höhere Priorität als der Reaktionsfähigkeit.

Im dritten Teil dieser Doktorarbeit wurde die Realisierbarkeit eines Beta Rebound basierten Brain Switches bewiesen. EEG Daten, die während Bewegungsdurchführungen und Bewegungsvorstellungen aufgenommen wurden, wurden für das Klassifikatortraining verwendet. Der Klassifikator analysiert das EEG-Signal von einer einzelnen Laplace-Ableitung in einer offline Simulation eines asynchrones Brain Switches, und detektiert das Auftreten des Beta Rebounds. Die Ergebnisse zeigen eine durchschnittliche TPR von 0.74 und 0.59 für die Klassifikation von Bewegungsdurchführung bzw. Bewegungsvorstellung.

Die FPR war in beiden Fällen auf 0.10 begrenzt. Die Ähnlichkeit des Beta Rebounds zwischen Bewegungsdurchführung und Bewegungsvorstellung wurde genutzt, um den Graz Brain Switch nach dem Bewegungsdurchführungmuster einzustellen. Nach einer Kalibrierungsphase wurde der Graz Brain Switch am Bewegungsvorstellungsmuster getestet. Eine offline Simulation zeigte eine durchschnittliche TPR von 0.46 (FPR = 0.11).

Im vierten Teil dieser Doktorarbeit wurden die online Evaluierung des Graz Brain Switches und die Realisierung eines hybriden BCI gezeigt. Das hybride BCI besteht aus einer Kombination des Graz Brain Switches mit einem auf steady-state visuell evozierten Potentialen basierendem BCI. Ein experimentelles Paradigma mit definiertem Zeitablauf diente als Vergleichsanwendung für die online Evaluierung des Brain Switches. Sechs Probanden nahmen an der Evaluierung teil und erreichten durchschnittlich 7.5 richtige und 3.5 falsche Aktivierungen (perfekte Ausführung bestand aus fünf richtigen und null falschen Aktivierungen) und 0.74 FP/min. Zum Vergleich, andere Brain Switch Arten erreichen 0.7 FP/min (offline) und 1.4 FP/min (online).

Resumen

Esta tesis doctoral presenta una interfaz cerebro-computadora (BCI por sus siglas en Inglés) asíncrona y no-invasiva, que proporciona la función de un interruptor. El Graz Brain Switch está basado en la sincronización del ritmo central beta (entre 15 y 35 Hz) que sigue la ejecución y la imaginación de movimiento (dorsiflexión) de ambos pieses, y que se conoce como beta rebound. La primera parte de esta tesis presenta una revisión bibliográfica sobre el beta rebound, un fenómeno fisiológico que corresponde a un cambio en la interacción entre grupos neuronales (sincronización), y que se presenta como un incremento del componente espectral beta del electroencefalograma (EEG). El beta rebound coincide con un estado de excitabilidad reducida de grupos neuronales corticales. La primera parte presenta, además, una comparación del beta rebound entre ejecución e inhibición de movimiento y entre la inhibición de movimiento real e imaginario. En estas condiciones, el beta rebound se presenta en la misma banda de frecuencia y en la misma localización topográfica, con diferencias en amplitud y distribución: (i) mayor amplitud entre ejecución e inhibición de movimiento y (ii) mayor amplitud y distribución más amplia entre inhibición de movimiento real y de movimiento imaginario.

La segunda parte de esta tesis presenta una revisión de diseños de brain switch actuales y sus métodos de evaluación. La mayoría de estos diseños estan basados en patrones cerebrales motores. Usualmente, el desempeño es evaluado fuera de línea, mediante la estimación de la tasa de verdaderos positivos (TPR) y la tasa de falsos positivos (FPR). Debido a que los falsos positivos pueden ser definidos de diferente manera y a que las clases no están balanceadas, la comparación entre dos o más diseños es complicada. Adicionalmente, se puede estimar el número de falsos positivos por minuto (FP/min). Medida que busca reducirse con mayor prioridad que el tiempo de respuesta de un brain switch.

La tercera parte de esta tesis demuestra la realización de un brain switch basado en el beta rebound. Señales de EEG registradas durante la ejecución e imaginación de movimiento son utilizadas para entrenar un clasificador. Este clasificador utiliza características espectrales para analizar el EEG y detectar la ocurrencia del beta rebound. Para obtener una BCI práctica, sólo una derivación (Laplaciana) de EEG es utilizada. Simulaciones de un brain switch asíncrono muestran un TPR de 0.74 para la detección de movimientos reales y de 0.59 para la detección de movimientos imaginarios. En ambos casos, el FPR esta limitado a 0.10. La similitud del beta rebound entre ejecución e imaginación de movimiento, permite entrenar el clasificador con el patrón cerebral de movimiento y, después de una fase de calibración, utilizar la imaginación de movimiento para el control del brain switch.

La simulación de este esquema resulta en un TPR promedio de 0.46 (FPR = 0.11).

La cuarta parte de esta tesis presenta la evaluación en línea del Graz Brain Switch, y la realización de una BCI híbrida. Esta BCI híbrida resulta de la combinación del Graz Brain Switch con una BCI basada en potenciales evocados visuales de estado estacionario. Un paradigma experimental bien definido y con temporización específica sirve como referencia para esta evaluación. Seis participantes completaron la evaluación con un promedio de 7.5 verdaderos positivos y 3.5 falsos positivos (el desempeño perfecto resultaría en cinco verdaderos positivos y cero falsos positivos) y un promedio de 0.47 FP/min. En comparación, otros diseños han reportado 0.7 FP/min en análisis fuera de línea y 1.4 FP/min para experimentos en línea.

Acknowledgements

This thesis would not have been possible without the help and support of several persons. First, I would like to thank Prof. Dr. Gert Pfurtscheller for supervising this work, and for his guidance through the several development stages of this dissertation. He shared with me his knowledge and ideas about the beta rebound, which became the basis for the Graz Brain Switch.

I would like to express my sincere gratitude to Prof. Dr. Christa Neuper and Prof. Dr. Gernot R. Müller-Putz, for allowing me to be part of the Institute for Knowledge Discovery throughout the duration of my doctoral studies. Working at the Laboratory for Brain-Computer Interfaces has provided invaluable experience for my professional career, as well as the support for my stay in Graz.

Many thanks to my colleagues at the Institute for sharing their knowledge, for the helpful discussions and recommendations, for the constructive criticism, and for the working atmosphere; but also for their friendship. Special thanks to Günther Bauernfeind, Martin Billinger, Christian Breitwieser, Clemens Brunner, Josef Faller, Raphaela Haring, Hannah Hiebel, Petar Horki, Vera Kaiser, Daniela Klobassa, Alex Kreilinger, Robert Leeb, Gernot Müller-Putz, Patrick Ofner, Reinhold Scherer, Johanna Wagner, Brigitte Wahl, and Selina Wriesnegger. Additional thanks to Vera Kaiser and Ian Daly for their help with the German and English parts of the abstract.

I am infinitely grateful to my father, my mother, my brother, and my sister, for believing in me and for their endless love and support. Also, I'm very much obliged to Elisabetta, for sharing with me a *Lebensabschnitt* in Graz.

I would like to acknowledge the financial support from the European research projects Eye-to-IT (IST-517590), PRESENCCIA (IST-2006-27731) and BETTER (ICT-2009-247935), and the FWF project "Coupling Measures in BCIs" (P20848-N15).

Contents

List of Figures

List of Tables

Chapter 1

Introduction

1.1 Brain-computer interfaces

A brain-computer interface[1] (BCI) is a communication system that provides a direct link between the human brain and a computer without involving peripheral nerves or muscles [1, 2], thus installing a non-muscular channel for the translation of brain activity (thoughts) into control commands (actions). The principal goal of a BCI is to improve the quality of life of persons with severe motor impairments, who may not have other means of communication. Brain-driven human-computer interaction is attractive to healthy persons who could use BCIs as novel controllers or hands-free devices. Therefore, current BCI research targets both disabled and able-bodied persons. Development in the BCI field has demonstrated applications that enable communication, provide control over devices, restore or replace lost motor functions, and contribute to recreation and creative expression [3–15]. Other applications offer thought-based control over robots and video games, as well as, navigation of virtual worlds [16–21]. Novel applications include the assessment of consciousness of non-responsive persons, and the assessment and promotion of cortical recovery after stroke [22–27]. Recent developments include the combination of one or more BCIs with other assistive technologies into *hybrid* systems [28–32].

Figure 1.1 illustrates the basic scheme of a BCI. In a nutshell, the BCI monitors the ongoing brain activity for characteristic patterns that represent the user's control intentions. Relying on signal processing and pattern recognition methods, the BCI identifies one of several predefined patterns and produces a distinct control command. The BCI informs the user about the current command and prepares itself for decoding the next instruction. A BCI complies with the following basic principles [29]:

Source: Control signals originate from the brain.
Control: Users are able to volitionally modulate the signal that enters the system.
Real time: Systems provide online control.
Feedback: Success or failure, i.e. system state, is fed back to the user.

[1] Also called brain-machine interface (BMI), and recently grouped under the term brain/neural-computer interaction (BNCI).

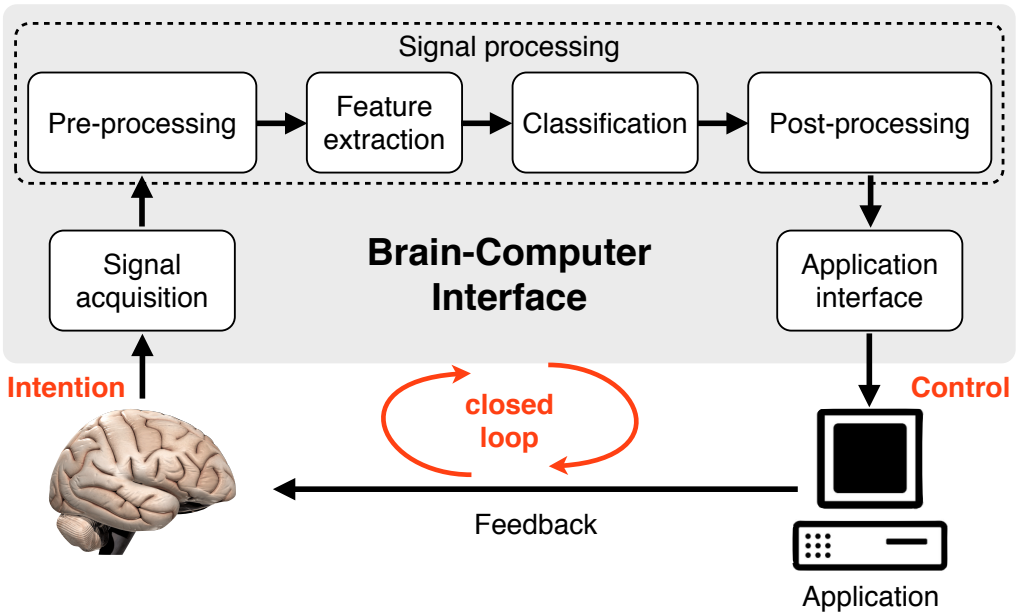

Figure 1.1: Scheme of a brain-computer interface (modified from [33]).

Control over a BCI is a skill that needs to be learned [2, 34]. A common approach is to train the BCI to recognize a user-specific brain pattern (machine learning), then allow the user to adapt his/her mental strategy to the BCI rule (operant conditioning). The latter procedure is known as user training or "feedback" training, where the BCI output guides the user to gain control over his/her own brain activity and over the machine. User training and machine learning are repeated until the system converges to an optimal control state. Coadaptation time varies among persons and BCI designs, and some users are unable to attain control [35–38]. Adaptive systems and machine learning methods help to ease the learning phase and to improve user's proficiency [39–41].

Existing BCIs can be grouped according to their operational characteristics [2, 42, 43]. Three main categories describe the operation mode of the BCI (asynchronous vs. synchronous), the type of technique that monitors brain activity (invasive vs. non-invasive), and the nature of the brain patterns that encode user's intentions (exogenous vs. endogenous). Noteworthy, these categories are not mutually exclusive, since they indicate different characteristics.

Operation of a BCI can be continuous or intermittent, meaning that control is available at any time or only during certain periods. Asynchronous BCIs provide continuous control to the user. On the other hand, synchronous BCIs allow control periodically, according to a system cue. Asynchronous and synchronous BCIs have been further divided depending on the inclusion of a *no-control* state [42], i.e. an additional command that does not execute any action. The no-control state allows the user to generate arbitrary brain patterns without producing unwanted control of the application. Following this subdivision, the four categories are: synchronized, system-paced, constantly-engaged, and self-paced. The for-

mer pair corresponds to the definition of synchronous BCI, and the latter pair corresponds to the definition of asynchronous BCI given above. In synchronized and constantly-engaged mode, the no-control state is not supported. Needless to say, an asynchronous BCI that supports the no-control state (self-paced) is preferred.

Brain activity is associated with changes in electrical potentials, magnetic fields, and blood flow that are useful as BCI inputs. Among these, bioelectrical signals are most practical due to their temporal resolution and the cost/portability of the measuring instruments. Bioelectrical brain activity can be monitored from inside the brain, from its surface (the brain cortex), and from the scalp. While invasive techniques record signals from electrodes inserted into the cortex (intracortical recordings) or laid on its surface (electrocorticogram, ECoG); non-invasive techniques record signals from electrodes placed on the scalp (electroencephalogram, EEG). Invasive BCIs use invasive techniques to obtain a high signal-to-noise ratio and a high temporal and spatial resolution; however, surgery is necessary to implant electrodes inside the head. Although signal quality decays with time after the implant, results from pilot clinical trials conducted by The BrainGate Co. (`http://www.braingate.com/`) showed that control over a computer mouse (2D movement and click) by a tetraplegic person is still possible 1000 days after implant [44]. Non-invasive BCIs use non-invasive techniques, which also have a high temporal resolution but lower signal-to-noise ratio and lower spatial resolution, to create systems that could be used on a daily basis by disabled persons and occasionally by able-bodied persons. Despite the differences in signal-to-noise ratio and spatial resolution, a recent comparison between invasive and non-invasive BCIs showed that the performance of 2D control of a computer cursor is comparable between both types [45]; furthermore, 3D control has been reported only with EEG-based BCIs in humans [46, 47].

Non-invasive BCIs based on hemodynamics use functional magnetic resonance imaging (fMRI) or functional near infrared spectroscopy (fNIRS), to quantify changes in the concentration of oxyhemoglobin and deoxyhemoglobin, which are an indirect measure of neuronal activity. Hemodynamic changes need around 6 to 12 s to reach a maximum value and 8 to 20 s to return to baseline levels; fast but weak changes appear 0.5 to 2 s after activity onset, thus setting the limit for temporal resolution of fMRI- and fNIRS-based BCIs [48]. Due to the complexity and cost of the equipment, applications of fMRI-based BCIs are limited to clinical rehabilitation and treatment [26, 49–51], e.g stroke rehabilitation, chronic pain, emotional and social disorders, and assessment of consciousness. Although fMRI is considered a standard for brain imaging, fNIRS is more practical and less expensive [52]. fNIRS-based BCIs could be considered practical for applications where time resolution is less important, e.g assessment of consciousness, or in hybrid systems [29, 53–57].

Brain activity patterns used for BCI control can be evoked by external stimuli or induced by internal processes. Evoked responses have known characteristics that are stable among persons, namely topography and latency; whereas induced responses create complex spatiotemporal patterns of brain activity with some general features that vary slightly among persons, i.e. topography and time-frequency characteristics. Exogenous BCIs take advantage of evoked responses to reduce user training and to maximize the information transfer rate (ITR), i.e. the amount of brain information that is correctly decoded by the

BCI in a certain amount of time [2]. However, exogenous BCIs require the users to focus their attention to an external stimulus, and unwanted commands often occur. Endogenous BCIs rely on induced patterns to convey control commands without the need of external stimuli, at a moderate ITR. The complexity of induced patterns reduces the probability of unwanted commands, but multichannel recordings are often necessary. Moreover, the capability of self-inducing these patterns varies among persons, which may increase the time for user training.

1.2 Event-related brain phenomena

Different types of events induce transient changes on the ongoing brain activity that are time-locked, but not always phase-locked. Phase-locked electrical responses are called event-related potentials (ERPs), and can be interpreted as the response of a stationary system to a stimulus [58]. ERPs occur in the EEG as small potential deflections immersed in the spontaneous activity. Averaging across several realizations reduces the contribution of spontaneous activity and isolates the ERP [59]. Non-phase locked responses are called event-related (de)synchronization (ERD/ERS), and represent changes in the functional connectivity of neuronal populations [60]. While the desynchronization of neuronal groups induces a suppression of a particular EEG rhythm, their synchronization induces an increment of a specific rhythm. Hence, the analysis of ERD and ERS require non-linear methods such as envelope detection or power spectral analysis. Time course of ERD/ERS is often computed with the inter-trial variance method [61], but other methods are available (see [62]). Since ERD and ERS are frequency specific, it is necessary to indicate the frequency band where the changes occur.

Many endogenous BCIs are based on the classification of event-related (de)synchronization of sensorimotor rhythms [42, 43, 63], i.e. oscillations in the alpha (8 to 13 Hz), beta (15 to 35 Hz), and gamma (>40 Hz) bands. Typically, ERD is interpreted as correlate of an active cortical area, whereas ERS in the alpha and beta bands is commonly associated with a deactivated or inhibited state of large neural networks; noteworthy, the ERS in the gamma band is considered a correlate of an active cortical area. In general, the ERD (power decrease) of the mu and lower beta (16 to 20 Hz) rhythms appears up to two seconds before movement onset and for the duration of the movement itself. The motor-related ERD reaches its minimum about half of a second to one second after movement onset [64]. After movement offset, a beta ERS (power increase) appears for about one second [65–67]. An ERS around 40 Hz appears shortly before movement onset [68, 69]. A similar ERD/ERS pattern is also visible during imagination of movements [34].

Interestingly, ERD and ERS are visible at the same time in different frequency bands (e.g alpha ERD and gamma ERS) and at the same cortical areas, thus indicating that underlying neuronal populations are engaged in different processes related to motor behavior, e.g somatosensory processing or motor control. Simultaneous ERD and ERS may also appear in the same frequency band on distant brain areas. This phenomenon is known as *focal ERD/surround ERS* [70, 71].

An example of focal ERD/surround ERS is observed during movement: hand/finger movement induces a contralateral ERD (cortical hand representation) and a mid-central ERS (cortical foot representation, overlapping with the supplementary motor area); similarly, foot movement produces a mid-central ERD and a bi-lateral ERS [70]. Focal ERD/surround ERS may result from a distribution of cortical resources, which might facilitate task performance by an additional suppression or inhibition of the surrounding cortical areas [72]. Antagonistic patterns, similar to the focal ERD/surround ERD of sensorimotor rhythms, can be found on the concentration changes of oxy- and deoxyhemoglobin (fNIRS) in the prefrontal cortex during mental arithmetic [57, 73]; and in form of positive and negative blood-oxygen-level-dependent (BOLD) signal measured by functional magnetic resonance imaging (fMRI) during toe movements [74] (positive BOLD in foot area, and negative BOLD in hand areas).

1.3 Bringing BCIs out of the lab

Widespread use of BCIs would require non-invasive techniques and affordable systems to record brain activity. The EEG meets these requirements and it offers a good temporal resolution (in the order of milliseconds), although the signal-to-noise ratio is low and multichannel recordings are often required. To bring an EEG-based BCI into every day life, additional features are necessary. The BCI must be simple and easy to set up, it must be robust and reliable, and it must provide on demand control. Hence, the BCI must be continuously available to the user and the number of unwanted commands must be minimized. Furthermore, the BCI should not depend on external stimuli and use as few channels as possible.

Ideally, a BCI that identifies stable brain patterns from ongoing single channel EEG would fulfill these requisites. A BCI that distinguishes a single brain pattern from all other brain activity is called a brain switch [75]. A brain switch provides a simple mechanism to trigger an action, to start/stop an application, or to sequentially execute a series of actions. Prerequisite for a robust BCI is a simple mental task associated with an stable EEG pattern, suitable for online detection in only one EEG channel or derivation. Such an EEG pattern could be the *beta rebound* reported after active and passive movement, electrical nerve stimulation, observation of movement, withholding of movement, and motor imagery. The beta rebound presents a strict somatotopic organization [62, 65], somatotopically-specific frequency components [76], "cross-talk" between hand representation area and mesial cortex [77], and coincidence with a reduced excitability of motor cortex neurons [78].

1.4 Aim of this work

This dissertation presents the asynchronous Graz Brain Switch, an EEG-based BCI trained to detect the event-related synchronization of the central beta rhythm (beta rebound) present after termination of a motor task, particularly, after brisk foot motor imagery.

Outline

This dissertation is organized in seven chapters. This chapter, Chapter 1, introduces brain-computer interfaces, the problem of bringing BCIs out of the lab, and the aim of this dissertation. Chapter 2, provides a brief literature review on the beta rebound and its characteristics. It also includes a novel comparison between the beta rebound following overt foot movement and its inhibition. Chapter 3 presents a brief literature review on other asynchronous brain switch designs and the methods for evaluation. Chapter 4 demonstrates that the beta rebound is suitable for realizing a brain switch, and compares the classification performance when ERD or ERS are used as features. Chapter 5 presents the methods for setting up a brain switch for healthy users, based on the similarity between the post-movement and the post-imagery beta rebound. Chapter 6 describes an online application and performance evaluation of the brain switch, as part of a hybrid BCI. Finally, Chapter 7 presents the conclusions and future prospects of this work.

Previously published work

Parts of this dissertation have appeared in peer-reviewed journals.

T. Solis-Escalante, G. R. Müller-Putz, and G. Pfurtscheller. Overt foot movement detection in one single Laplacian EEG derivation. *Journal of Neuroscience Methods*, 175: 148–153, 2008.

G. Pfurtscheller and **T. Solis-Escalante**. Could the beta rebound in the EEG be suitable to realize a "brain switch"? *Clinical Neurophysiology*, 120:24–29, 2009.

T. Solis-Escalante, G. R. Müller-Putz, C. Brunner, V. Kaiser, and G. Pfurtscheller. Analysis of sensorimotor rhythms for the implementation of a brain switch for healthy subjects. *Biomedical Signal Processing and Control*, 5:15–20, 2010.

G. Pfurtscheller, **T. Solis-Escalante**, R. Ortner, P. Linortner, and G. R. Müller-Putz. Self-paced operation of an SSVEP-based orthosis with and without an imagery-based "brain switch": a feasibility study towards a hybrid BCI. *IEEE Transactions on Neural Systems and Rehabilitation Engineering*, 18:409–414, 2010.

T. Solis-Escalante, G. R. Müller-Putz, G. Pfurtscheller, and C. Neuper. Cue-induced beta rebound during withholding of overt and covert foot movement. *Clinical Neurophysiology*, 123:1182–1190, 2012.

Chapter 2

The beta rebound

Beta rebound is the term for the induced burst of beta activity that follows somatosensory stimulation or motor behavior [64, 79]. The beta rebound is a short lasting beta ERS observable in ECoG, EEG, and MEG. It typically appears in the motor cortex, the somatosensory cortex, and the supplementary motor area [80–85]; but it also appears in the prefrontal cortex [86], and the parietal cortex [65, 87]. Figure 2.1 illustrates the burst of beta activity in the EEG and the corresponding beta ERS.

It is generally accepted that the beta rebound reflects a process of active inhibition after termination of a sensorimotor program [66, 67, 72, 88], but its exact functional meaning is still uncertain. Support for the active inhibition role of the beta rebound comes from studies demonstrating that the beta rebound coincides with a reduced excitability of the neurons in the motor cortex [89], that the beta rebound is suppressed during enhanced activation of the motor cortex [90–94], and that the beta rebound correlates inversely with the blood-oxygen-level-dependent (BOLD) signal measured by fMRI [95–97]. Additionally, there are studies showing an influence of the concentration of the inhibitory neurotransmitter γ-Aminobutyric acid (GABA) on the power and frequency of the beta rhythm at rest [98] and the beta rebound [99, 100], and a decreased beta rebound in patients with myoclonic epilepsy (Unverricht-Lundborg disease), which leads to an enhanced excitation and deficient inhibition of cortical regions [101, 102].

Other observations indicate that the beta rebound partly correlates with the processing of afferent inputs [103–107], and that changes to somatosensory pathways affect the beta rebound [108–111]. However, motor output and somatosensory stimulation are not a requisite for the beta rebound since motor imagery [91, 112] and motor inhibition [86, 113, 114] are also followed by a beta rebound.

A general interpretation of beta activity has been recently proposed [115]. Engel and Fries [115] suggest that beta band activity could "signal the status quo", of motor control and cognitive processes. Regarding motor control, the authors cite several studies where the beta band activity helps to *restore* a motor state after some dynamic change, e.g. after motor planning, motor termination, somatosensory stimulation, or response inhibition. Although there is no consensus on the functional meaning of the beta rebound, the active inhibition role seems to be appropriate.

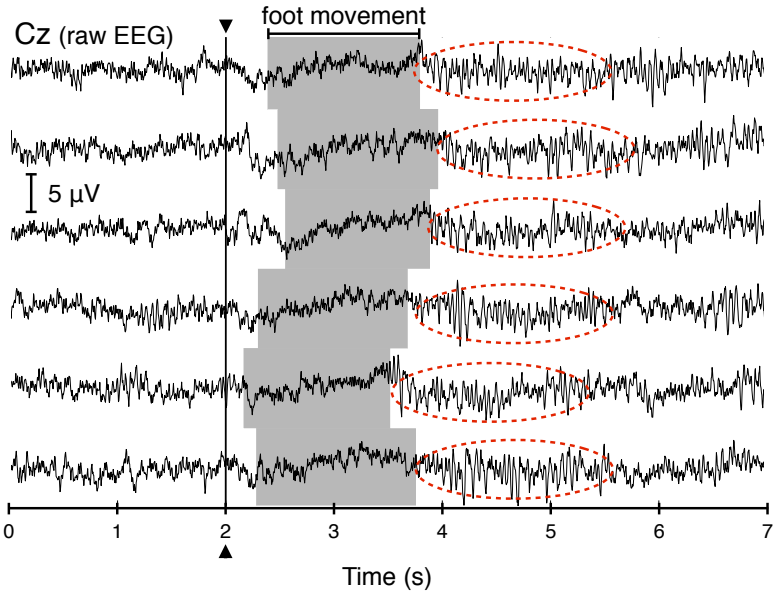

(a) Induced beta activity after movement (beta rebound).

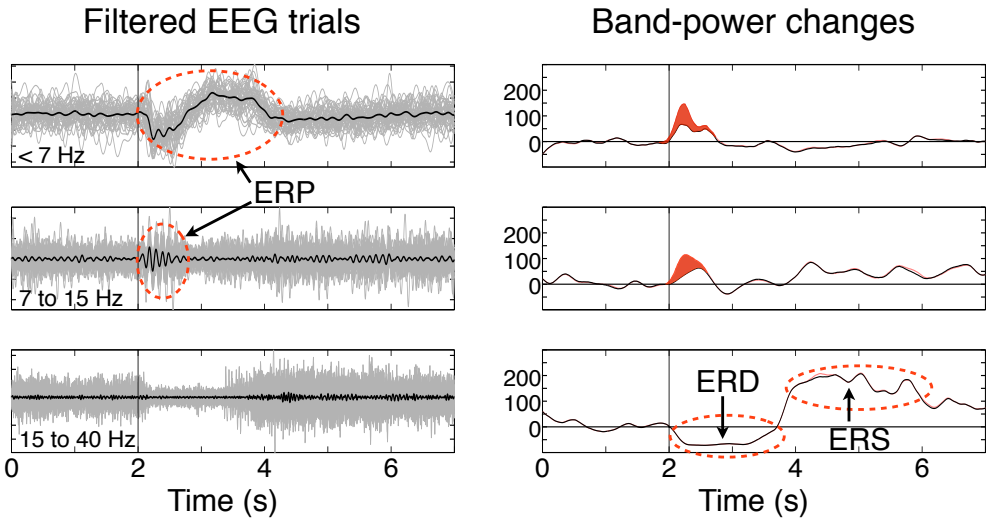

(b) Phase-locked and non phase-locked event-related phenomena.

Figure 2.1: Quantification of the beta rebound. (a) Raw EEG (0.5 to 100 Hz) recorded from a Laplacian derivation at the vertex (electrode position Cz), during cue-paced foot movement, cue onset at t=2 s. Shaded areas indicate the duration of individual movements. (b) Event-related brain responses during cue-paced foot movement (cue at t = 2 s, vertical line), the left panel shows the event-related potentials (average) obtained after filtering below 7 Hz, between 7 and 15 Hz, and between 15 and 40 Hz; the right panel presents the corresponding event-related (de)synchronization computed with the power method (red) and the *inter-trial variance* method [61] (black). The inter-trial variance method reduces the contribution of phase-locked responses by subtracting the average waveform to each individual EEG epoch (differences marked in red). Reference for the ERD/ERS curves was between 0.5 and 1.5 s.

2.1 Beta rebound after movement and stimulation

Voluntary movements

The post-movement beta rebound appears over the sensorimotor cortex after self-paced and cue-paced movement of several body parts [64–67, 76, 79, 80, 85, 95, 103, 104, 116–118]. Following a strict somatotopic organization along the sensorimotor strip, the beta rebound is dominant in contralateral areas of the sensorimotor cortex after finger, wrist, and toe movements [65, 67, 80]; whereas a dominant beta rebound appears at the vertex after foot movement [66], and bilaterally in the parietal cortex after mouth movements [65].

Although the beta rebound is sometimes associated with cortical oscillations around 20 Hz [65, 81], the reactive bands of the beta rebound present a somatotopic frequency specificity with higher components for foot movements than for hand movements [76, 84]. Figure 2.2 exemplifies the somatotopic specificity of the beta rebound. Interestingly, self-paced brisk finger movement induces a beta rebound in the contralateral hand representation area, and a midcentral beta rebound around the foot representation area and the supplementary motor area (SMA) [84]. This observation suggests the information transfer between the primary motor cortex (M1) and the SMA, which has also been reported in response inhibition experiments with humans [119] and non-human primates [120].

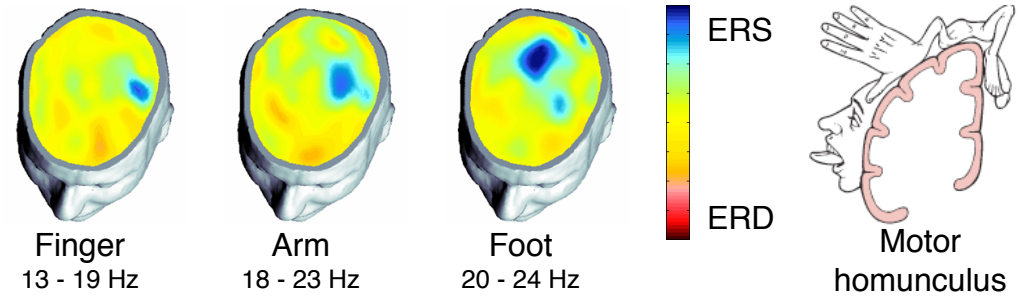

Figure 2.2: Somatotopic organization and frequency specificity of the beta rebound. Topography of the beta rebound after hand, arm, and foot movement; noteworthy are the different frequencies where the beta rebound occurs. The cortical representation of different body parts on the motor cortex is shown on the far right (modified from [76]).

Different characteristics of the movement have a direct influence on the post-movement beta rebound. Brisk/ballistic movements induce a stronger beta rebound than sustained movements [103, 117]; the duration of the beta rebound is related to the muscle force [121] and the muscle mass [67] involved in the movement; the strength of the beta rebound reduces gradually and inversely with the speed of the movement [95]; the beta rebound is stronger for movements of the non-dominant side than for the dominant side, for hand [122] and foot [66].

Passive movements

Besides voluntary movements, passive movements are also followed by a beta rebound. Since passive movements do not require motor planning or execution of a motor program, it is concluded that these are not a requisite for the beta rebound. The beta rebound has been observed after passive movements [88, 104, 123, 124], movements induced by nerve stimulation [90, 93], and movements induced by functional electrical stimulation (FES) [125]. Also displaying a somatotopic organization, the beta rebound after passive movements is generally more intense than the beta rebound after voluntary movement [123, 124]. The presence of the beta rebound after induced movements suggest that at least some components of the beta rebound are related to somatosensory stimulation. Figure 2.3 shows a comparison between active and passive movements, as well as somatosensory stimulation.

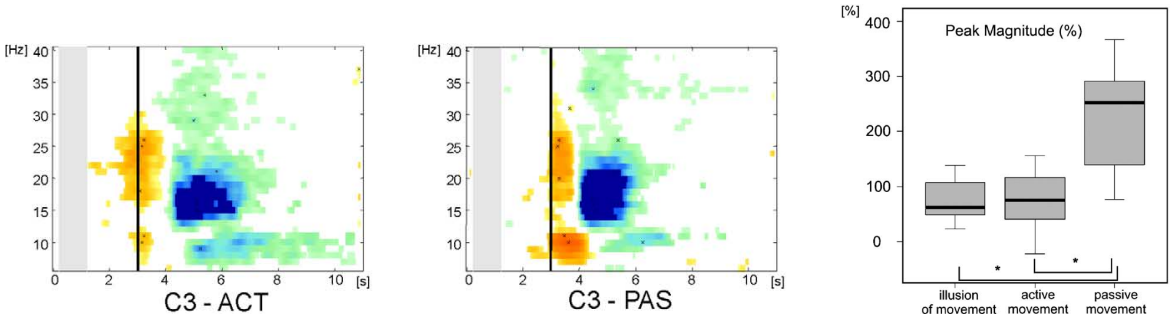

(a) Time-frequency. (b) Amplitude.

Figure 2.3: Beta rebound after active and passive movements. (a) Time-frequency map of the ERD/ERS during active and FES-induced wrist movement. Note the lack of ERD before movement onset (vertical line) in the passive (PAS) movement condition (modified from [125]). (b) Statistical analysis of the amplitude of the beta rebound after movement illusion (nerve stimulation without movement), active movement, and passive movement of the arm (modified from [123]).

The role of somatosensory stimulation in the beta rebound after voluntary and induced movements has been addressed in several experiments. In healthy persons, the beta rebound after passive movements and nerve stimulation disappears following blocking of the median nerve with an ischemic maneuver [91, 104]. Accordingly, the beta rebound after active movement, passive movement, and nerve stimulation is reduced in patients with sensory deafferentation due to Parkinson's disease [109]; and the beta rebound after self-paced finger movement is reduced in patients with sensory deafferentation due to chronic pain [108]. Furthermore, the beta rebound is reduced or abolished in persons with spinal cord injury [124], and the amplitude of the rebound is correlated to the severity of the lesion [110].

Somatosensory stimulation

Somatosensory stimulation can induce a beta rebound even without inducing movement. A beta rebound occurs after median nerve stimulation below motor threshold [76, 106, 123] and tactile stimulation [105, 126]. The beta rebound after somatosensory stimulation also follows somatotopic organization and frequency specificity. Figure 2.4 shows a comparison between the beta rebound after movement and stimulation of hand an foot.

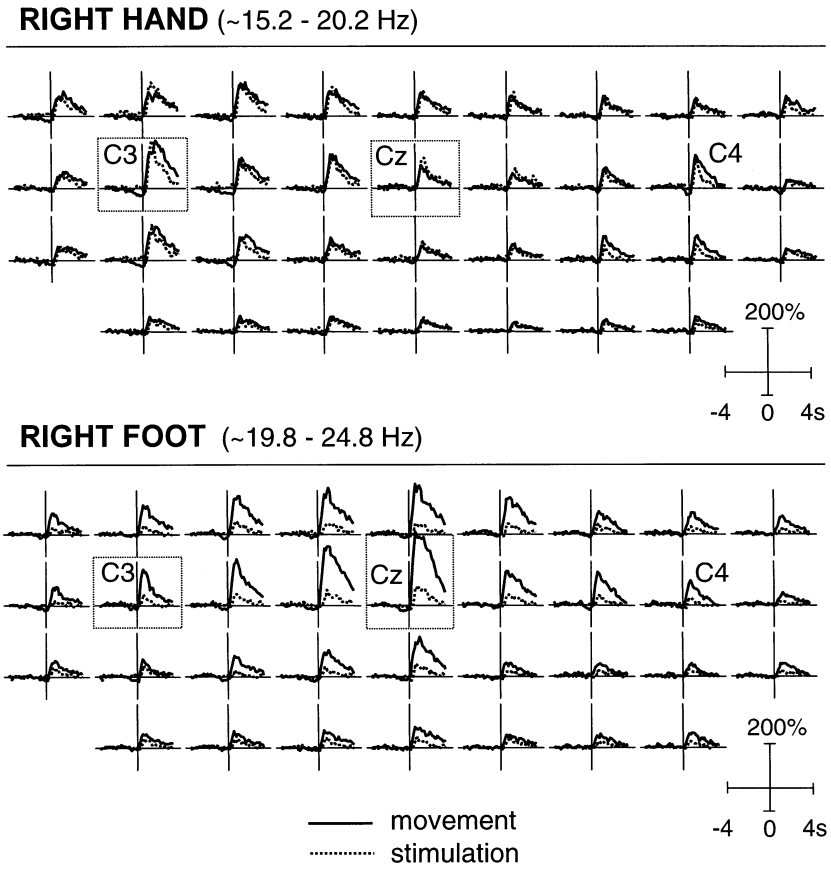

Figure 2.4: Beta rebound after somatosensory stimulation. Comparison of the beta rebound following movement and nerve stimulation. Vertical lines indicate the offset of movement or stimulation (modified from [76]).

Action observation

Action observation activates parts of the primary motor cortex and the premotor cortex through the mirror neuron system, which is believed to help understanding the meaning of observed actions and learning by imitation [92, 127, 128]. Activation of the mirror neuron system through action observation creates an interference in the primary motor system

that reduces the amplitude of the beta rebound after nerve stimulation [129]. Even without nerve stimulation, the beta rebound is also present after observation of movement [130] and hearing of motor actions (drum tapping) [107]. Interestingly, the beta rebound after observation of movements is reduced in patients with a dysfunctional mirror neuron system associated with autistic spectrum disorder [131].

Noteworthy, the beta rebound after observation of motor tasks is modulated by the *semantics* of the movement (see Figure 2.5). Observation of goal directed movement suppresses the beta rebound more than non-goal directed movement [94]. Also, the execution and observation of movement, as well as observation of somatosensory stimulation (brushing of a mannequin hand), reduced the amplitude of the beta rebound, whereas observation of aimless thumb movement does not [129]. The amplitude of the beta rebound correlates inversely with the correctness of the observed action [87]. Similarly, the beta rebound after tactile stimulation is stronger when the stimulus has the relevance of a cue [132].

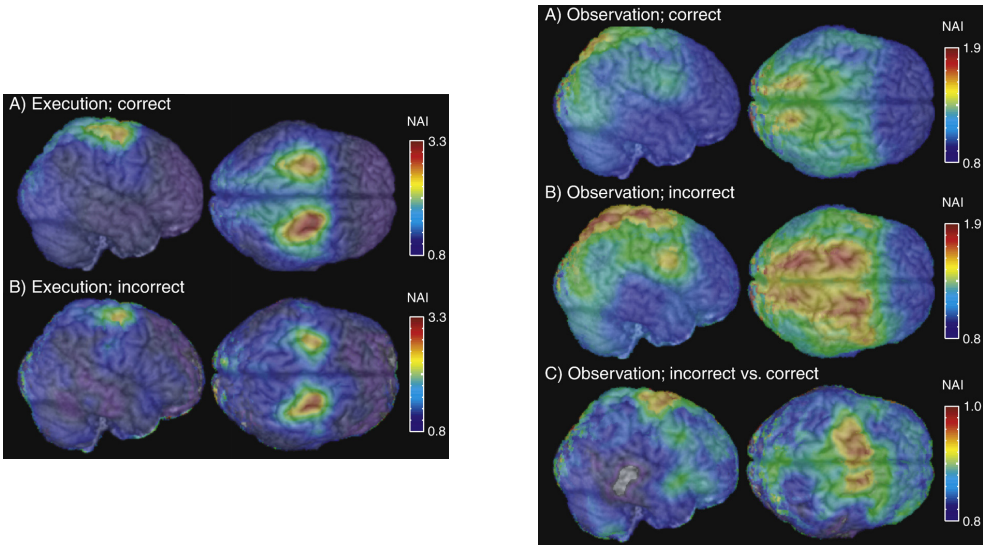

Figure 2.5: Beta rebound during action observation. (left) Beta rebound after execution of correct and incorrect responses. (right) Brain activity during observation of correct and incorrect responses. Differences between observation of correct and incorrect responses are stronger in precentral areas, including the SMA (modified from [87]).

2.2 Beta rebound after motor imagery

Motor imagery is the mental simulation of a movement without motor output. It activates cortical areas in the sensorimotor cortex that are also active during execution of movement [91, 133]. Consequently, a beta rebound is also observed after motor imagery, although with a smaller amplitude than the post-movement beta rebound [124]. Besides the amplitude differences, the post-imagery beta rebound is similar in topography and

time course to those patterns accompanying motor execution [134]. It also follows the somatotopic organization [135, 136], the somatotopic frequency specificity [124, 135], the contralateral dominance [136], and the negative covariation with the BOLD signal [97] previously mentioned for the post-movement beta rebound.

Execution and imagination of foot movement

The beta rebound after execution [76] and imagination [112] of foot movement is particularly interesting due to its dominance. This beta rebound appears at the vertex, near the SMA and the cortical foot representation area. Considering the close proximity of these areas [137] and the possible cross talk between M1 and SMA [84], it is reasonable that a large amplitude beta rebound occurs after foot movement or its imagination. Figure 2.6 illustrates the cross talk between these M1 and SMA, as well as the dominance of the midcentral beta rebound. Figure 2.7 demonstrates the similarity between the beta rebound after foot movement execution and imagination. It can be stated that the beta rebound after foot movement displays a high signal-to-noise ratio, thus it is specially suitable for detection of foot motor imagery in single EEG trials.

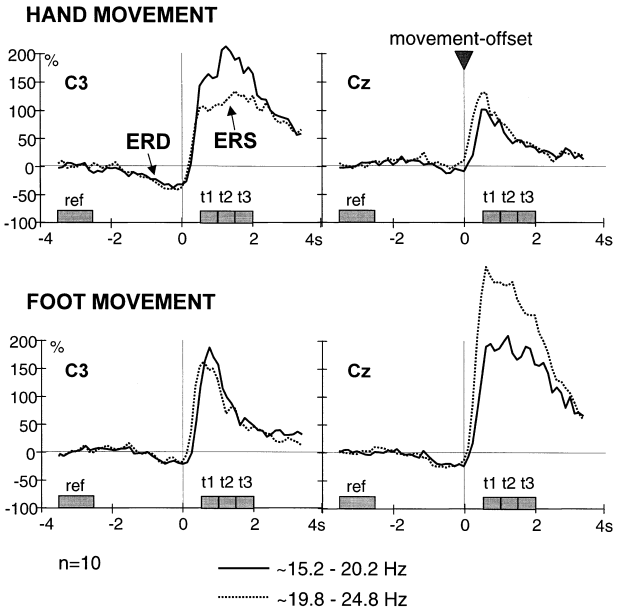

Figure 2.6: Cross talk and dominance of midcentral beta rebound. (left) Contralateral and midcentral beta rebound after right *hand* movement. The midcentral beta rebound has a slightly shorter latency than the contralareal beta rebound. (right) Contralateral and midcentral beta rebound after *foot* movement. The midcentral beta rebound following foot movement has a larger amplitude than the contralateral beta rebound following hand movement. In both cases, the beta rebound displays a somatotopic frequency specificity (modified from [76]).

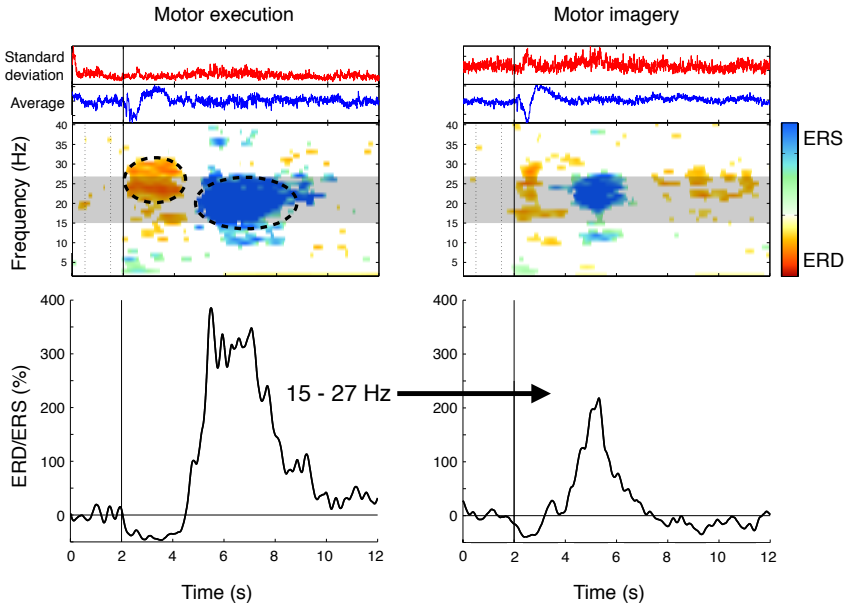

Figure 2.7: Beta rebound after foot movement and its imagination. (top) Time-frequency maps of statistically significant ($p < 0.01$) ERD/ERS values and the mean and standard deviation across trials ($N = 36$ for execution, and $N = 60$ for imagination). (bottom) Time course of the beta rebound, same frequency band used for motor execution and imagery (15 to 27 Hz). ERD and ERS are observed in slightly different bands (dashed circles in top-left map).

2.3 Inhibition of overt and covert foot movement

Inhibition processes, along with decision making, are studied with Go/NoGo paradigms. In such paradigms, participants are required to execute or withhold an action in response to a cue. Several studies have observed a beta rebound induced by the *NoGo* cue, in the human EEG [86, 113, 114, 119] and local field potentials (LFP) of non-human primates [120]. Moreover, Zhang et al. [120] observed the beta rebound following the NoGo cue, even when the decision was to maintain an arm extension (continuous depression of a lever). The beta rebound during response inhibition appears with a latency between 200 to 300 ms after the cue, over the prefrontal (electrode positions Fz or Cz) and premotor cortex (FC3, F3 or F8) near the cortical representation areas of the motor response, e.g. finger/wrist movements.

A beta rebound has also been observed in the inhibition of voluntary action. Walsh et al. [138] observed a burst of beta activity 12 ms before the intention to move in a self-inhibition experiment, only in the trials that included self-inhibition. Using a self-reporting scheme, the participants of that study decided when to complete or inhibit a movement

(key press), at their own freewill. These observations support the active inhibition role of the beta rebound.

Interestingly, the beta rebound after motor execution and during response inhibition have not been directly compared. Moreover, investigations of withholding of movement are exclusively done with hand movement; while foot movements have not been considered. In this section we present a comparison of the beta rebound following the Go/NoGo cues in an experiment with dorsiflexion of both feet, and between the withholding of execution and imagination of the same movement. The goal is to investigate the differences between the beta rebound following the Go/NoGo cues for experiments with foot movement, and the differences between the beta rebound during withholding of overt and covert foot movement.

Participants and experimental setup

Our analysis included sixteen participants (8 males and 8 females, age 23.6 ± 3.5 years). From an original group of twenty persons, the data from three participants was discarded due to movement or EMG artifacts. Data from one additional participant was discarded because the beta rebound showed an atypical power increase ($> 1000\%$). All participants gave informed consent. During the experiment the participants sat on an armchair, one meter in front of a computer screen. The computer screen showed the cues for a Go/NoGo experiment and a first person perspective of a virtual character's feet. The participants' task was to perform or imagine a brisk movement (dorsiflexion) of both feet following a green circle (Go), and to withhold the movement if a red circle (NoGo) appeared.

The experimental paradigm consisted of a single session of cue-paced motor execution (ME) without feedback, and another session of cue-paced motor imagery (MI) with feedback. None of the participants had previous experience with MI. The ME session consisted of two runs and the MI session of three runs. Each run contained 40 trials and Go/NoGo class probability of 50%. Trials with feedback were not considered in this analysis. Both sessions were conducted in the same day with several pauses in between. The paradigm timing is shown in Figure 2.8.

Data recordings

We recorded the EEG from the participants' scalp with five Ag-AgCl electrodes arranged around electrode position Cz. Reference and ground electrodes were attached to the left and right mastoid, respectively. Additionally, we recorded the electromyogram (EMG) from the *tibialis anterior* muscles in both legs using bipolar derivations. A reference electrode for EMG was attached to the right hip. Figure 2.9 shows the montage for both EEG and EMG. Prior to digitization, the EMG was band-pass filtered between 1 and 1000 Hz, full-wave rectified, and integrated with a time constant of 100 ms. EEG and EMG were recorded with a biosignal amplifier (g.UBSamp, Guger Technologies, Schiedlberg, Austria). Sampling rate was 250 Hz, with a band-pass filter between 0.5 and 100 Hz, and a notch filter at 50 Hz.

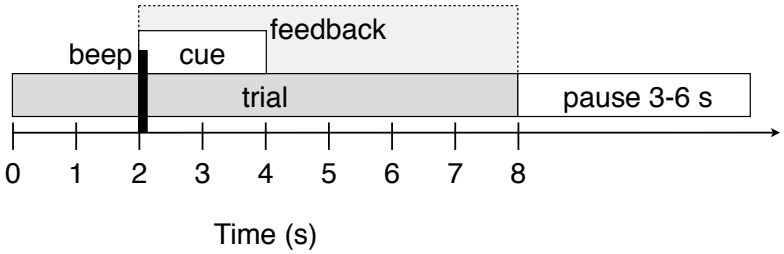

(a) Trial timing

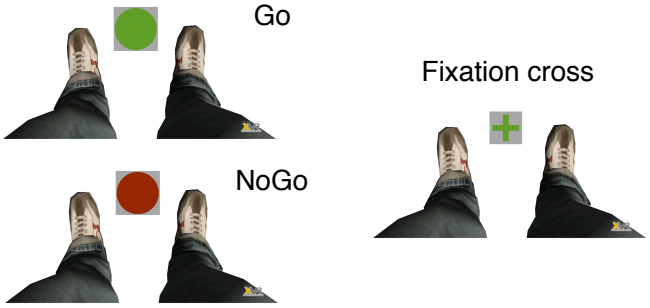

(b) Visual cues

Figure 2.8: Experimental paradigm Go/NoGo. (a) The trials in each run lasted 8 s plus a random pause between 3 and 6 s. Auditive (beep, 70 ms) and visual (ball, 2 s) cues were presented to the participants two seconds after the beginning of a trial. (b) A green ball indicated the execution (or imagination) of brisk foot dorsiflexion, while a red ball indicated the withholding of such task. Participants observed a fixation cross during the rest of the trial and the pause (inter-trial period). Modified from [139].

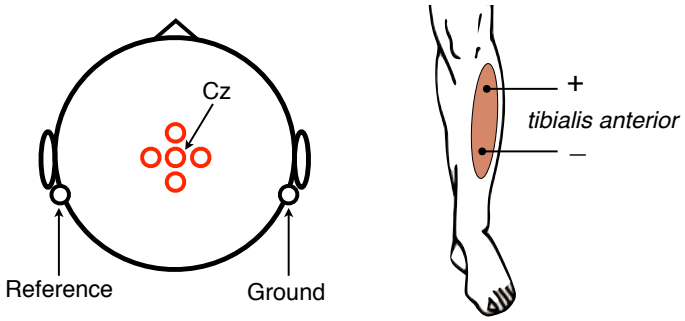

Figure 2.9: Electrode montage for EEG and EMG. EEG was recorded from five monopolar channels arranged in a Laplacian derivation around position Cz. Inter-electrode distance was 2.5 cm. EMG was recorded from the *tibialis anterior* muscles from both legs using two bipolar derivations. The ground electrode for EMG was located on the right hip (not shown). Modified from [139].

Artifact rejection

We computed a Laplacian filter [140] over Cz to improve the signal-to-noise ratio of the EEG. Then, we rejected the EEG trials automatically: (i) if the kurtosis of each trial exceeded the mean plus five times the standard deviation of the EEG data, or (ii) if the amplitude of the signal exceeded $20\,\mu$V. Additionally, for NoGo trials and MI runs, we rejected trials if the EMG from either leg was larger than a threshold. For NoGo trials, this threshold was equal to the mean plus three times the standard deviation of the EMG at rest. For Go trials in the MI runs, the threshold was equal to the mean plus five times the standard deviation of the EMG at rest, since imagined movements can increase the tonus of the target muscles [141]; although MI-Go trials were not further analyzed. We defined the *EMG at rest* period as a five second interval before the cue onset. Data sets from two participants were discarded after artifact rejection due to excessive number of movement artifacts in the EEG (ME-Go trials). One additional data set was discarded due to large EMG activity during MI (Go trials). MI-NoGo trials were discarded if feedback, i.e. moving legs of the avatar, occurred between five seconds before and six seconds after the cue onset.

Beta rebound quantification

We used the inter-trial variance method [61] to quantify the amplitude and time course of the beta rebound. Furthermore, visualization of ERD/ERS patterns was completed with ERD/ERS maps, a time-frequency representation of significant ERD/ERS values [142]. Quantification and visualization were managed by the BioSig toolbox [143]. Data was analyzed between 8 and 45 Hz in intervals of 2 Hz. Reference interval for the relative power changes was between 0.5 and 1.5 s after beginning of the trial. We used the ERD/ERS maps and the discriminability (Cohen's kappa) between the beta rebound and the reference interval to define a participant-specific frequency band.

To complete the quantification of the beta rebound we applied the inter-trial variance method once again, after selection of the individual frequency band. The ME-Go trials were re-triggered to the end of the movement to avoid attenuations due to inter-trial differences in movement duration. Alignment of individual trials has been used previously for similar reasons [103, 144]. Since NoGo trials and MI produced no EMG, we processed those trials relative to the cue onset. Reference interval for the beta rebound quantification was 4.5 to 3.5 s before the end of the movement (ME-Go) or the cue onset (ME-NoGo and MI-NoGo). After quantification of the beta rebound, the data of one participant was discarded due to a very strong beta rebound ($> 1000\%$).

Beta rebound characteristics

Sixteen participants showed a post-movement beta rebound following the brisk dorsiflexion of both feet (ME-Go). Average reaction time was 367 ± 124 ms, and movement duration was $1.6\,\text{s} \pm 310$ ms. Twelve out of sixteen participants showed a beta rebound after the ME-

NoGo cue, whereas only seven participants showed a beta rebound after the MI-NoGo cue. The beta rebound ranged between 13 and 37 Hz, with an average frequency band between 19 and 28 Hz (s.d. 4.7 Hz in both cases). The post-movement beta rebound (ME-Go) reached an average amplitude of $322 \pm 169\%$ with an average peak latency of 0.9 ± 0.4 s, relative to the end of the movement. During withholding of movement, the amplitude decreased to $191 \pm 99\%$ and $152 \pm 75\%$, for ME-NoGo and MI-NoGo respectively. In both cases, latency was 1.0 ± 0.2 s relative to cue onset. Figure 2.10 presents the individual and grand average ERD/ERS curves. Details about the participants' average reaction time and movement duration, as well as the number of artifact-free trials, individual frequency bands, peak amplitude, and peak latency of the beta rebound are given in Table A.1 and Table A.2 (Appedix A).

Statistical analyses

We compared the beta rebound between pairs of conditions: (i) ME-Go vs. ME-NoGo, and (ii) ME-NoGo vs. MI-NoGo; considering only those participants with a significant beta rebound in each condition, i.e. sixteen in ME-Go, twelve in ME-NoGo, and seven in MI-NoGo. For the first analysis, ME-Go vs. ME-NoGo, we aligned the beta rebound of individual participants to 100 ms before a certain ERS threshold. This threshold was equal to 30%, i.e. the average ERS across participants at the end of the movement (EMG triggered). For the second analysis, ME-NoGo vs. MI-NoGo, the alignment time point was the cue onset. Bear in mind that in the second analysis, the two conditions refer to the inhibition task only; hence, motor execution or imagery should not occur. The power from the reference intervals between pairs of conditions were compared with a paired t-test, since significant differences in the reference interval affect the beta rebound quantification. We observed that the power of the reference interval of the first comparison was significantly different ($p < 0.05$). To correct this, three participants with the largest differences in power were removed from the analysis. After recomputing a t-test between the references of the nine remaining participants, we found no significant difference. For the second comparison, no significant differences in the power of the reference period were found in the original sample of seven persons.

To improve the topographical information of our study, we analyzed the beta rebound from all five EEG electrodes (see Figure 2.9). Once the trials were selected and aligned (see above), we applied a common average reference to the EEG channels. Time course of the beta rebound between conditions was compared with a three-way ANOVA with factors TASK×CHANNEL×TIME. The factor TASK indicates the motor task to perform, i.e. ME or MI in Go or NoGo conditions. The factor CHANNEL had five levels, i.e. the channel locations relative to Cz: anterior, lateral left, Cz, lateral right, and posterior. The factor TIME refers to the time course of the ERD/ERS. The factor TIME considered only time points from $t = 0$ to 2.5 s, in steps of 500 ms, relative to the alignment point of each analysis (see previous paragraph). The dependent variable was the average beta ERD/ERS over a 300 ms window centered at each of the time points under analysis. Pair-wise post-hoc tests (Bonferroni corrected) provided the confidence intervals for

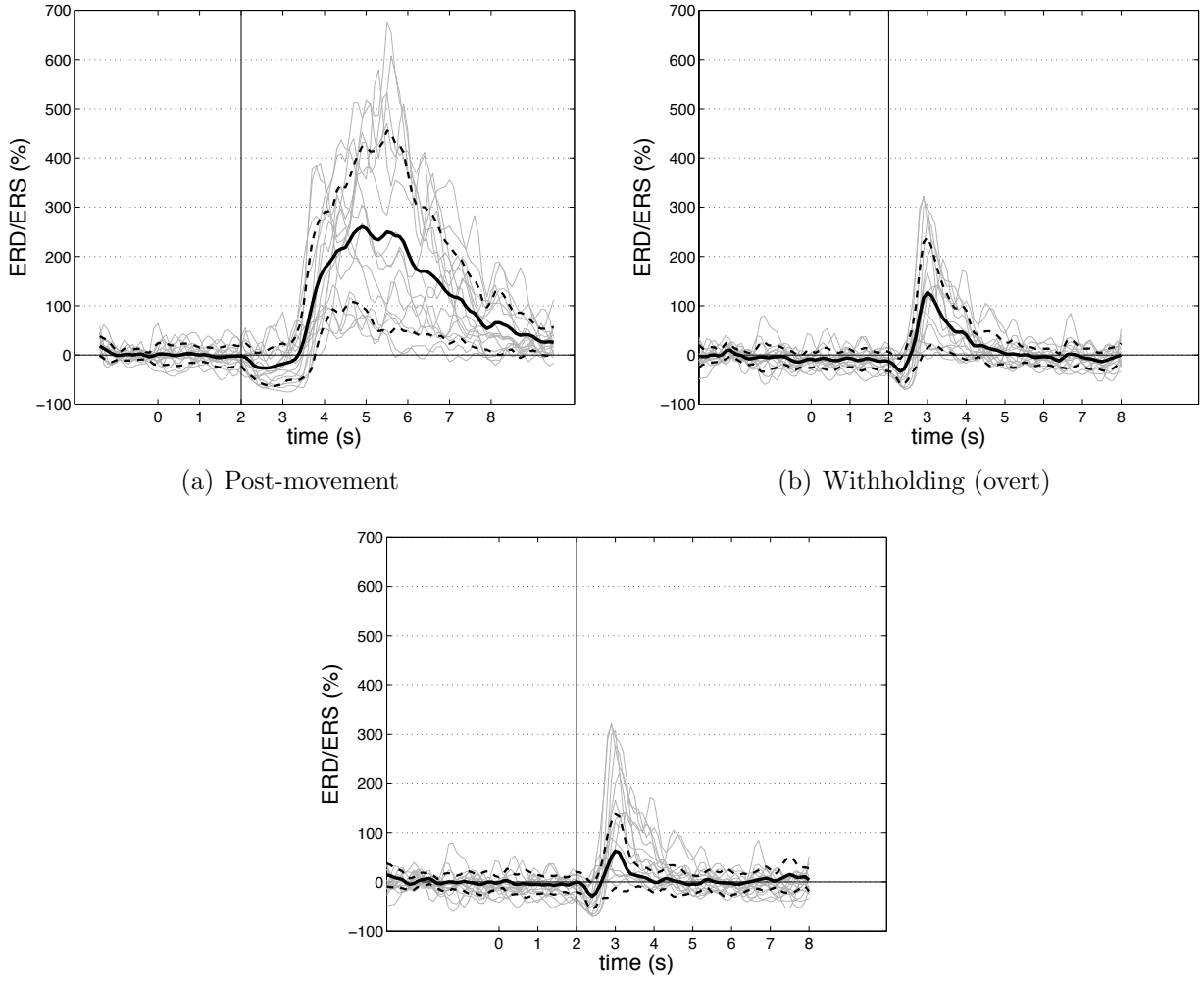

(a) Post-movement

(b) Withholding (overt)

(c) Withholding (covert)

Figure 2.10: Time course of the Go/NoGo beta rebound. (a) Beta rebound after foot movement execution (dorsiflexion). Individual curves were computed according to the end of the movement of individual trials, and then re-aligned according to the average movement duration for display only. (b) Beta rebound after/during withholding of overt foot movement. (c) Beta rebound after/during withholding of covert foot movement (motor imagery). Gray lines show the individual beta rebound of individual participants. A thick black line presents the grand average curve and dashed black lines show the standard deviation. Vertical lines indicate the cue onset ($t = 2\,s$). All curves obtained from the Laplacian derivation at Cz. Modified from [139].

the TASK×CHANNEL×TIME interaction comparisons. Significance levels were corrected (Greenhouse-Geisser) if sphericity violations occurred.

All factors and their interactions showed statistically significant differences. These differences are summarized in the next sections. Please refer to Table A.3 and Table A.4 (Appendix A) for the exact mean and standard deviation values of the comparisons.

ME-Go vs. ME-NoGo

For the factor TASK, the beta ERS was stronger during ME-Go than during ME-NoGo. For the factor CHANNEL, the ERS was strongest on channel Cz. For the factor TIME, the ERS at time t = 0 s was weaker than all other time points, and the ERS at time t = 0.5 s was stronger than at time t = 2.5 s. For the interaction TASK×CHANNEL, the strongest ERS during ME-Go appeared on channel Cz. There were no significant differences across channels during ME-NoGo. On channel Cz, the beta ERS was stronger during ME-Go than during ME-NoGo. For the interaction TASK×TIME, the beta ERS during ME-Go was stronger than during ME-NoGo between t = 1 and 2.5 s. The strongest ERS during ME-NoGo occurred at t = 0.5 s. For the interaction CHANNEL×TIME, the beta ERS was stronger on channel Cz than other channels between t = 0.5 and 2.5 s. For the interaction TASK×CHANNEL×TIME, significant differences between ME-Go and ME-NoGo occurred only on channel Cz, between t = 0.5 and 2.5 s.

ME-NoGo vs. MI-NoGo

For the factor TASK, the beta ERS was stronger during ME-NoGo than during MI-NoGo. For the factor CHANNEL, the ERS was strongest on channel Cz. For the factor TIME, the ERS was strongest at t = 1 s. The beta ERS at t = 1.5 s was stronger than at t = 0, 0.5, and 2.5 s. For the interaction TASK×CHANNEL, the beta ERS was stronger during ME-NoGo than during MI-NoGo on all channels. The beta ERS on channel Cz was stronger than any other channel during both ME-NoGo and MI-NoGo. For the interaction TASK×TIME, the beta ERS was stronger at time t = 1 s than at any other time point, during both ME-NoGo and MI-NoGo. The beta ERS during ME-NoGo was stronger than during MI-NoGo between t = 1 and 2.5 s. For the interaction CHANNEL×TIME, the beta ERS on each channel was strongest at t = 1 s. The beta ERS was stronger on channel Cz than in other channels between t = 1 and 2.5 s. For the interaction TASK×CHANNEL×TIME, the beta ERS during ME-NoGo was strongest on all channels at t = 1 s, with the maximum located on channel Cz. The beta ERS was also strongest on channel Cz at t = 1.5 and 2 s. All channels presented a strong beta ERS at t = 1.5 s, compared with time points t = 0, 0.5, and 2.5 s. During MI-NoGo, the strongest beta ERS occurred on channel Cz at t = 1 s. There were no differences across time in all other channels. The beta ERS during ME-NoGo was stronger than during MI-NoGo at t = 1 s on all channels, except lateral right. At t = 1.5 s, the beta ERS was stronger on channels lateral left and posterior. On channel Cz, the ME-NoGo beta ERS was stronger than the MI-NoGo between t = 1 and 2 s.

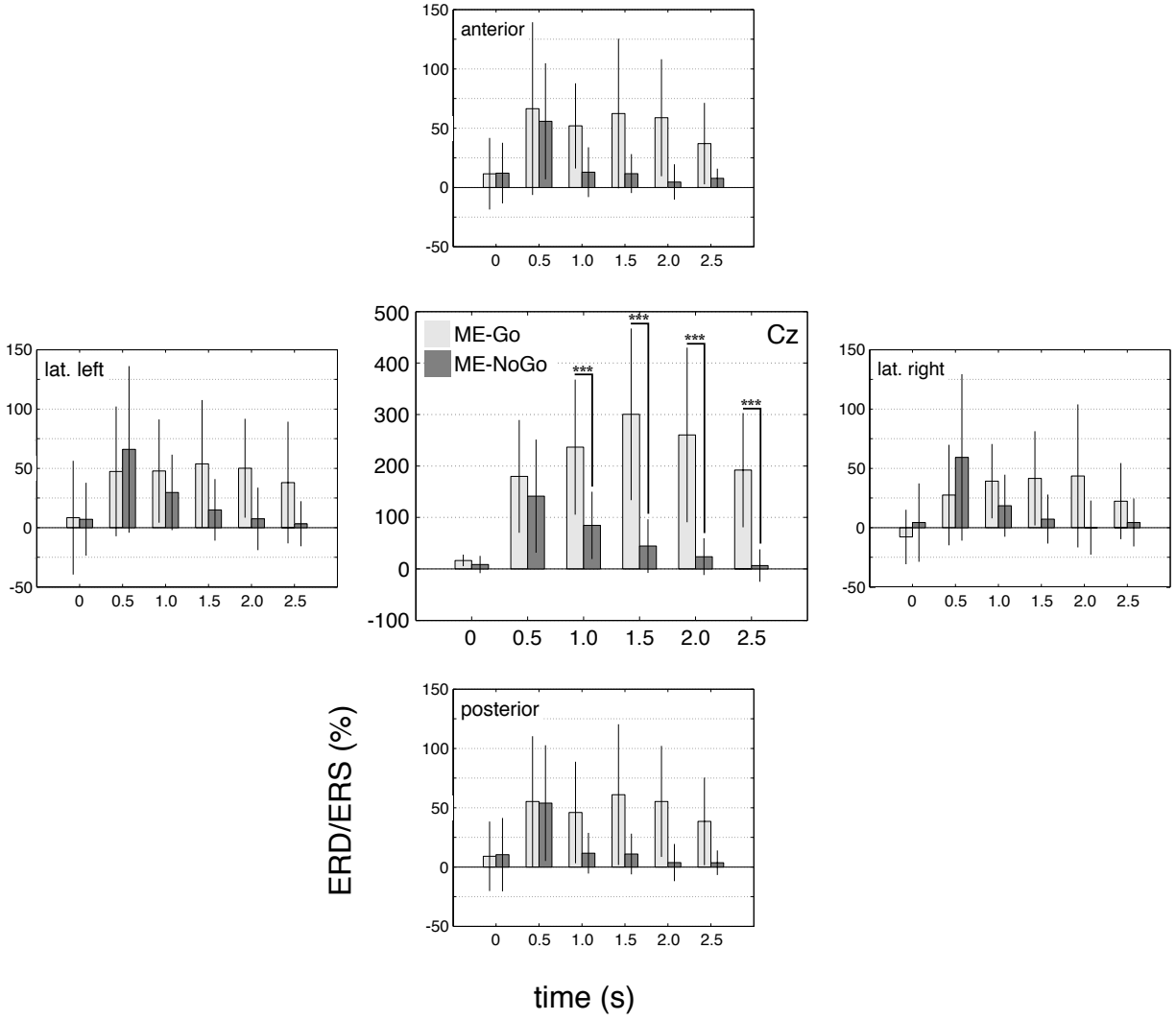

Figure 2.11: Execution and inhibition of foot movement. The post-movement beta rebound is shown in light gray, and the beta rebound during withholding of movement is shown in dark gray; vertical lines in the middle of each bar indicate the standard deviation. Thick black lines indicate significant differences. Statistically significant differences ($p < 0.001$) appear only in electrode position Cz. The beta rebound after the ME-Go cue (post-movement) is stronger and lasts longer than the beta rebound following the ME-NoGo cues (inhibition). There are no statistical significant differences between the two conditions in any other electrode position and during the first second (electrode Cz). Modified from [139].

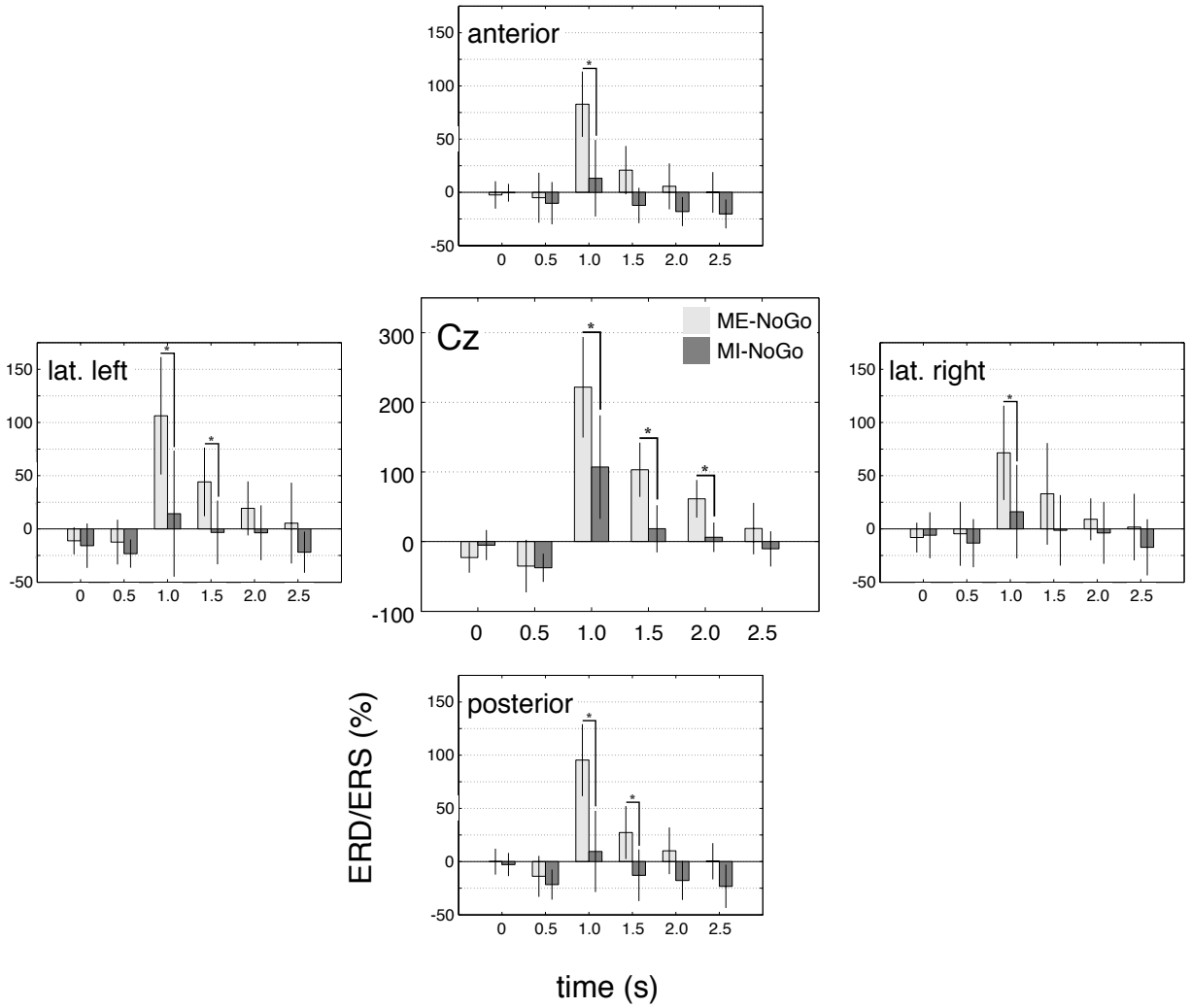

Figure 2.12: Inhibition of overt and covert foot movement. The beta rebound during withholding of overt foot movement is shown in light gray, and the beta rebound during withholding of covert foot movement is shown in dark gray; vertical lines in the middle of each bar indicate the standard deviation. Thick black lines indicate significant differences. Statistically significant differences ($p < 0.05$) appear in all electrodes between 1 and 1.5 s after the cue. In electrode position Cz, these differences continue until 2 s after the cue. The beta rebound after the ME-NoGo cue (withholding of overt movement) is stronger, more widespread, and lasts longer than the beta rebound following the MI-NoGo cues (withholding of covert movement). Modified from [139].

Findings

Our main findings show that the beta rebound is not only observed after motor execution [64, 66, 67, 76, 79–82, 85, 95, 103, 116–118], motor imagery [97, 124, 135, 136], action observation [107, 129–131], and other kinds of somatosensory stimulation [88, 90, 93, 104–106, 123–126], but also after withholding of overt and covert movements [120, 138, 139]. To our knowledge, we have compared for the first time the post-movement beta rebound with the beta rebound during withholding of foot dorsiflexion, and the beta rebound during withholding of overt and covert foot movement. Our results suggest that the magnitude of the beta rebound may depend on motor task preparation prior to cue onset. In other words, the active inhibition represented by the beta rebound may be stronger when the pre-activation of cortical areas is larger [65, 67, 121, 122].

The beta rebound following physical motor execution (ME-Go) has a larger magnitude than the beta rebound during withholding of movement (ME-NoGo), but only after the first second of recovery of the beta rhythm. To explain this observation, we assume that the ME-Go and the ME-NoGo beta rebound share a common functional meaning, at least within the first second, i.e. the active inhibition of neuronal networks activated during movement execution (ME-Go) and/or movement preparation (ME-NoGo). Besides the different processes that precede the beta rebound, there are other factors that should be further considered, namely, the re-afferent input after ME-Go, and the contributions of movement onset to the beta ERD/ERS [103].

The beta rebound during withholding of movement, i.e. in the NoGo condition, begins after an early beta ERD (power decrease around 500 ms after cue onset) and reaches its maximum around one second after cue onset. Although the responses to NoGo cues are similar for motor execution and motor imagery, withholding of motor execution presents a larger magnitude than withholding of motor imagery. This difference can be interpreted as the result of a more intense and/or widespread inhibition of neuronal networks for withholding the execution of physical movement.

No clear statement can be made about the origin of the midcentral beta rebound. In addition to the reduced topographic information of our study, whole head MEG recordings have shown evidence of an inter-participant variability of the sources of beta oscillations along peri-Rolandic areas [145]. Furthermore, the contributions of the foot representation area and the supplementary motor area can not be differentiated because of the close proximity of both areas [137].

Chapter 3

Asynchronous brain switch

A brain switch is a two-state BCI that differentiates between a specific brain state and any other mental state. In its asynchronous mode, the brain switch remains inactive during periods of rest or *non-intentional* control, and reacts only when the user performs a specific mental task, i.e. *intentional* control. This means that the brain switch is continuously available to the user, who decides freely when to activate the brain switch. Figure 3.1 illustrates the brain switch operation. In order to be practical, activations during non-intentional control must not occur. First reports on asynchronous brain switch began to appear around the year 2000, when several research groups presented system prototypes for asynchronous operation. Since asynchronous BCIs dismiss the use of external cues, exogenous BCIs were the first to support the continuous analysis of ongoing brain activity. Most brain switch designs rely on the detection of motor related brain phenomena, i.e. motor-related potentials [75, 146] and event-related (de)synchronization [8, 136]. Nevertheless, slow cortical potentials [147], steady state visual evoked potentials [148], and brain hemodynamics [54, 149] have also been used.

Even though many research groups are working towards out of the lab applications of asynchronous BCIs, most researchers target multi-class systems. However, it is not uncommon that multi-class BCIs operate under a *one vs. the rest* scheme, which can be regarded as a brain switch. Still, only a few groups work specifically on brain switch systems. Although binary classification has been extensively analyzed and standardized methods for performance evaluation exist, it is difficult to strictly compare the performance of different brain switch approaches because false activations are considered differently, and the non-intentional control is more prevalent that intentional control, contrary to the assumptions of performance evaluation methods. Interestingly, current brain switch systems attempt to provide near-zero false activations, prioritizing reliability over responsiveness.

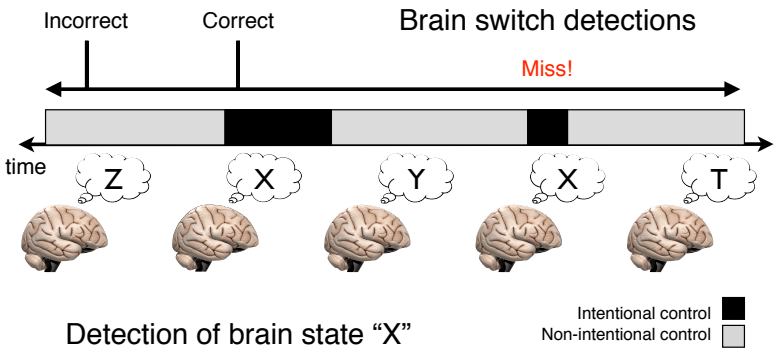

Figure 3.1: Brain switch operation. A brain switch identifies a specific brain state (**X**) from any other arbitrary activity(**T**, **Y**, or**Z**). In the example, the brain switch produces an impulse every time it detects brain state **X**, which is produced by the user at any time and for any lapse of time.

3.1 Detection of motor-related potentials

The low frequency asynchronous switch design

The first report of an asynchronous brain switch introduced the low-frequency asynchronous switch design (LF-ASD) [75]. The LF-ASD could identify the intention to perform an index finger flexion, based on frequency components of the EEG between 1 and 4 Hz. Such low frequency features correspond to the motor-related cortical potential (MRCP) that precedes a movement [150, 151]. Offline performance of the original LF-ASD showed a true positive rate[1] (TPR, the fraction of correct activations) that varied between 0.38 and 0.81, whereas the false positive rate (FPR, the fraction of false activations) ranged between 0.003 and 0.12. Online evaluation led to a similarly low FPR for the detection of real movements and the intention to perform imagined movements [152]. Since its introduction, the LF-ASD has reduced the number of false activations through several optimization steps such as normalization and dimensionality reduction [153], inclusion of temporal features [154], and parameter optimization [155]. The latest modifications to the LF-ASD include the addition of two supporting brain phenomena (modulations of the mu and beta rhythms) and a classifier ensemble [156, 157].

Beyond the LF-ASD, the Birch-Ward's group investigates the feasibility of a two-state BCI with different mental strategies [158, 159] (rest, multiplication, letter composing, 3D object rotation, mental arithmetic, sentence visualization, and motor imagery). These mental strategies are compared one vs. the rest, and the BCI is tuned to obtain a FPR equal zero and the highest possible TPR. Offline results from this approach show that the best mental strategies lead to an average TPR of 0.67 while maintaining a FPR equal to zero [159].

[1]Definitions of true positive rate and false positive rate are given in Section 3.4.

Brain switch designs based on motor-related potentials

The strategy from the original LF-ASD is similar to template matching. This idea forms the basis of several brain switch designs. Ongoing EEG is compared to a template of the MRCP by means of the cross-correlation, and the brain switch generates a detection event if the comparison exceeds a threshold. In the LF-ASD, the 1 to 4 Hz filter serves as template for the MRCP.

Detection of motor related potentials based on template matching was presented by Levine et al. [146] (see Figure 3.2(a)). Analyzing ECoG, the authors demonstrated that using this scheme it was possible to obtain an average TPR of 0.94 and FPR of 0.20. In an analysis of the original LF-ASD, Yom-Tov and Inbar [160] demonstrated the similarity between the LF-ASD and the template matching approach (see Figure 3.2(b)). Additionally, the authors improved the LF-ASD performance by including a feature extraction scheme that allows for variations of the MRCP template and evaluating different classifiers.

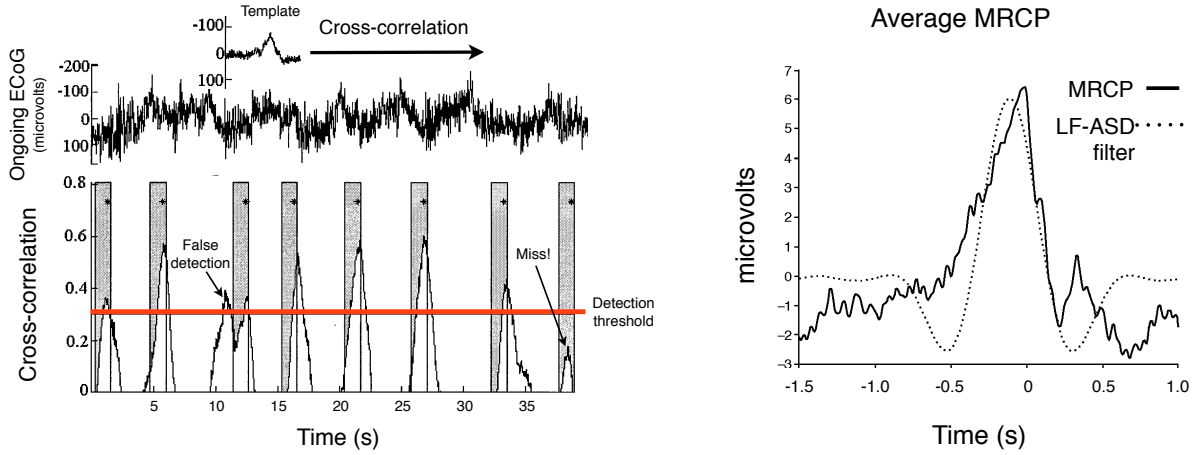

(a) MRCP template matching (modified from [146]).

(b) MRCP template (modified from [160]).

Figure 3.2: Template matching for detection of motor-related potentials. (a) Cross-correlation of ongoing ECoG and an MRCP template. (b) Similarity between the MRCP template and the low-pass filter from the LF-ASD.

A prototype system presented by Boye et al. [161] introduced an optimal spatial filtering algorithm to maximize the signal-to-noise ratio of the MRCP, and principal component analysis for dimensionality reduction [161]. The performance of the system achieved a TPR of 0.84 and an FPR of 0.01, evaluated offline with a single participant. Niazi et al. [162] developed this idea into a system for detection of MRCPs with an optimal spatial filter and template matching for detection. The authors demonstrated the online performance of their brain switch with a group of healthy persons performing overt and covert foot movements, and stroke patients attempting to perform foot movements. All experiments

were self-paced, without any external cues. For healthy persons the average TPR was 0.83 for motor execution (n = 15) and 0.64 for motor imagery (n = 10). For stroke patients it was 0.55 for attempted movements (n = 5). Instead of reporting FPR values, the authors counted the number of false activations (false positives) in a period of rest (non-intentional control) five minutes. This brain switch generated 1.38, 3.16, and 3.38 FP per minute, for overt and covert foot movement in healthy persons and attempted foot movements in stroke patients, respectively.

Instead of relying on template matching, the brain switch described by Hasan and Gan [163] uses a Gaussian mixture model to differentiate the non-intentional control period from motor onset, motor execution (wrist extension), and a post-movement period. The offline performance of this approach was reported by counting true and false activations from the intentional control epochs of a cue-paced experiment. The average TPR can be estimated to 0.89 and the FPR to 0.10.

3.2 Detection of event-related (de)synchronization

The asynchronous Graz BCI

Although most work from the Graz group is not defined as a brain switch, some of it presents a switch-like behavior. Early work focused on offline ERD detection from continuous ECoG [164], and simulations of an asynchronous BCI [165]. Graimann et al. [164] compared the template matching scheme with the detection of ERD from the ongoing ECoG (Figure 3.3). Across participants and four motor tasks, the average TPR was 0.97 and the FPR was 0.22 for the detection of ERD, in comparison with an average TPR of 0.93 and FPR of 0.35 for the template matching scheme. This findings highlighted the signal-to-noise ratio differences between ERD and MRCP. Townsend et al. [165] evaluated the inclusion of post-processing parameters (a threshold, a dwell time, and a refractory period) to transform a continuous BCI classification into control events (Figure 3.4).

Pfurtscheller et al. [136], presented an asynchronous BCI for online control of functional electrical stimulation (FES) for grasp restoration in a tetraplegic person. Later, Müller-Putz et al. [8] reported on the online control of an implanted neuroprosthesis (Freehand system [166]) in another tetraplegic person. Both BCI users were able to switch between the phases of a grasp sequence by imagining foot or hand movements. The methodology of the Graz group consisted on selecting the most discriminative features between two motor imagery tasks (cue-paced training), and training a linear classifier (Fisher's linear discriminant analysis) to distinguish between the two mental states. By adding a threshold, one of these two mental strategies can be identified against other arbitrary states or EEG at rest [167] (see Figure 3.5). This well established methodology has been used for online control of a virtual keyboard [168] and navigation of virtual environments [169, 170].

Regarding brain switch development, Leeb et al. [169] focused on the use of the asynchronous BCI to switch between stand and move phases, while exploring a virtual environment along a predefined path. The performance of the BCI was estimated to TPR

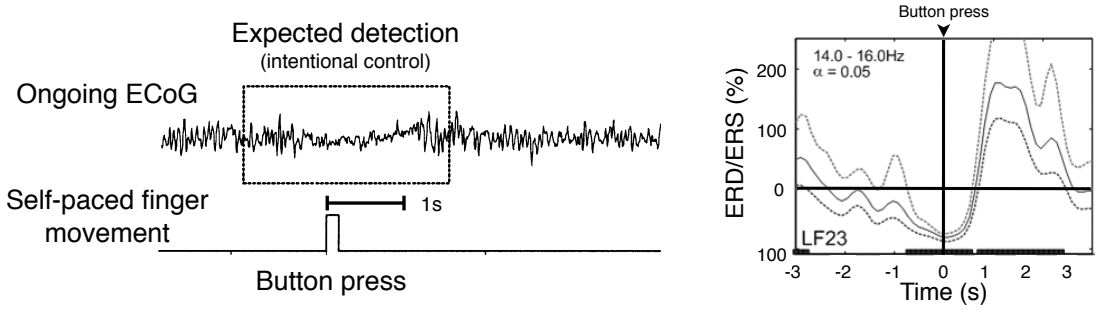

(a) Single trial ECoG (b) ERD/ERS

Figure 3.3: ERD detection from ongoing ECoG. (a) An amplitude decrease is observed around the button press. (b) Event-related (de)synchronization of ECoG during button press (dotted lines represent the confidence intervals $\alpha = 0.05$). Modified from [164].

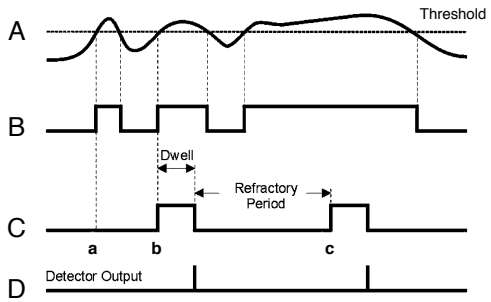

Figure 3.4: Post-processing parameters for asynchronous BCIs. (A) The classifier output is compared to a threshold (a). To generate an event, the classifier output must exceed the threshold for a dwell time (b). (C) After this, the classifier output is overridden during a refractory period (c). (D) The result is an impulse train that correspond to control events. Modified from [165].

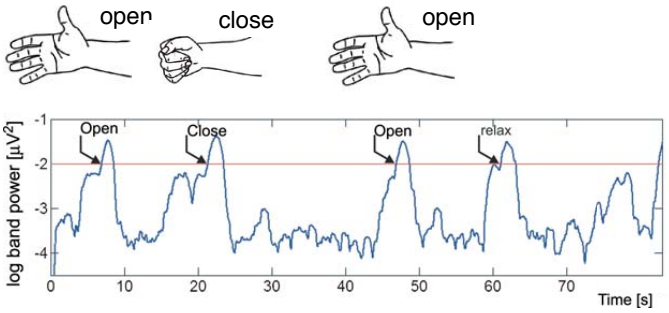

Figure 3.5: Neuroprosthesis control using a two-state BCI. Tetraplegic persons control a BCI to switch a FES neruoprotsthesis to open/close their own hands. Modified from [167].

0.23 and FPR of 0.04, where the special focus was the low FPR achieved online. Latest developments on the Graz asynchronous BCI include the introduction of *pulse width modulation* of the brain switch [171], to extend the number of commands that are available to the user with a two-state BCI, and the combination of a brain switch with other assistive technologies [29].

Other ERD/ERS-based brain switch

Other research groups have also developed BCIs based on ERD and ERS, but only a few have targeted the brain switch. Lauer et al. [172] presented an online system that allowed the users (two healthy persons and one tetraplegic person) to open/close a neuroprosthesis, by modulating the band power of a frontal beta rhythm (25 to 28 Hz). After 20 training sessions, the accuracy of the system was above 90 % in all cases. Heasman et al. [173] showed an online system that relied on the occipital alpha rhythm (8 to 13 Hz) of the users for the same task. TPR was around 0.70 and FPR below 0.10, for one tetraplegic user and one healthy person.

Relying on modulations of the mu and beta rhythms (8 to 30 Hz), Bai et al. [174] reported on the online prediction of movement from the EEG. The authors trained a BCI to differentiate between rest periods and preparation of movements of the right wrist of healthy participants. After a session of about 40 movements, the authors modeled the differences between these two phases. Then, in a validation run, a threshold was added to the classifier output to minimize the FPR (close to zero). In a final evaluation run, the system obtained a TPR close to 0.40, but the FPR was not reported. Previously, Bai's group investigated different combinations of features and classifiers for such a BCI [175]. Also from Bai's group, Qian et al. [176] recently presented a new paradigm for an asynchronous brain switch. The novel paradigm goes against the brain switch convention and provides the user with an external periodic cue, which the user is free to use or to ignore. If the user desires to activate the brain switch, he or she performs a mental task (imagination of thumb-index pinch) after every cue. The user must keep performing the mental task (synchronously) until the system provides a detection. The BCI averages the ERD/ERS from previous "epochs" to detect the user's intention. This strategy helps to improve the signal-to-noise ratio of the ERD/ERS features and to reduce false activations, at the expense of limiting the responsiveness of the system. Online evaluation of this system achieved an average FPR of 0.008, with an average response time of 37 s.

3.3 Detection of alternative brain phenomena

Slow cortical potentials – the thought translation device

Kaiser et al. [147] showed the self-paced initiation of the thought translation device (TTD), a spelling application for BCIs based on slow cortical potentials [4, 177]. In the original TTD, a user is trained to produce a negative or positive shift in the ongoing EEG. Contin-

uous feedback informs the user on the development of the slow cortical potential and, at the end of each trial, the TTD informs the user on the outcome. The work of Kaiser et al. [147] consisted on extending the TTD to include an on/off function. To volitionally switch on/off the spelling application, users produce a predefined sequence of ten potential shifts without continuous feedback. Two locked-in persons learned to self-initiate the spelling application following this control strategy. Performance from both users was above 84 % classification accuracy after several sessions, including user training and evaluation of the system. Two major points need to be noticed: (i) external cues about the start/end of the trial are still included, and (ii) a long sequence of commands is required. Although it is not a brain switch in the strict sense, it is worth considering this device and strategy because of its novelty.

Steady state visual evoked potentials

Steady state visual evoked potentials (SSVEP) provide one of the fastest information transfer rate among existing BCIs, but require focused attention on external stimuli and unintended activations often occur. Cheng et al. [148] developed a SSVEP-based BCI that operated in a self-paced mode, and included an on/off button between the BCI commands. The on/off button operated as a main switch for the system, enabling or disabling twelve other visual stimuli. To minimize the false activations of the SSVEP switch, a control command was generated only after the BCI detected two seconds of sustained visual attention on the on/off button. In online experiments, six out of seven participants needed between 3.9 and 7.5 s to turn on the BCI, and between 4.2 and 7.2 s to turn it off. Two additional participants were unable to control this brain switch, thus the BCI was turned on/off manually. Noteworthy, only the performance of the on/off stimuli is discussed here.

Hemodynamic responses

Coyle et al. [54] realized a brain switch based on hemodynamic responses using a custom built, one-channel fNIRS system and motor imagery. Although the system didn't operate in an asynchronous mode, it was the first fNIRS-based brain switch. In a two-class, cue-paced paradigm, the BCI presents a period when users are supposed to perform motor imagery and when to avoid doing it. After the two classes have been shown, the BCI selects the class with the largest oxyhemoglobin concentration change. In online, cue-paced experiments, the average classification accuracy was 82 %, the TPR was 0.72, and the FPR was 0.10.

Bauernfeind et al. [149] presented another fNIRS-based brain switch. This system operated online in an asynchronous mode. Included into a hybrid BCI, the fNIRS switch was used to turn on/off a SSVEP-based BCI, in a paradigm that required a specific control sequence [29, 178]. To start the experiment, a trained user operated the fNIRS-based BCI to turn on the second BCI (SSVEP). Next, the user controlled the SSVEP-based BCI in a given sequence. Finally, the fNIRS-based BCI turned off the second BCI. After four runs and parameter adaptation, the user achieved complete control over the hybrid system.

Both fNIRS brain switch used only one channel and a custom system, which could be developed into a portable system. There are three main differences between both fNIRS-based BCIs: (i) the two systems operated online, but only Bauernfeind's system operated in an asynchronous mode; (ii) brain activities were motor imagery and mental arithmetic; and (iii) Coyle's brain switch prompted the user to perform two mental tasks, whereas Bauernfeind's system relied on relative changes (from a baseline recording) and a threshold. The two systems are limited by the latency of hemodynamic responses.

3.4 Evaluation

Confusion matrix, true positive rate, and false positive rate

Assuming that a binary classifier assigns a class label equal to $+1$ to the intentional control and equal to -1 to non-intentional control, correct detection of intentional control is called true positive (TP), and correct detection of the non-intentional control is called true negative (TN). Consequently, incorrect activations are false positives (FP) and missed intentions are false negatives (FN). These events compose the confusion matrix

$$\mathbf{M} = \begin{bmatrix} \mathrm{TP} & \mathrm{FN} \\ \mathrm{FP} & \mathrm{TN} \end{bmatrix} \tag{3.1}$$

The confusion matrix fully describes the performance of a classifier [179]. In BCI research, $\mathbf{M}$ represents the correspondance between the user's intention and the BCI's detections [180].

It is usual to summarize the information from the confusion matrix into one or two values, for easy comparisons between classifiers or BCIs. These comparisons need to be carefully interpreted. When comparing classifiers or BCIs, special attention needs to be paid to the *chance agreement*, i.e. the performance of a random classifier. A random classifier assigns a random class label to every input. Furthermore, it assigns random class labels even if the same input is presented more than once.

The classification accuracy $\left(\mathrm{ACC} = \frac{\mathrm{TP+TN}}{\mathrm{TP+FN+FP+TN}}\right)$ is the most common way to present the performance of a classifier. It reports the overall performance by indicating the proportion of correct decisions made, and it is usually reported as a percentage. Theoretically, the chance agreement of a binary classifier is associated with a 50% classification accuracy, but depending on class prevalence, the classifier bias, and the number of training/testing patterns, the classification accuracy of a random classifier accuracy can be well above the theoretical value [181].

The true positive rate (TPR) and false positive rate (FPR) are another form of summarizing the confusion matrix. The TPR indicates the ratio of user's intentions correctly detected, and the FPR is the ratio between false detection and the total number of decisions from non-intentional control periods. The pair TPR and FPR is easily computed

from the confusion matrix as

$$\mathrm{TPR} = \frac{\mathrm{TP}}{\mathrm{TP} + \mathrm{FN}} \tag{3.2}$$

$$\mathrm{FPR} = \frac{\mathrm{FP}}{\mathrm{FP} + \mathrm{TN}} \tag{3.3}$$

In the particular case of brain switch evaluation, the main problem with TPR and FPR is the prevalence of classes and the number of total activations of the brain switch, specially when considering FPR because TN can be overestimated, causing the FPR to tend to zero.

Asynchronous operation of a brain switch in a cue-paced paradigm

Construction of a confusion matrix for evaluation of a brain switch faces several practical problems. First, the evaluation can be done sample-by-sample or event-by-event [165], i.e. counting correctly and incorrectly classified samples or single detection events. Since periods of non-intentional control are more common than periods of intentional control, the evaluation based on events is preferred because offers a smaller difference between class prevalences. Moreover, while brain switch activations can be either correct or incorrect, the correct detection of the non-intentional control does not generate brain switch activations; posing the problem of estimating the number of TNs.

TNs can be correctly estimated in a cue-paced paradigm, where the non-intentional periods are well defined. Hence, it is possible to continuously classify the EEG from a cue-paced paradigm for performance estimation. Additionally, it is possible to conduct a simulation of an asynchronous brain switch, preferably from runs without feedback. A variation of this is the evaluation of an asynchronous two-class BCI or a brain switch with *experimenter given* cues, where the paradigm is defined, and the experimenter guides the participants through its execution. An example of this type of evaluation can be found in [169]. Leeb et al. [169] completed an experiment where the participants were instructed to navigate a virtual environment through sustained motor imagery (hand vs. foot), with several stops along a predefined path. The participants knew beforehand where they were supposed to stop, and the experimenter informed them about the duration of the stops. A generalization of these methods can be described as the control of a benchmark application. This means that a simple application with a predefined timing can be used to evaluate the participant's control over the brain switch.

Self-report of the brain switch performance

Another way to evaluate the performance of a brain switch relies on the participants self-report of their own intentions [152, 182]. For example, the participant could confirm the correct detection of his/her intentions after every brain switch detection; failing to do so, would automatically generate a FP. Noteworthy, TNs are impossible to count in this way. One possibility is to indicate the intention to activate the brain switch, prior to the actual

brain switch detection. Nonetheless, the execution of a motor/cognitive task before the activation of the brain switch could lead to a misinterpretation of false activations, biasing the performance estimation. This type of evaluation is discouraged.

False positives per minute

False positives per minute (FP/min) offer a way to evaluate the reliability of a brain switch during the non-intentional control periods [156]. One way to estimate the FP/min consist on counting all false activations that appear during a run or the whole experiment. However, it is common to segment the data for offline analysis, and to discard contaminated epochs. In a better way to estimate the FP/min, the brain switch user is instructed to remain relaxed (rest with eyes open) for a certain period of time [162, 178]. FP/min is not restricted to the non-intentional control periods, it could also be computed from periods where intentional control is expected, e.g. if two or more activations occur when only one is expected. Nonetheless, a well designed paradigm is needed to differentiate TP from FP. The recommendation for evaluation of a brain switch is the combination of a benchmark application with inclusion of non-intentional control periods for estimation of the FP/min.

3.5 Overview

The majority of brain switch designs rely on non-invasive techniques and endogenous brain phenomena. Most of them are based on motor-related brain phenomena, but few other options have been explored. A brain switch might not result very attractive for fast communication and control applications. However, it is the simplest case of an asynchronous BCI and could be considered a *building block* for multi-class BCIs, as many of them operate under a one vs. the rest scheme. A brain switch could be combined with multi-class BCIs and other assistive technologies into a hybrid BCI. The number of sensors needed for on/off control is low, in comparison to multi-class BCIs, which is an appealing property for out of the lab applications. Some brain switch prototypes have been used to control a neuroprosthesis for grasp (open/close) and elbow (up/down) function, and to provide detection of movement intention (foot movement) in stroke patients, these are current BCI applications of growing interest. Performance evaluation is usually measured in terms of true and false activations, and it should be completed with the online control of a benchmark application that includes periods of non-intentional control, and the report of FP/min.

Chapter 4

Beta ERS-based brain switch

4.1 Detection of overt foot movement

Data description

We analyzed a database of EEG recordings from ten healthy persons (4 female, aged 24.6 ± 1.4 years). The EEG was recorded while the participants completed several runs of cue-paced motor tasks, including passive movement, motor execution, and motor imagery. Here we present the analysis of the motor execution runs only. Details about other experimental runs can be found elsewhere [124]. The EEG was recorded with sixteen Ag-AgCl electrodes placed on the scalp around electrode position Cz. Distance between electrodes was 2.5 cm. Reference and ground electrodes were attached to the left and right mastoid, respectively. The EEG was filtered between 0.5 and 30 Hz before digitalization. In all recordings, a notch filter at 50 Hz was on and the sampling rate was $f_S = 250$ Hz.

Cue-paced motor execution

The paradigm corresponded to cue-paced execution of foot movements. In the paradigm, a trial began when a fixation cross appeared on screen ($t = 0$ s). Two seconds later ($t = 2$ s) an arrow pointing downwards was displayed as a cue. Following the cue, the participants performed a *brisk* dorsiflexion of both feet, lasting about one second. The arrow disappeared from screen at $t = 3.25$ s, and the cross disappeared at $t = 6$ s. Afterwards, the screen displayed a blank screen until the end of the trial ($t = 7.5$ s) and during a random inter-trial interval (maximum duration of one second). Figure 4.1 illustrates the timing of a trial. Each participant completed three runs with 30 trials each, for a total of 90 movements. All runs were conducted on the same day with few minutes in between.

Spatial filtering and ERD/ERS maps

To improve the signal-to-noise ratio of the EEG, we computed a Laplacian derivation from five electrodes around electrode position Cz (see Figure 2.9 in Chapter 2). Data quality

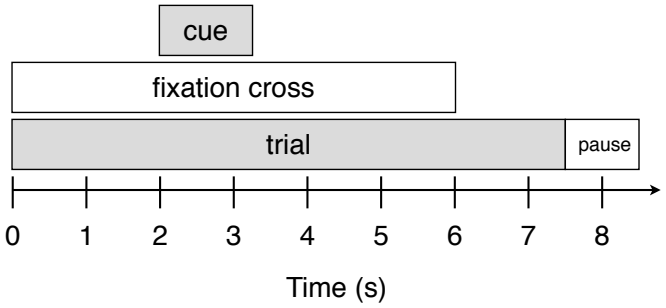

Figure 4.1: Paradigm timing for overt and covert foot movement. The trials in each run lasted 7.5 s plus a random pause with maximum duration of one second. Two seconds after the beginning of the trial, an arrow pointing downwards appeared as cue for the execution of brisk foot movement (dorsiflexion of both feet).

was visually inspected from the mean and standard deviation across trials. No artifacts were rejected or labeled for exclusion. ERD and ERS embedded in the Laplacian derivation were quantified with the inter-trial variance method and visualized with the computation of ERD/ERS maps [142]. We used Morlet[1] wavelets for the spectral analysis between 6 and 36 Hz (non-ovelapping bands of 2 Hz). Statistical significance ($p < 0.05$) was determined using a bootstrap algorithm. Reference interval for the relative power changes was between t = 0.5 and t = 1.5 s. The data from three participants was discarded for analysis due to lack of significant post-movement beta ERS.

Feature extraction

For our analysis, we considered trials of 10 s (t = -1 s to t = 9 s, relative to the onset of the fixation cross). Each trial was segmented in epochs of one second with 50 % overlap. A total of 29 spectral features were extracted from each epoch by means of the logarithmic band power (logBP), i.e. filtering the epoch, squaring every sample, and averaging across samples. These features corresponded to spectral components between 6 and 36 Hz. Each component had a bandwidth of 2 Hz, with an overlap of 1 Hz between consecutive components. Filtering was performed with a 62^{nd} order band-pass finite impulse response filter (FIR). In this way, an epoch yielded a feature vector with 29 logBP values.

The feature vectors were labeled twice for the independent classification of ERD or ERS against all other brain activity. Because ERD and ERS occur in slightly different frequency bands and at different times, they can be treated as mutually exclusive. On one hand, for the ERD-based classification, a *class +1* label was assigned to all feature vectors lying in the interval t = 2.5 s to t = 3.5 s. On the other hand, for the ERS-based classification, the class +1 label was assigned to all feature vectors in the interval t = 4 s

[1] According to an implementation of the ERD/ERS maps developed by Clemens Brunner (`clemens.brunner@tugraz.at`). An updated version can be found with the BioSig Toolbox [143].

to t = 5 s. In both cases, the *class −1* label was assigned to all feature vectors outside these intervals. Noteworthy, the feature vectors labeled as class +1 for ERD are labeled as class −1 for ERS, and vice versa. Figure 4.2 illustrates the labeling procedure for each trial.

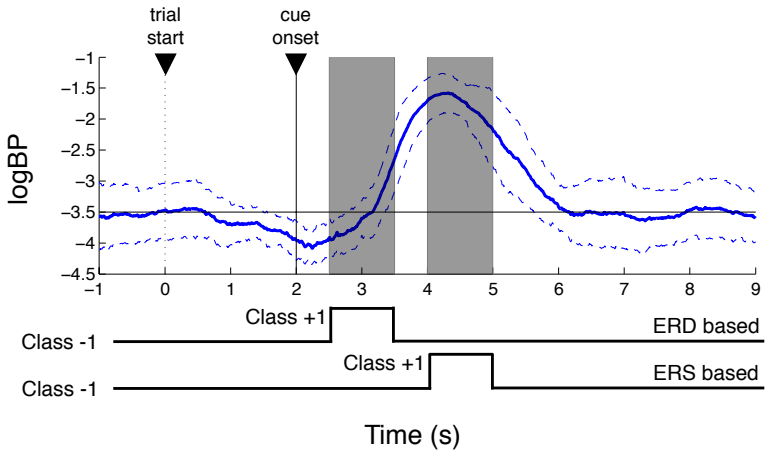

Figure 4.2: Labeling of feature vectors. The feature vectors extracted from each epoch were labeled twice for comparison of ERD- and ERS-based detection of foot movement. All vectors are considered as class −1, except those from the intervals t = 2.5 s to t = 3.5 s (ERD-based) or t = 4 s to t = 5 s (ERS-based), which where labeled as class +1. These windows are exclusive.

Classifier training

Support vector machines (SVM) with Gaussian kernels handled the classification of feature vectors. We used the library libSVM [183] in combination with the Matlab interface from BioSig [184] for the implementation of the SVM. Kernel parameters of the SVMs, i.e. the regularization factor C and the kernel width σ, were selected after an exhaustive search in a parameter grid. Inside the grid C varied from 2^{-10} to 2^{1} and σ varied from 2^{-15} to 2^{1}. These parameters doubled their value at each step inside the grid.

The three runs were shuffled before parameter selection. One run was kept apart for evaluation and the remaining two runs were assigned to training and testing phases (one run each). Training and testing runs entered the following iterative process:

1. Train a $\text{SVM}_{i,j}$ with a specific pair of parameters (C_i, σ_j) and the data from the training run, including a 10-fold cross-validation.
2. Test the $\text{SVM}_{i,j}$ with the data from the testing run. Obtain the confusion matrix and compute TPR and FPR. Summarize the performance of $\text{SVM}_{i,j}$ with the index $Y = \text{TPR} - \text{FPR}$.
3. Repeat from step 1 until all parameters (C_i, σ_j) have been tested.

The parameters (C_i, σ_j) associated with the highest value of the index Y were chosen. A SVM was trained with those parameters and the feature vectors from the training and testing runs. At this point, the SVM was also trained to predict the posterior probability of a new feature vector [185].

We carried out a parameter selection process for ERD and ERS independently. Only the Gaussian kernel was considered because it has been proved that when using this kernel with a complete parameter search, there is no need to test linear kernels [186]. The classifier training process was repeated six times in total, one time for each combination of training/testing runs.

Post-processing

The evaluation run, a run set apart before classifier training, was analyzed and classified continuously. Features vectors were computed from the first until the last second of EEG data, using a sliding window of one second with an overlap of 249 samples ($f_S = 250\,\mathrm{Hz}$). All consecutive feature vectors were fed to the pair of SVMs obtained for classification of ERD and ERS. This procedure corresponds to the simulation of an asynchronous brain switch. Figure 4.3 demonstrates the ERD and ERS classification. The output of each SVM indicated the probability of a feature vector to represent ERD or ERS, hence the classifier outputs represent P (ERD) and P (ERS), respectively. The probability output of the classifiers was further processed with a threshold (TH), a dwell time (DT), and a refractory period (RP) [165]. A receiver operating characteristics (ROC) analysis over TH revealed the best threshold for fixed values of $\mathrm{DT} = 250\,\mathrm{ms}$ and $\mathrm{RP} = 2\,\mathrm{s}$. We considered these parameters to allow the system to make fast decisions (DT) and to limit the number of detections during the intentional control windows defined for evaluation (RP). Figure 4.4 presents an example of post-processing of the classifier output.

Performance assessment

The commands of an asynchronous brain switch may happen at any moment, depending entirely on the user's intention. A simulation of an asynchronous brain switch from a cue-paced paradigm, provides a useful way to evaluate the capability of the brain switch to detect intentional and non-intentional control. Knowing when a brain switch activation is supposed to occur allows for the estimation of TPs, FPs, and FNs. Additionally, since the periods of non-intentional control are know, the estimation of TNs is also possible. In our assessment, a TP was counted if a brain switch activation (foot movement detection) occurred between $\mathrm{t} = 2.5\,\mathrm{s}$ and $4.5\,\mathrm{s}$ for the ERD-based classifier, and between $\mathrm{t} = 3.5\,\mathrm{s}$ and $5.5\,\mathrm{s}$ for the ERS-based classifier. All detections outside these windows were counted as FPs.

TPR and FPR were estimated from TP, FP, the expected total of true detections

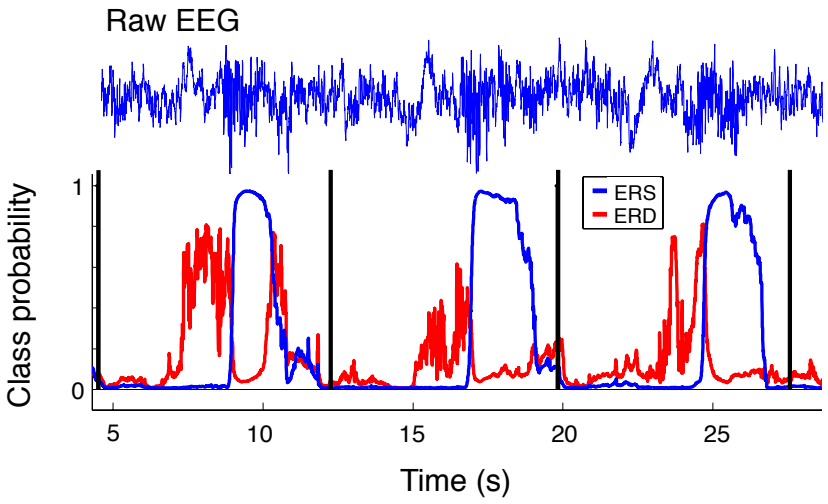

Figure 4.3: Simulation of an asynchronous brain switch. The validation run is analyzed to extract feature vectors from a 1 s sliding window. The feature vectors are fed to the SVMs, which predict the probability of a feature vector corresponding to ERD (red) or ERS (blue). Bursts of activity, the beta rebound, can be seen in the raw EEG (top). Black vertical lines indicate the beginning of individual trials.

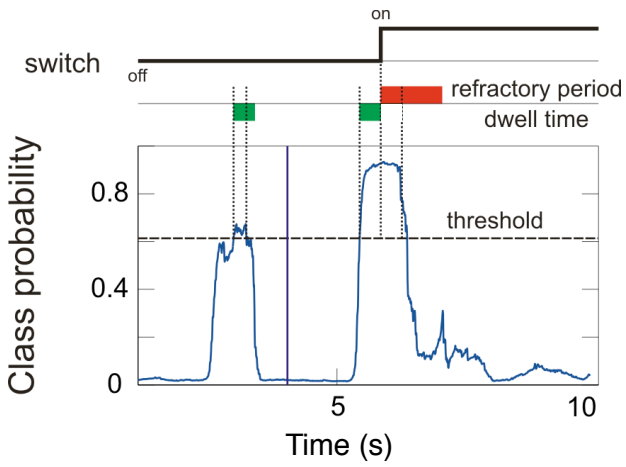

Figure 4.4: Post-processing of the classifier output. To generate detection events from the classifier output (blue), a threshold (dashed horizontal line), a dwell time (green squares), and a refractory period are used (red rectangle). A brain switch event occurs when the classifier output exceeds the threshold for a period of time given by the dwell time. After a detection, further events are suppressed during the refractory period.

$N_T = \mathrm{TP} + \mathrm{FN}$, and the maximum number of false detections

$$\mathrm{TPR} = \frac{\mathrm{TP}}{N_T} \tag{4.1}$$

$$\mathrm{FPR} = \frac{\mathrm{FP}}{N_F} \tag{4.2}$$

where N_T is equal to the number of trials, and N_F is the estimated count of possible events in the non-intentional control periods

$$N_F = \frac{\text{total number of samples}}{\lfloor f_S \times (\mathrm{DT} + \mathrm{RP}) \rfloor} \tag{4.3}$$

In this study, $N_T = 30$ and $N_F \sim 110$, due to the random duration of the inter-trial interval.

Combination of motor-related information

ERD and ERS are related to the execution of foot movement, therefore, it is reasonable to assume that combination of ERD and ERS features could improve the detection of foot movements. We combined the ERD and ERS information to try to minimize the number of false detections. The combination was based on the following assumptions:

- ERD is present in all foot movements.
- ERS follows ERD.
- Classification of ERD and ERS are independent.

These assumptions led to the computation of the joint probability as the product of independent probabilities

$$\mathrm{P}(\mathrm{ERD}, \mathrm{ERD}) = \mathrm{P}(\mathrm{ERD}) \cdot \mathrm{P}(\mathrm{ERS}) \tag{4.4}$$

where $\mathrm{P}(\mathrm{ERD})$ and $\mathrm{P}(\mathrm{ERS})$ are the output of the ERD- and ERS-based SVMs described above. Since co-occurrence of ERD and ERS is not considered, $\mathrm{P}(\mathrm{ERD})$ was delayed one second to match the $\mathrm{P}(\mathrm{ERS})$ events, before computing the product between classifier outputs. Figure 4.5 gives an example of the combination of classifiers. Foot movement detection with the classifier combination was completed with the additional post-processing parameters, and performance assessment described above.

Outcome

Figure 4.6 shows the TPR and FPR values obtained from each run combination per participant, and the participant individual average. Table 4.1 presents the individual averages and the grand average TPR and FPR for the classifiers under analysis. Detection of brisk foot movement based on ERD achieved an average TPR of 0.21 ± 0.12 and an FPR of 0.06 ± 0.06. The detection based on ERS achieved an average TPR of 0.74 ± 0.21 and

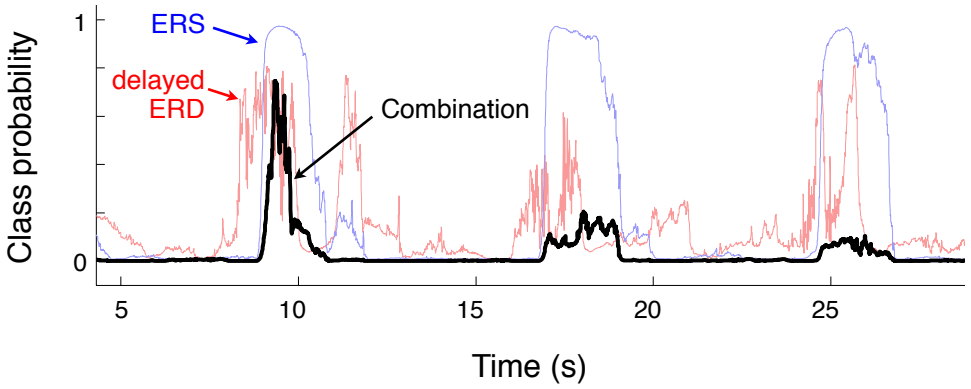

Figure 4.5: Combination of ERD- and ERS-based classifiers. The joint probability $P(ERD, ERD)$ is obtained from the individual classifier outputs $P(ERD)$ and $P(ERD)$. Before combining these two probabilities, the ERD-based classifier must be delayed to match the occurrence of the post-movement beta rebound. This figure can be compared to Figure 4.3.

an average FPR of 0.06 ± 0.03. Detection of foot movement based on the combination of ERD and ERS classifiers resulted in a TPR of 0.74 ± 0.20 and an FPR 0.06 ± 0.03. These results were obtained from the ROC analyses as the maximum TPR associated with an FPR ≤ 0.1, to show the best performance possible. The highest individual performance was achieved in all cases for ERS-based classification, although in some cases the classification based on the combination of ERD and ERS led to a slight performance improvement (a2, a3, a5, and a7). A two tailed t-test for repeated measurements applied to the results of each participant showed no significant differences ($p \geq 0.05$) between the combination of classifiers and the ERS-based classification.

We used a wide spectral description and no feature selection to let the SVMs learn the differences between intentional and non-intentional control from the EEG of each participant. The SVMs automatically adjust the decision border to the intra-subject variability, by assigning smaller weights to non-relevant features during the optimization of the decision boundary. This classification scheme showed a stable performance despite the lack of feature selection. Dimensionality of the feature vectors (29 features) did not represent a problem, but the parameter selection for the SVM was a time consuming task, and the number of feature vectors has to be controlled to avoid overfitting. It is important to notice that the same Laplacian derivation was used for all participants, and that the analyses were made without artifact selection. Furthermore, a unique set of features was used for every participant and only two runs are needed to find the parameters of the SVMs.

For the first time, information related to brain signal dynamics during and after movement were combined to improve the performance of single trial classification. Even though no significant differences were found between ERS and the combination of classifiers, it can be speculated that there is considerable potential of improvement if ERD and ERS are

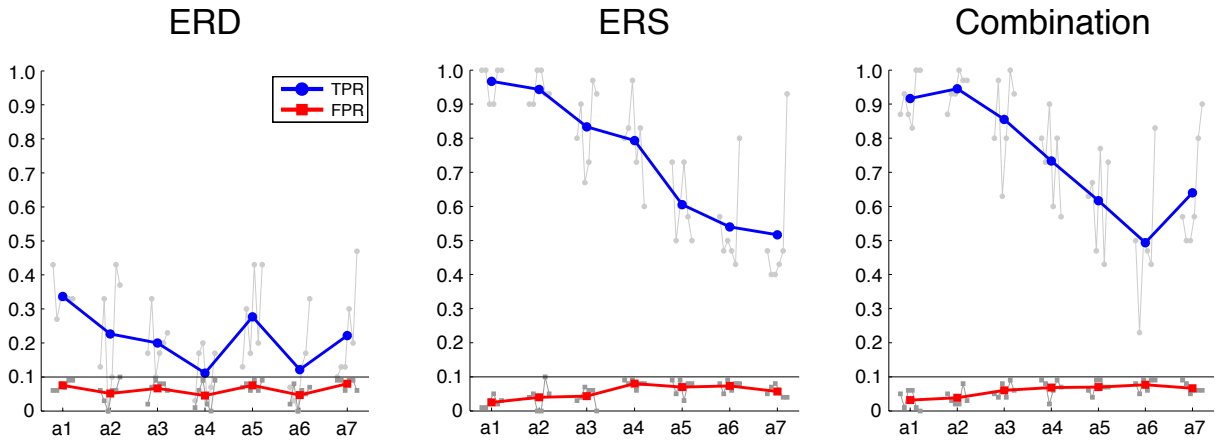

(a) (b) (c)

Figure 4.6: Detection of overt foot movement. (a) ERD-based classifier, (b) ERS-based classifier, and (c) Classifier combination. Performance of the individual evaluation folds is shown in gray. TPR is represented by circles and FPR is represented by squares. The horizontal black line marks the limit where FPR = 0.10.

Table 4.1: Participant average performance (overt foot movement)

ID	ERD				ERS				Combination			
	TPR		FPR		TPR		FPR		TPR		FPR	
	mean	s.d.	mean	s.d.	mean	s.d.	mean	s.d.	mean	s.d.	mean	s.d.
a1	0.34	0.05	0.08	0.01	0.97	0.05	0.03	0.02	0.92	0.07	0.03	0.03
a2	0.23	0.17	0.05	0.03	0.94	0.05	0.04	0.04	0.95	0.05	0.04	0.02
a3	0.20	0.08	0.07	0.03	0.83	0.12	0.04	0.03	0.86	0.14	0.06	0.02
a4	0.11	0.08	0.05	0.04	0.79	0.12	0.08	0.01	0.73	0.13	0.07	0.03
a5	0.28	0.13	0.08	0.01	0.61	0.10	0.07	0.02	0.62	0.14	0.07	0.02
a6	0.12	0.12	0.05	0.03	0.54	0.14	0.07	0.02	0.49	0.19	0.08	0.02
a7	0.22	0.14	0.08	0.02	0.52	0.20	0.06	0.02	0.64	0.17	0.07	0.02
mean	0.21		0.06		0.74		0.06		0.74		0.06	
s.d.	0.12		0.06		0.21		0.03		0.20		0.03	

successfully combined.

4.2 Detection of covert foot movement

Data description, experimental paradigm, and analysis

To further evaluate the use of the beta ERS for the realization of a brain switch, we analyzed a second database of EEG recordings. The data was collected from five healthy participants (3 female, aged 25.8 ± 2.9 years) during a cue-paced motor imagery experiment without feedback. During the experiments the participants were seated on a comfortable armchair about 1.5 m in front of a computer screen, in an electrically shielded room. The participants' task was the kinesthetic imagination of a brisk foot movement, similar to the movement described in Section 4.1. Before the experiment, the participants gave informed consent and were allowed to practice the motor task with real feet movement. All participants were familiar with hand and foot imagery but, only two of them had participated experiments with feedback. Electrode montage and amplifier settings were the same as described above. We applied the methods described in Section 4.1 for feature extraction, classifier training, post-processing, and performance assessment. Only ERD- and ERS-based classification was investigated. Combination of features was disregarded because no significant improvements were found before.

Performance

With all possible combinations of training/testing/evaluation, each run served twice for evaluation. Hence, the performance was estimated six times per participant. Figure 4.7 shows the individual TPR and FPR values obtained from every run combination per participant and the individual average. Table 4.2 shows the individual averages and the grand average TPR and FPR. By design, in all cases the FPR was less or equal to 0.10. The average TPR for detection of ERD was 0.28 ± 0.13 (FPR 0.08 ± 0.01) and the TPR for detection of the ERS was 0.59 ± 0.20 (FPR 0.07 ± 0.02).

In accordance with our previous analysis regarding motor execution, the ERS-based classifier performed better than the ERD-based classifier. For both overt and covert foot movement, the most dominant feature is the beta ERS, which appears as a strong broad pattern in the visualization of ERD/ERS. In contrast, the beta ERD is less pronounced and has a larger inter-participant variability (not shown). For covert movements, part of this variability is an effect of the timing for motor imagery, since it is difficult to exactly know when the imagery starts and it is not easy to repeat the motor task with the same time span every time, specially without online feedback. Such inherent variability could affect the training of the SVMs because errors may occur while labeling the training patters, due to the fixed latency and length of the labeling windows. Optimization strategies, e.g. identification of the most discriminant time points, could help to improve the SVM training and thus the classification performance too.

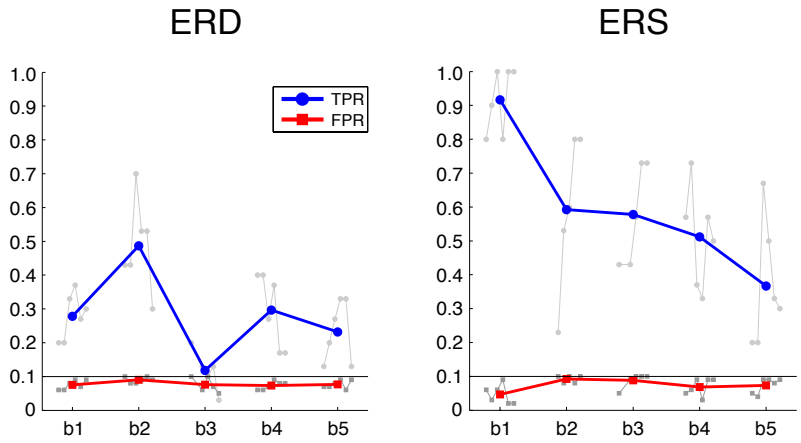

(a) (b)

Figure 4.7: Detection of covert foot movement. (a) ERD-based classifier and (b) ERS-based classifier. Performance of the individual evaluation folds is shown in gray. TPR is represented by circles and FPR is represented by squares. The horizontal black line marks the limit where FPR = 0.10.

Table 4.2: Participant average performance (covert foot movement)

ID	ERD				ERS			
	TPR		FPR		TPR		FPR	
	mean	s.d.	mean	s.d.	mean	s.d.	mean	s.d.
b1	0.28	0.07	0.08	0.01	0.92	0.10	0.05	0.03
b2	0.49	0.13	0.09	0.01	0.59	0.24	0.09	0.01
b3	0.12	0.06	0.08	0.02	0.57	0.14	0.09	0.02
b4	0.30	0.11	0.07	0.01	0.51	0.15	0.07	0.03
b5	0.23	0.09	0.08	0.01	0.37	0.19	0.07	0.02
mean	0.28		0.08		0.59		0.07	
s.d.	0.13		0.01		0.20		0.02	

4.3 Discussion

The analyses presented in this chapter demonstrate that the beta rebound (ERS) is a better feature than the ERD for the detection of overt and covert brisk foot movement. By selecting a fixed FPR limit ($\leq$0.10) we managed to obtain an average TPR of 0.74 ± 0.21 for detection of overt foot movement, and 0.59 ± 0.20 for detection of covert foot movement. Because of the relative stability of the beta rebound, its similarity during executed and imagined foot movements [112, 124], and the activation of similar cortical areas during overt and covert movement [187, 188], we propose that movement execution data may be suitable to train a classifier that could be applied to motor imagery data.

A limitation of using the beta rebound as feature for a brain switch is the time delay between an intended command and its detection. We estimated the information transfer rate of the ERS-based detection of overt foot movement to range between 8 and 18 bits/min (average ITR of 11 bits/min) [189]. It can be expected that the average ITR is maintained or improved after some training sessions with feedback. For operating complex applications, like a spelling device or an arm prosthesis, 11 bits/min is relatively low. However, such ITR is sufficient for simple switching tasks or for leisure. In this way, an acceptable ITR can be achieved after a few training runs, meaning that a working BCI could be set up very fast. The next chapter presents a methodology for setting up a brain switch relying on data from motor execution; thus, a brain switch for the able-bodied.

Chapter 5

A brain switch for the able-bodied

5.1 Methods

Data description

We analyzed the EEG recordings from nine healthy persons (3 female, aged 25.1 ± 0.9 years). Six participants were experienced with BCIs and motor imagery, including real time feedback sessions, but they were unfamiliar with our particular paradigm. The remaining three participants had no previous experience with motor imagery, BCI or similar experiments. EEG was recorded from five Ag-AgCl electrodes placed on the scalp around electrode position Cz, during cue-paced runs with motor execution and motor imagery without feedback. A single Laplacian derivation was computed from the multichannel EEG data. Amplifier settings were the same as described in the previous Chapter.

Experimental paradigm and analysis overview

Each participant completed three runs of cue-paced foot motor execution and another three runs of cue-paced foot motor imagery. One run consisted of 30 trials. All runs were completed on the same day, with several minutes in between. During the experiment, participants sat in comfortable armchair about 1.5 m in front of a monitor, inside an electrically shielded room. They were asked to perform a brisk foot movement, or its imagination, in response to a cue. Paradigm timing (Figure 5.1) was similar to the experiments described in Chapter 4 with two minor variations: (i) addition of an audible cue, and (ii) longer inter-trial pauses. At the beginning of the trial ($t = 0\,s$) a fixation cross appeared on the center of the screen. Two seconds lated ($t = 2\,s$), a beep (1 kHz tone, with a duration of 70 ms) and an arrow pointing downwards served as cue for the motor task (motor execution or motor imagination). The arrow remained on screen for 1.25 s ($t = 3.25\,s$). At the end of the trial ($t = 6\,s$) the cross disappeared. Participants observed a blank screen in between trials, during a short pause with a random duration between 1.5 and 3 s.

The analysis of the data was divided into synchronous and asynchronous processing. In the synchronous phase, two SVMs were trained with the data from the motor execution

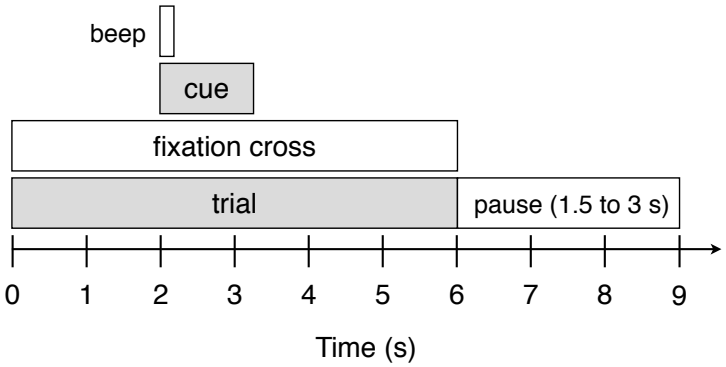

Figure 5.1: Paradigm timing. The timing of a trial is similar to that of Chapter 4. Minor differences include: (i) addition of an adible cue (beep), (ii) reduction of the trial duration, and (iii) extension of the inter-trial interval.

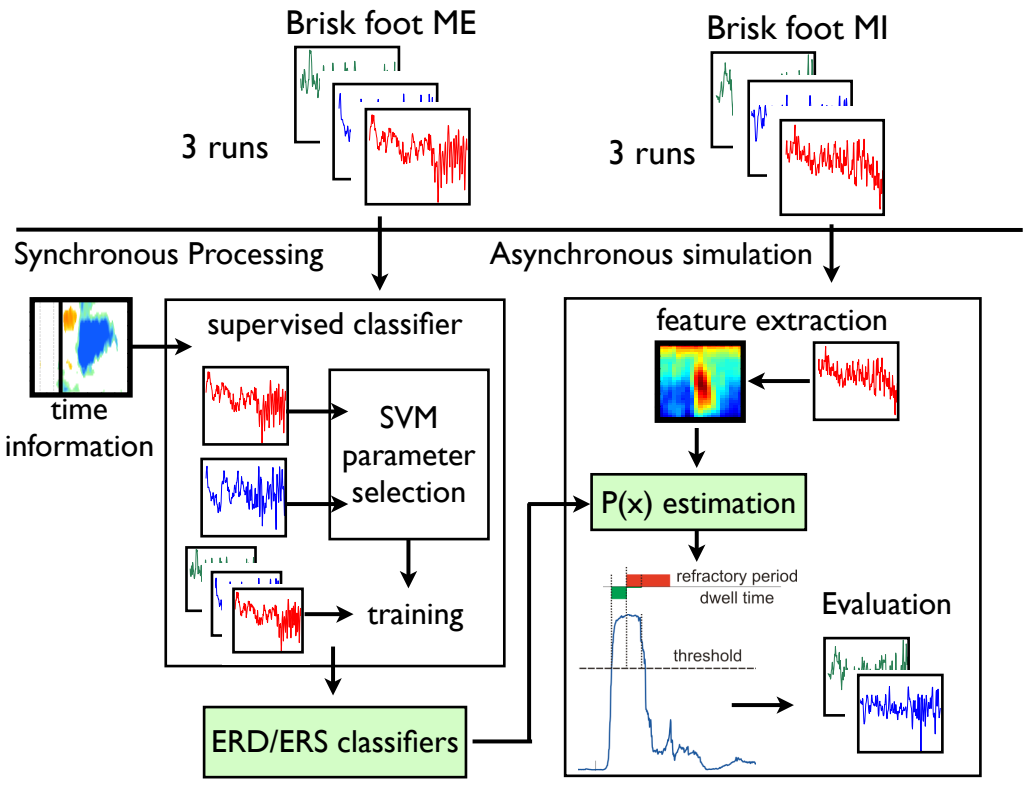

Figure 5.2: Analysis overview. The analysis is divided into a synchronous and an asynchronous phase. In the synchronous phase, a pair of SVMs are trained to detect foot movements based on ERD or ERS. In the asynchronous phase, post processing parameters are setup from a single run of motor imagery, and a simulation of an asynchronous brain switch is conducted. Modified from [190].

runs, according to the methods presented in Chapter 4. Each SVM was trained to classify either ERD or ERS against other brain activity. Labeling of feature vectors was adapted for each participant using the information from ERD/ERS maps computed from the motor execution runs. In the asynchronous phase, the post-processing parameters DT, TH and RP were obtained from the first motor imagery run. Then, a simulation of an asynchronous brain switch was performed with the remaining two motor imagery runs. Figure 5.2 gives an overview of the methods. Synchronous and asynchronous processing are described in detail below.

Synchronous processing

Labeling of feature vectors

Labeling of feature vectors was customized to the ERD/ERS patterns of each participant. We computed an ERD/ERS map for each participant using the data from the motor execution runs. Again, sinusoidal wavelets were used to assess changes in the frequency domain, and a bootstrap algorithm revealed statistically significant changes ($p < 0.05$). The maps analyzed the frequencies between 6 and 40 Hz and the interval between $t = 0$ and $t = 7$ s, relative to the beginning of the trial. The reference interval for ERD/ERS calculation was between $t = 0.5$ and $t = 1.5$ s. We identified the time intervals with the largest, significant ERD or ERS from the ERD/ERS maps. The periods selected were regarded as intentional control period. Three constraints were imposed to the selection of the intervals:

- Only patterns between $t = 2.5$ s and $t = 6$ s were considered.
- ERD patterns may precede ERS patterns, but not the other way around.
- ERD duration is restricted to one second.

Feature extraction

Features were extracted from the motor execution recordings according to the methods described in the previous Chapter, i.e. 29 logBP features between 6 and 36 Hz (2 Hz bandwidth with 1 Hz overlap), extracted using a set of 62^{nd} order band-pass FIR filters, and applying a moving average filter of one second length (250 samples). Each trial was segmented in epochs of length one second with 50% overlap. Feature labeling was done separately for each participant. In this case, the class +1 window was selected individually for each participant as described above. All patterns outside these windows were labeled as class -1.

Classifier training

After labeling the segments from all trials from the motor execution data, one of the runs was chosen randomly to train a SVM with a specific set of parameters for the Gaussian kernel. This classifier was tested with one of the remaining motor execution runs, and the

performance was measured with the TPR and FPR. The procedure was repeated in an iterative manner during an exhaustive search for parameters C_i and σ_j.

The parameters that achieved the maximum TPR and the minimum FPR were selected for the next phase. Note that there was no limitation on the FPR, contrary to the FPR ≤ 0.10 constraint imposed in Chapter 4. In the case of a tie between two or more parameter pairs (C_i, σ_j), the pair that included the smallest regularization parameter C was chosen. During training of the SVMs, a small C penalizes less the misclassification of feature vectors close to the separation hyperplane, thus offering a *softer* margin and improving generalization. The winning parameters were used to train a SVM using all feature vectors from the three motor executions runs. These SVMs were trained to predict the posterior class probability of each new feature vector. Classifier training was carried out for ERD and ERS independently. After the classification procedure, the data from one participant was discarded because the performance was close to random (ERD: TPR = 0.28, FPR = 0.22; ERS: TPR = 0.17, FPR = 0.15).

Asynchronous processing

Post-processing parameters (calibration)

The first recorded run of foot motor imagery was continuously classified by the SVMs trained on the motor execution data. The motor imagery run was described with the same 29 logBP features with one-sample shift for consecutive feature vectors. All feature vectors were fed to the classifiers and two output signals were obtained, namely the ERD and the ERS posterior probabilities. This processing corresponds to the continuous classification of the motor imagery run, i.e. the simulation of an asynchronous brain switch.

A ROC analysis determined the optimal values of the post-processing parameters TH, DT and RP. Parameter TH varied from 0 to 1 in steps of 0.01. The parameter DT took the values 25, 50, 62, 75 and 100 samples. Larger values (up to 200 samples) were tested in a preliminary study but the results showed no improvement. RP was computed according to DT + RP = $2 \times f_S$. For continuous processing, the intentional control period was extended to t = 2 s to 4 s for ERD, and t = 3 s to 4 s for ERS. Noteworthy, the ERD interval include the time of the cue and the beep (t = 2 s). Feature vectors around t = 2 s were labeled as *class −1* during training, because the cue is shown always at the same time and the participants could start preparing themselves for the motor imagery. Thus, early ERD due to motor preparation could be detected.

Classification performance was estimated for every combination of TH, DT, and RP. TPR and FPR were used for performance evaluation. In this analysis, the maximum number of false detections N_F = FP + TN was estimated from

$$N_F = \sum_i \left\lfloor \frac{NS_i}{\mathrm{DT} + \mathrm{RP}} \right\rfloor \tag{5.1}$$

where NS_i corresponds to the number of samples outside the detection window for trial i; all values are given in samples. The parameters TH, DT and RP that lead to the maximum

TPR, subject to the condition FPR ≤ 0.10, were chosen for further analysis.

Asynchronous simulation

The remaining two motor imagery runs were described with the same logarithmic band power features and classified by the motor execution-trained SVMs. The post-processing parameters were included, and the performance was measured with the TPR and FPR. This process was equivalent to the simulation of an asynchronous brain switch.

5.2 Results

Figure 5.3 presents the results for the ERD-based classification, and Figure 5.4 presents the results for the ERS-based classification. Please refer to Table B.1 and Table B.2 (Appendix B) for the individual TPR and FPR values of each participant. The average TPR for ERD-based classification was 0.52 ± 0.20 and the FPR was 0.14 ± 0.07, during the training phase (motor execution). For ERS-based classification, the average TPR was 0.63 ± 0.17 and the FPR was 0.11 ± 0.05, in the same phase. Contrary to the results presented in the previous chapter, there were no significant differences between ERD- and ERS-based classification (t-test, $p > 0.05$ for TPR and $p > 0.05$ for FPR). We attribute this result to the use of participant specific windows for the labeling of feature vectors. No significant differences (t-test, $p > 0.05$) were found during the calibration of post-processing parameters either. Average TPR values were 0.32 ± 0.22 and 0.51 ± 0.28 for ERD- and ERS-based classification, respectively. FPR was restricted to be less or equal to 0.10.

In the evaluation phase, the average TPR was 0.27 ± 0.19 for ERD-based classification, and 0.46 ± 0.26 for ERS-based classification. Average FPR was 0.11 ± 0.03 and 0.11 ± 0.05 for ERD- and ERS-based classification, respectively. There were no significant differences between the two approaches for neither for TPR (t-test, $p > 0.05$) nor FPR (t-test, $p > 0.05$) estimations.

Table 5.1 indicates, for each participant, which neurophysiological phenomenon is associated with the highest performance (TPR) during motor execution (training) and motor imagery (calibration and evaluation). This table also shows the segment where the class +1 label was assigned during training, and the parameters TH and DT from the calibration phase, also used during evaluation. Six out of eight participants achieved a better performance with the ERS-based classifier during the classifier training phase (motor execution runs). During the simulation of an asynchronous BCI, it was not possible to select one particular phenomenon for participants c7 and c8. In four from the remaining six participants, the ERS-based classifier performed better than the ERD-based classifier. Overall, the threshold was set around 0.3 (median 0.22) and the dwell time was longer than 250 ms (median 350 ms).

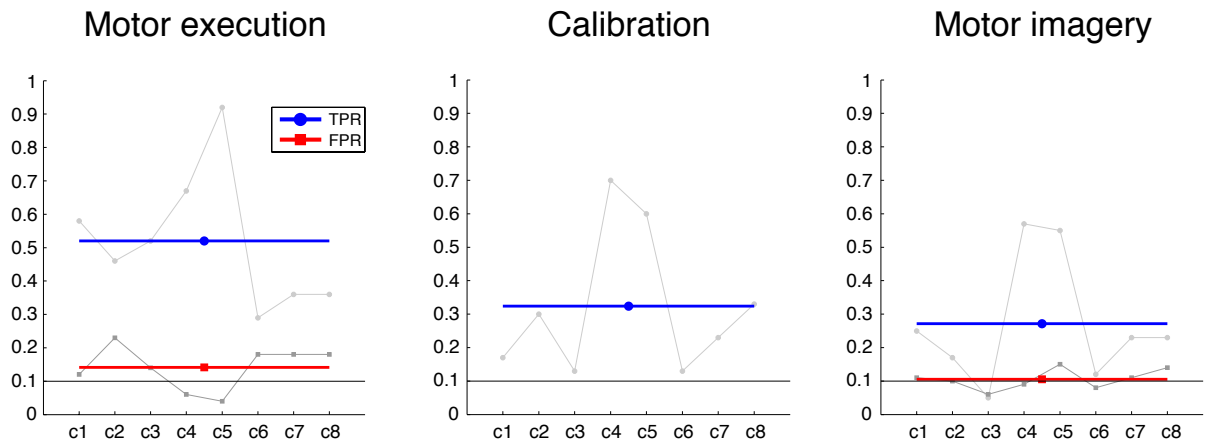

(a) (b) (c)

Figure 5.3: ERD-based classification results. (a) Training phase with motor execution data, (b) calibration phase with data from the first motor imagery run, and (c) evaluation phase, i.e. simulation of an asynchronous brain switch. A horizontal black line indicates 0.10.

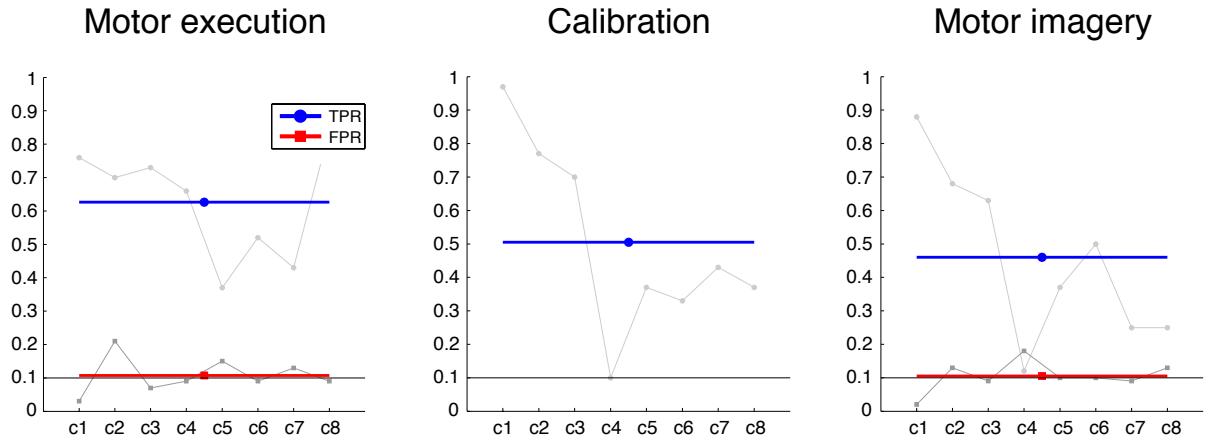

(a) (b) (c)

Figure 5.4: ERS-based classification results. (a) Training phase with motor execution data, (b) calibration phase with data from the first motor imagery run, and (c) evaluation phase, i.e. simulation of an asynchronous brain switch. A horizontal black line indicates 0.10.

Table 5.1: Physiological phenomena and post-processing parameters

ID	Training			Calibration & Evaluation		
	Phenomenon	Labeling window (s)		Phenomenon	DT (ms)	TH $\left(P_{(x)}\right)$
c1	ERS	4	5	ERS	300	0.24
c2	ERS	3.5	4.5	ERS	248	0.22
c3	ERS	3	4	ERS	400	0.15
c4	ERD	5	6	ERD	248	0.66
c5	ERD	4	5	ERD	400	0.56
c6*	ERS	4.5	5.5	ERS	300	0.15
c7*	ERS	3.5	4.5	–	400	0.29
c8	ERS	4	6	–	400	0.22

Naive participants marked with an asterisk (*).

5.3 Discussion

This chapter shows that a brain switch can be implemented by training a classifier with motor execution data, and then, applying it directly to motor imagery with only a minor calibration. This approach proved to be successful because both motor tasks (execution and imagery) result in similar ERD/ERS patterns, as expected. To use a classifier trained with motor execution on motor imagery data can be seen as a measurement of similarity between the patterns of both motor tasks. Hence, if the patterns differ significantly, the classification performance degrades. The results in Table 5.1 suggests that, when comparing motor execution to motor imagery, the post-movement ERS is more stable than the peri-movement ERD.

ERD/ERS pattern reshaping comprises frequency shifts and increments/decrements of the time/frequency span. For the particular case of post-movement ERS, those changes may be present in harmonic frequencies too, because the EEG can present a characteristic arc shape during the beta rebound. Frequency shifts could result from adjustments of the somatosensory and motor cortex during covert movement, specially for the beta ERS, when different neural networks may be responsible for its generation. The same principle applies to the increment/decrement of the frequency spread, while time span changes could result from variations in the duration of the motor imagery. The lack of somatosensory input and the inexperience with kinesthetic imagery, influences the activation of the neural networks involved in motor execution. Being unable to activate a specific motor related neural network impacts the generation of ERD patterns, and the subsequent inhibition of such network and the post-imagery ERS.

Another naive participant, c6, presented a stable ERS-based classification, meaning that the beta ERS from motor execution and motor imagery was similar between motor tasks. Most interesting is the case of participant c7, also naive, which presented a similar performance with both ERD- and ERS-based classifiers (motor imagery), even though the

ERS-based classification was better during motor execution. The rest of the participants were experienced with BCIs, meaning that they were able to produce ERD/ERS patterns with motor imagery. Similarity between execution and imagery related ERD/ERS patterns was not tested before on those participants.

In comparison with the previous chapter, the selection of an optimum window for labeling of feature vectors helped to reduce the gap between ERD- and ERS-based classification. No significant difference was found between ERD- and ERS-based classification for synchronous or asynchronous processing.

Since the design of the brain switch is based on motor execution, this methodology could not be used to create a brain switch for severely disabled patients. It is instead, a simple way to train a BCI for applications controlled by healthy users. However, it would be possible to obtain data from attempted movements or even through passive movements, possibly for clinical applications for persons with stroke, spinal cord injuries, or in a minimally conscious state.

5.4 Toward online operation

The offline analyses described so far rely on a full description of the EEG's power spectrum and a SVM to detect the beta rebound following a brisk foot movement, or its imagination. Labeling of training patterns in Chapter 4 considered only the timing of the training paradigm. Such strategy is suboptimal because the individual time span of the ERD/ERS patterns is not examined. In this chapter, individual differences were inspected, and participant-specific labeling was carried out. Such simple refinement reduced the difference between ERD- and ERS-based classification, by improving the performance of both classifiers.

One further improvement to our methods is feature selection. Until now, the SVMs dealt with a feature set that contained both relevant and irrelevant features. As discussed above, frequency shifts of the ERD/ERS patterns influence the performance of the brain switch. If a relevant feature changes from the training to the testing set, or in this case from execution to imagery, the classifier's performance will change. Identification of relevant features, i.e. feature selection, could cope with this problem. Moreover, reduction of the feature set would make the use of SVMs unnecessary and simpler, linear classifiers could be used. Additionally, training a SVM is a time consuming task that presents an obstacle for a quick setup of a brain switch. This section describes the comparison between the methods from this chapter and a similar analysis including feature selection and a Fisher's linear discriminant analysis (LDA) [179] instead of the SVMs.

Analysis

We analyzed the data presented at the beginning of this chapter once again, centering our analysis in the post-movement beta ERS. Feature extraction was repeated with a set of 5^{th} order Butterworth filters, to obtain a similar set of 29 logBP features extracted from

motor execution data. Each trial was segmented in epochs of length 0.5 s without overlap. We changed the labeling of training patterns in preparation for feature selection. First, we considered class -1 to match the reference interval for the ERD/ERS map computation (between $t = 0.5$ and $t = 1.5$ s). Then, any training pattern outside the reference interval was considered as class $+1$.

The most discriminative time intervals (segments) and features were revealed by a DSLVQ analysis [191]. In an iterative way, features from a given time interval were compared against the features from the reference interval and, ranked according to their discriminability. The most discriminative features corresponding to the beta rebound were clustered into broader bands. A clustering algorithm found the most discriminative time interval for each feature and its matching ERD/ERS value. Only features with significant ERD/ERS were considered. Features were merged if they differed at most in 2 Hz and if their associated time segments were at most 1 s apart from each other. Merging of features continued until no further merging was possible.

Once a frequency band was selected, a single logBP feature was computed from the motor execution data. Trials were segmented again in epochs of length 0.5 s without overlap. The epochs were labeled as described above. The most discriminative time interval was found by evaluating an LDA classifier with the features from each segment against the reference interval. We use Cohen's kappa (κ), estimated from a 10×10 cross-validation, as discrimination index. The segment with the highest κ was identified. An LDA was computed with the training patterns from the most discriminative time interval and the reference interval. The computation of post-processing parameters (calibration) as well as the simulation of an asynchronous BCI (evaluation), were repeated as described above. These methods are based on the standard methods from the Graz BCI group, which have been modified to include the automatic selection of features and the post-processing parameters.

Results and discussion

Figure 5.5 presents the classification performance of the different analysis stages (training, calibration and evaluation). Please refer to Table B.3 in Appendix B for the individual TPR and FPR values of each participant. Although our analysis focused on the beta rebound, participant c4 did not present a post-imagery ERS, therefore, the classifier was trained with features corresponding to a peri-imagery ERD. The average TPR during training was 0.92 ± 0.07, significantly higher than the ERS-based classification presented above ($p < 0.001$). The average FPR was 0.24 ± 0.11, also significantly higher than previous results for ERS-based classification ($p < 0.05$). After calibration, the classification performance between LDA and SVM leveled ($p > 0.05$ for TPR). At this stage, the LDA achieved a TPR of 0.49 ± 0.25, while FPR was kept below 0.10. Remarkably, the performance was maintained between calibration and the evaluation stage with both classifiers. For the simulation of an asynchronous brain switch (evaluation), the average TPR was 0.51 ± 0.20 ($p > 0.05$) and the average FPR was 0.08 ± 0.03 ($p > 0.05$).

Table 5.2 list the parameters from the feature selection and calibration phases. As

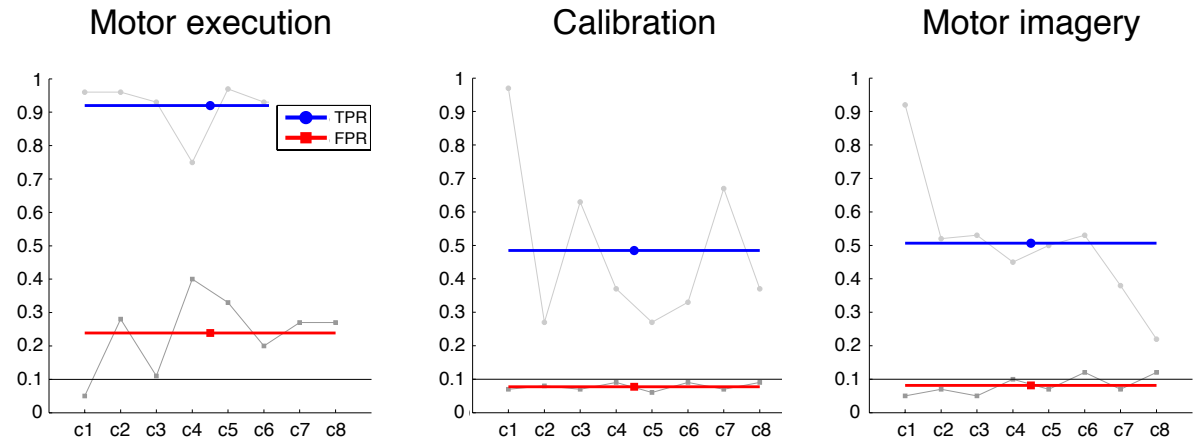

Figure 5.5: LDA-based classification results. (a) Training phase with motor execution data, (b) calibration phase with data from the first motor imagery run, and (c) evaluation phase, i.e. simulation of an asynchronous brain switch. A horizontal black line indicates 0.10.

mentioned before, ERS was used as neurophysiological phenomena for seven out of eight participants. The DT was again longer than 250 ms with median 300 ms. Direct comparisons of the TH parameter are not possible, because the SVMs computed a probability between 0 and 1, whereas the LDA computes a distance between $-\infty$ and $+\infty$.

Summarizing, both schemes presented in this chapter are equivalent. The inclusion of feature selection in our training scheme allows for the use of a simpler classifier, i.e. LDA. Classifier raining is completed faster for LDA than for SVMs, even though a series of DSLVQ analyses are necessary. Another boost on the setup of the brain switch, is the selection of the beta ERS as supporting neurophysiological phenomena. Focusing on the beta ERS reduces the feature space where DSLVQ must be applied. These results indicate that it would be feasible to set up an asynchronous brain switch for naive able-bodied persons, after a short time, with only a few repetitions of foot movement.

With a similar approach, Müller-Putz et al. [182] reported on the *fast and easy* setup of a brain switch, and its online operation through motor imagery. Six healthy persons completed a session of cue-paced foot movement, while their EEG was recorded from a single Laplacian derivation over Cz. After computing ERD/ERS maps, the authors selected a participant-specific frequency band to train an LDA classifier. During training, the overall classification accuracy was 91.8%. Then, four of the six participants completed a session of cue-paced motor imagery, with online feedback provided by the LDA trained with motor execution. The online classification accuracy was 68.8%, close to a chance agreement. EEG data recorded from the feedback sessions was used to update the classifier, defining a second participant-specific frequency band, and retraining the classifier. The improved

Table 5.2: Physiological phenomena and post-processing parameters (LDA)

ID	Training				Calibration & Evaluation		
	Frequency band (Hz)		Labeling window (s)		Phenomenon	DT (ms)	TH
	f_1	f_2					
c1	15	20	5.5	6.5	ERS	400	0.43
c2	26	30	5	6	ERS	100	0.78
c3	18	25	4	5	ERS	248	0.68
c4	26	31	4.5	6	ERD	300	0.60
c5	15	19	6	7.5	ERS	100	0.84
c6*	21	26	6	7	ERS	400	0.41
c7*	9	11	5	6	ERS	300	0.69
c8	19	23	6	7	ERS	300	0.54

Naive participants marked with an asterisk (*).

classification accuracy went up to 80.8% (offline analysis).

The same four participants completed a third experiment of self-paced motor imagery. All participants completed five runs (3 min each), with a total of eight (intended) activations per run. To evaluate this experiment, the participants were instructed to press a button with their right thumb *before* attempting to activate the brain switch through motor imagery (feet dorsiflexion). In this way, TP, FP, and FN could be estimated. Performance was evaluated with the TPR and the positive predictive value $\left(\mathrm{PPV} = \frac{\mathrm{TP}}{\mathrm{TP+FP}}\right)$. The average TPR was 0.79, and the PPV was 0.84. FP/min (not reported) can be estimated around 0.5 FP/min. However, it is possible that the brain switch reacted to a central beta rebound following the button press instead of the participant's motor imagery, biasing the results.

Chapter 6

Online application: a hybrid BCI

One way to evaluate the online performance of an asynchronous brain switch, consists on assessing the user's control over a simple *benchmark* application (see Chapter 3). A benchmark application provides a specific task and a set of rules, which the participant must observe while operating the brain switch (or BCI). For example, Müller-Putz et al. [192] used a video game to evaluate the control of a brain switch based on motor imagery, and to facilitate user training. In another example, Cheng et al. [148] conducted a self-paced experiment consisting of focusing visual attention on a set of flickering lights (LEDs), following a strict order, to evaluate the control of a SSVEP-based BCI. Noteworthy, these experiments were designed to evaluate motor imagery and focused visual attention independently.

A novel benchmark application could integrate motor imagery and focused visual attention into a single experiment controlled by a hybrid BCI. Hybrid BCIs result from the combination of a BCI (e.g. a brain switch) and another system, possibly a second BCI or an assistive device [28–31]. Besides combining two or more systems, a hybrid BCI offers some advantages over its individual components.

In this chapter, we realize a hybrid BCI by combining a brain switch with a SSVEP BCI. To operate the hybrid BCI motor imagery and visual attention are sequentially performed by the user. The hybrid BCI constitutes a benchmark application for the online evaluation and development [1] of brain switch concepts.

6.1 Brain switch as a component of a hybrid BCI

A brain switch could be integrated into a hybrid system to enable/disable a secondary, more complicated, multi-class BCI or another assistive technology. In this way, the brain switch could disable the system during periods of non-intentional control, avoiding the occurrence of false activations, should these happen. Additionally, a self-paced paradigm with a well defined and expected behavior, allows evaluating the online operation of the

[1] Bauernfeind et al. [149], Bauernfeind [193] have used this application to evaluate an optical brain switch based on fNIRS.

brain switch. This Chapter presents the online operation of an ERS-based brain switch, and its effect on the performance of a hybrid BCI composed by a SSVEP-based BCI and the beta rebound based brain switch.

6.2 Methods

Data description

Six healthy participants (male, age 26.1 ± 2.9 years) completed an experimental session involving motor imagery and SSVEP. Five out of six participants had previous experience with motor imagery and SSVEP, but were unfamiliar with this particular paradigm. We recorded the EEG form a Laplacian derivation over Cz and a bipolar derivation at electrode position O1. Five Ag-AgCl were placed around Cz, and two additional electrodes were placed 2.5 cm anterior and posterior to O1. Reference and ground electrodes were attached to the left and right mastoid, respectively. EEG was recorded with a biosignal amplifier at 256 Hz, with a band-pass filter between 0.5 and 100 Hz and a notch filter at 50 Hz, applied before digitalization.

We conducted the experiments in a quiet, unshielded room. During the experiments, the participants sat comfortably on an office chair, in front of a table. A monitor placed on the table, one meter away from the participants provided cues and online feedback. A hand orthosis was also placed on the table, 40 cm away from the participant. This hand orthosis was controlled by a SSVEP-based BCI. With this configuration, the participants simultaneously observed the monitor and the orthosis.

The experiments were divided into three main parts. The first part included the training of a brain switch based on the post-imagery beta rebound, and the calibration of a SSVEP-based BCI. The second part involved the self-paced operation of a hybrid BCI composed by the ERS brain switch and the SSVEP-based BCI. Finally, as a control condition, the participants repeated the self-control paradigm with the SSVEP-based BCI only. These main stages are described in the following sections.

Cue-paced motor imagery

Each participant completed two runs of cue-paced motor imagery without feedback. A run consisted of trials with imagination of brisk feet dorsiflexion or rest (relaxed with eyes open), with fifteen trials per class. At the beginning of the trial ($t = 0\,s$) a fixation cross appeared on the center of the monitor. Two seconds later ($t = 2\,s$) an audible cue was played, and an arrow was displayed as a cue. An arrow pointing downwards indicated a trial of motor imagery, and an arrow pointing upwards indicated a trial of rest. Cue presentation was randomized. The arrow disappeared at $t = 3.25\,s$, followed by the cross at $t = 6\,s$. A blank screen was presented until the end of the trial ($t = 8\,s$) and during the inter-trial interval (random duration between 0.5 and 1.5 s). The trial timing is shown in Figure 6.1.

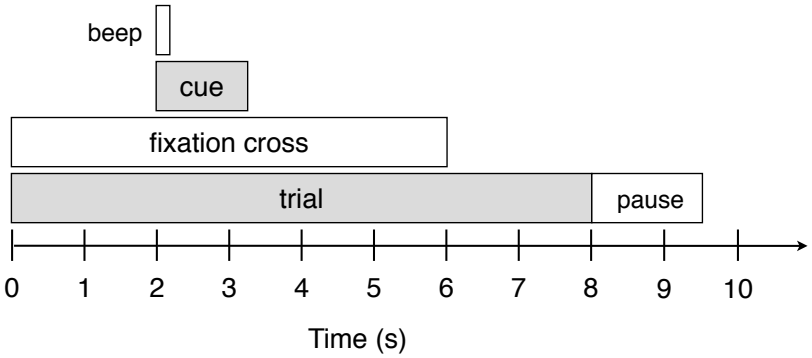

Figure 6.1: Cue-paced training paradigm. Besides minor differences in timing, the runs of this paradigm included two classes: motor imagery and rest (relaxed with eyes open). Two seconds after the beginning of the trial ($t = 2\,s$) an arrow appeared on screen for 1.25 s, the arrow could point downwards or upwards, indicating imagination of foot movement (dorsiflexion) or rest (relax with eyes open).

Brain switch setup

We completed the brain switch setup by selecting the reactive band of the beta rebound, and a specific time segment, which offered the best classification between the post-imagery beta rebound and a reference interval ($t = 0.5$ to $1.5\,s$), for each participant. As described in the last section of Chapter 5, we estimated the performance (10×10 cross-validation) of a LDA classifier trained on different logBP features at different time segments within a trial. The frequency bands with the best performance (Cohen's κ) were merged for computation of a single, broad band feature. Finally, we selected the time segment where the classification performance reached its maximum for setting up the classifier for online operation.

To further reduce the setup time, we avoided the ROC analysis for selection of post-processing parameters. Instead, we adapted the methods of Müller-Putz et al. [182] and defined preliminary values for threshold (TH) and dwell time (DT). These two parameters were manually adjusted for every participant during a test run. The initial threshold was defined as the mean plus one standard deviation of the LDA output from the training segments, and the dwell time was defined to be one second. To complete the set of parameters, and reduce the possible number of activations, the refractory period (RP) was fixed to two seconds (512 samples). It is necessary to mention that length of the refractory period has a direct impact on the ITR of a BCI.

SSVEP-based BCI calibration

Participants operated a SSVEP-based BCI to control a 4-step electrical hand orthosis (Otto Bock Healthcare Products GmbH, Vienna, Austria). Details about this orthosis can be

found elsewhere [194]. The hand orthosis supports wrist flexion, with four intermediate steps (see Figure 6.2). Two LEDs attached to the orthosis deliver the visual stimulation for the SSVEP-based BCI. One LED flickering at 8 Hz is used for wrist flexion, and another LED flickering at 13 Hz is used for wrist extension.

Operation of the SSVEP-based BCI relied on the harmonic sum decision (HSD) [195]. The HSD evaluates the weighted sum of the spectral power at each stimulation frequency and its 2nd and 3rd harmonics. The results of the HSD for n stimulation frequencies are compared, and the maximum value is selected as command. The weights for the HSD are computed as the average harmonic sum of each stimulation frequency during a period of rest (one minute EEG recordings, relaxed with eyes open). In this period of rest, the visual stimuli are inside the visual field, but the participants are instructed to avoid attending any of the flickering elements. The SSVEP-based BCI evaluates the HSD based on the discrete Fourier transform computed from the last second of EEG recordings (bipolar derivation over O1). The output of the SSVEP-based BCI was further processed with a DT (1.56 s) and RP (4 s).

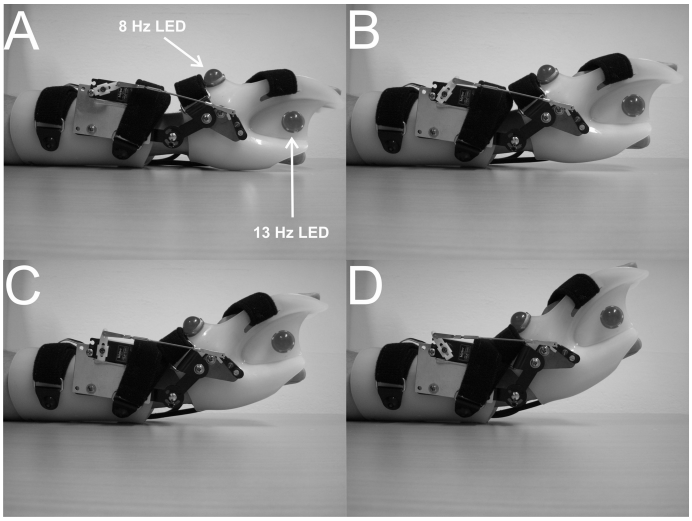

Figure 6.2: SSVEP controlled hand orthosis. A 4-step (A→D) electrical hand orthosis (Otto Bock Healthcare Products GmbH, Vienna, Austria) was fixed with a pair of LEDs flickering at 8 and 13 Hz. Participants could control the movement of the orthosis by focusing on one of these two LEDs (modified from [178]).

Hybrid BCI and self-paced paradigm

We realized a hybrid BCI by combining the ERS-based brain switch and the SSVEP-based BCI (see Figure 6.3). The ERS-based brain switch enabled/disabled the flickering elements of the SSVEP-based BCI, while the SSVEP-based BCI controlled the hand orthosis. The self-paced paradigm required the participants to operate both BCIs sequentially. At the

beginning of a self-paced run, the participants activated the brain switch to turn on the visual stimulation, i.e. LEDs on the orthosis, enabling the SSVEP-based BCI. Next, the participants operated the SSVEP-based BCI to change the positions of the hand orthosis from fully extended to fully flexed, and back to fully extended. After completing this task, the participants were required to activate the bran switch to turn off the visual stimulation and to disable the SSVEP-based BCI. A non-intentional control period (one minute) followed. The participants repeated the SSVEP control three times, with two non-intentional control period in between (see Figure 6.4). Maximum duration of a self-paced run was ten minutes. Participants were instructed to correct the false activations of the brain switch, and the SSVEP-based BCI during the intentional control periods. As a control experiment, each participant repeated the self-paced paradigm with the SSVEP-based BCI only, i.e. the brain switch was removed and the LEDs were continuously on.

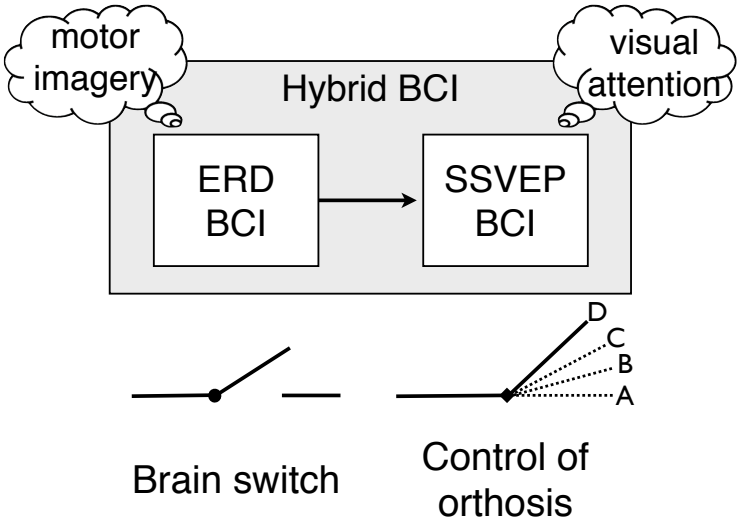

Figure 6.3: Realization of a hybrid BCI. A brain switch and a SSVEP-based BCI were combined to create a hybrid system. To operate the hybrid BCI, users need to sequentially change their mental strategy between motor imagery and visual attention (modified from [29]).

Performance evaluation

The performance of the classifiers used for online operation of the brain switch was estimated from the confusion matrix during training, and summarized with the classification accuracy (class prevalence was the same at this stage). Activations of both BCIs were the basis for performance evaluation of the hybrid system. We counted the true and false activations of the SSVEP-based BCI, during intentional and non-intentional control periods separately, and the activations of the brain switch during the complete run.

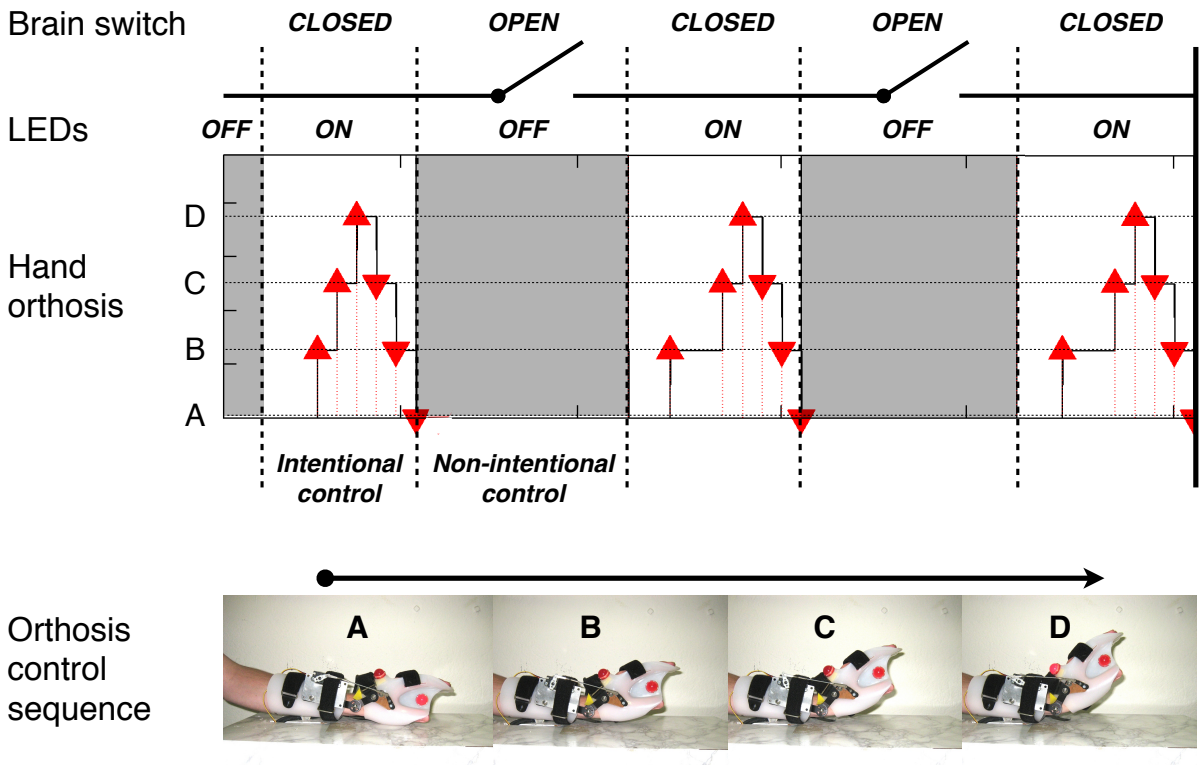

Figure 6.4: Self-paced paradigm for the hybrid BCI. At the beginning of a run, the participants perform motor imagery to *close* the brain switch and to turn on the LED's on the hand orthosis (top). By focusing on the different LEDs, the participants move the hand orthosis (red triangles). After completing a control sequence ($A \rightarrow D \rightarrow A$, see Figure 6.2) with the orthosis, a period of non-intentional control (duration: 60 s, showed in gray) for the SSVEP-based BCI starts. The participants perform motor imagery to *open* the brain switch and turn off the LED's, avoiding movements of the orthosis. Participants were instructed to correct false activations of the brain switch at any time, and false activations of the orthosis only during the intentional control periods. A run ends after completing the third sequence with the hand orthosis, or if the time limit is reached (ten minutes). For illustration purposes, the bottom of the figure shows half of the orthosis control sequence. Noteworthy, the participants did not wear the orthosis on their hand.

To facilitate the interpretation of the performance evaluation, we combined true and false activations into the positive predictive value $\left(\text{PPV} = \frac{\text{TP}}{\text{TP+FP}}\right)$. The PPV equals one when there are no false activations, it equals 0.5 if the number of true and false activations is the same, and it tends to zero if the number of false activations is larger than the number of true activations. Although it might seem that this strategy disregards the importance of the non-intentional control period, we consider that the estimation of the true and false negatives is highly affected by class prevalence. As an alternative, we estimated the false positives per minute (FP/min) from the periods of non-intentional control (SSVEP-based BCI only), and for the brain switch during the whole run.

6.3 Results

Figure 6.5 shows an example of the self-paced paradigm with the hybrid system. For comparison, Figure 6.6 shows an example of the self-paced paradigm without the brain switch. Both figures correspond to the evaluation runs of participant d4. Table 6.1 presents the frequency band selected for each participant, and the classification accuracy obtained during the setup of the brain switch. Average classification accuracy was $85.0 \pm 6.6\%$. Notably, classifier training does not impose any restrictions to the FPR. Table 6.2 shows the performance evaluation for the brain switch. Figure 6.7 shows the average PPV and FP/min of each participant in their individual runs, obtained during the self-paced operation of the brain switch. Each participant completed two runs with the online self-paced paradigm, except participants d3 and d4. On average, the FP/min was 0.47 ± 0.37. Additionally, there were 7.58 ± 2.35 TPs and 3.50 ± 3.35 FPs, yielding an average PPV of 0.74 ± 0.14. All PPV values were above 0.50, and above 0.70 in four out of six participants.

Table 6.1: Brain switch setup.

ID	Frequency band (Hz)		Accuracy (%)
	f_1	f_2	
d1	20	24	95
d2	26	32	90
d3	25	27	76
d4	22	26	84
d5	25	29	82
d6	34	36	83
mean	25.3	29.0	85.0
s.d.	4.8	4.4	6.6

Table 6.3 shows the performance of the SSVEP-based BCI as part of the hybrid BCI, whereas Table 6.4 shows the performance of the SSVEP-based BCI by itself, i.e. without inclusion of the brain switch. Considering the hybrid BCI, the average TP/min were

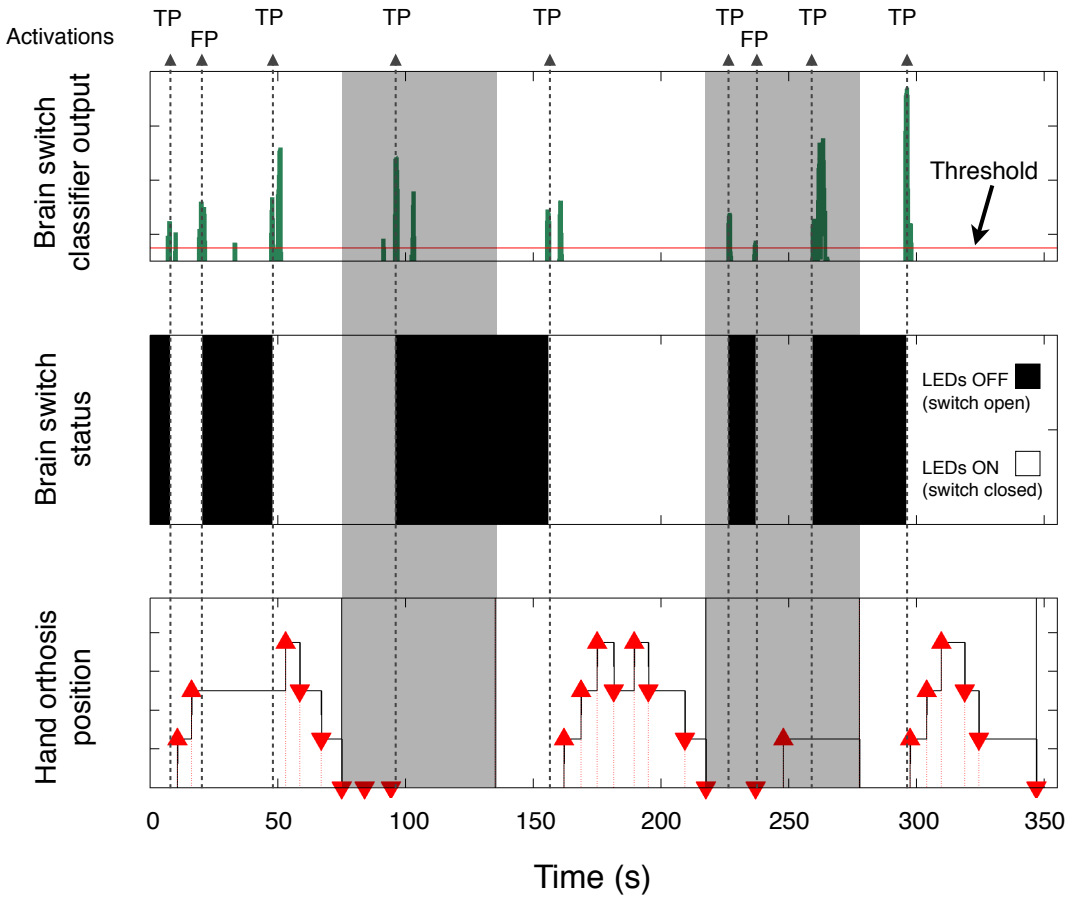

Figure 6.5: Example of online evaluation: hybrid system. Few seconds after the beginning of the run, the brain switch enables the LEDs on the hand orthosis. A false positive occurs after two movements of the hand orthosis. Motor imagery turns the LEDs back on ($t = 50\,s$), and the participant completes the sequence with the hand orthosis. The non-intentional control period (duration 60 s, marked in gray) starts immediately, and the participant is notified on the computer screen. Two false activations of the orthosis occur while attempting an activation of the brain switch ($t = 100\,s$). The second sequence is executed without problem, but false activations occur during the second non-intentional control period. Finally, the third sequence is also executed without problem. The figure corresponds to the data from participant d4.

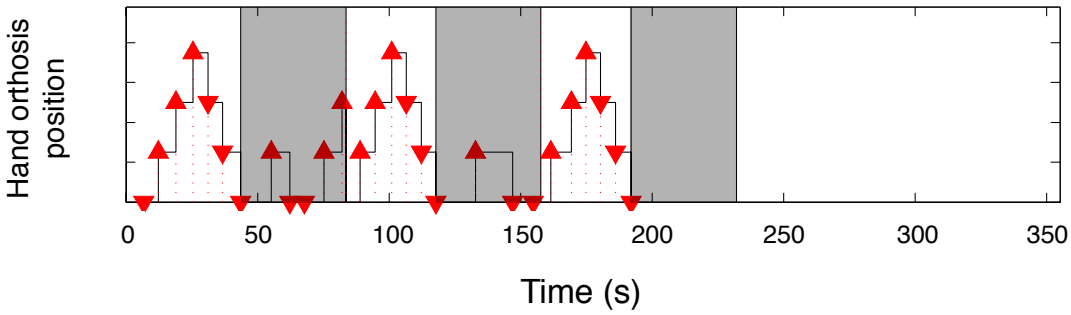

Figure 6.6: Example of online evaluation: SSVEP. All three control sequences with the hand orthosis are completed without problems. However, false activations occur during the periods of non-intentional control (duration: 40 s, marked in gray). The figure corresponds to the data from participant d4.

3.96 ± 1.34 and the FP/min were 0.84 ± 0.98 during intentional control. In addition, there were 1.46 ± 1.18 FP/min during non-intentional control. Considering the SSVEP-based BCI alone, the average TP/min were 6.87 ± 2.48 and the FP/min were 0.94 ± 0.76 during intentional control. Furthermore, there were 5.40 ± 0.90 FP/min during non-intentional control.

Noteworthy, the FP/min during non-intentional control were significantly reduced for the hybrid BCI ($p < 0.01$). Figure 6.8 illustrates the reduction of FP/min. Although the TP/min (intentional control) were also reduced significantly reduced ($p < 0.01$), there was only a slight reduction on FP/min (intentional control) and the PPV. Another difference between the operation of the hybrid BCI and the SSVEP-based BCI, is the time needed to complete a run. The average time for the hybrid BCI was 429.64 ± 86.06 s, while the operation of the SSVEP-based BCI required only 291.89 ± 48.23 s. This difference might caused by the time needed to operate the brain switch, and a higher workload required for control of the hybrid BCI.

Table 6.2: Online performance of the brain switch.

ID	TP		FP		PPV		Time (s)		FP/min
	mean	s.d.	mean	s.d.	mean	s.d.	mean	s.d.	
d1	5.50	0.71	0.50	0.71	0.92	0.10	468	87	0.06
d2	5.00	0.00	1.00	1.41	0.83	0.20	457	61	0.13
d3	8.00		3.00		0.73		306		0.59
d4	7.00		2.00		0.78		346		0.35
d5	8.50	4.95	5.00	2.83	0.63	0.00	465	34	0.65
d6	11.50	0.71	9.50	0.71	0.55	0.03	536	11	1.06
mean	7.58		3.50		0.74		430		0.47
s.d.	2.35		3.35		0.14		86		0.37

Table 6.3: Performance of the hybrid BCI.

ID	Intentional control			Non-intentional control	Time (s)
	TP/min	FP/min	PPV	FP/min	
d1	4.29	0.91	0.83	0.25	468
d2	2.69	2.73	0.50	0.25	457
d3	5.80	0.00	1.00	1.00	306
d4	5.04	0.27	0.95	2.00	346
d5	3.58	0.77	0.82	2.00	465
d6	2.38	0.37	0.87	3.25	536
mean	3.96	0.84	0.83	1.46	430
s.d.	1.34	0.98	0.18	1.18	86

Table 6.4: Performance of the SSVEP-based BCI.

ID	Intentional control			Non-intentional control	Time (s)
	TP/min	FP/min	PPV	FP/min	
d1	6.06	0.91	0.87	5.00	319
d2	3.70	2.18	0.64	5.63	321
d3	10.10	0.00	1.00	4.50	229
d4	9.64	0.54	0.95	6.00	232
d5	5.77	1.38	0.81	6.75	338
d6	5.97	0.63	0.90	4.50	311
mean	6.87	0.94	0.86	5.40	292
s.d.	2.48	0.76	0.13	0.90	48

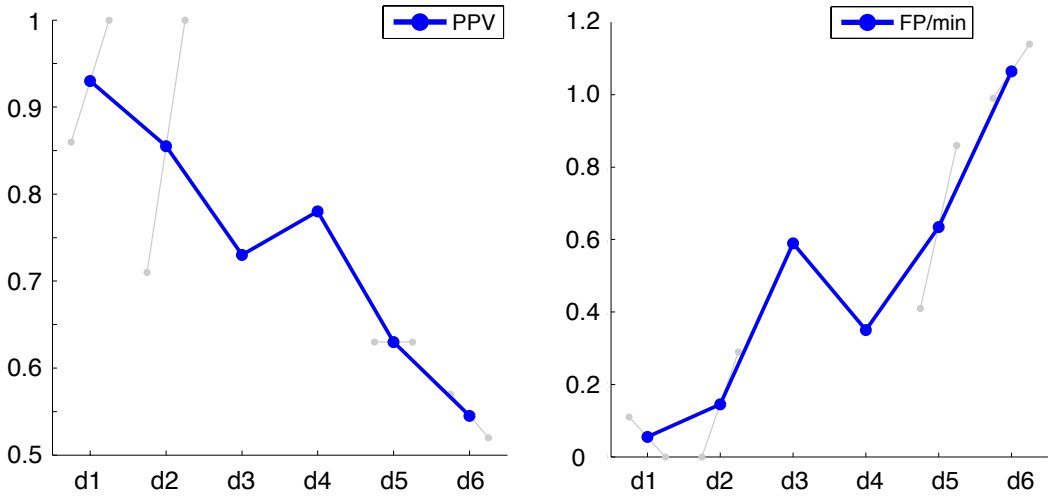

(a) (b)

Figure 6.7: Online performance of the brain switch. (a) Positive predictive value and (b) false positives per minute of individual participants and individual runs are shown in gray circles. Average values for each participant are marked with blue circles. All PPV values above 0.50. All FP/min values below 1.2. Participants d3 and d4 completed only one run of the self-paced paradigm.

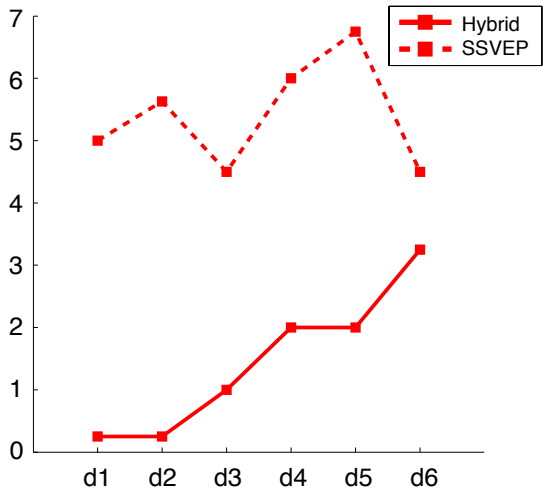

Figure 6.8: Reduction of FP/min in a hybrid BCI. False activations of the SSVEP-based BCI during periods of non-intentional control differ significantly ($p < 0.01$) between the hybrid BCI (continuous line), and the SSVEP-based BCI without the brain switch (dashed line); showing that the brain switch effectively reduces the false activations of the SSVEP-based BCI during periods of non-intentional control.

6.4 Discussion

In this Chapter we have demonstrated the online operation of the Graz Brain Switch, and its possible role as a component of a hybrid BCI. We realized a hybrid BCI with the sequential operation of a brain switch and a SSVEP-based BCI. The hybrid system provides control of a hand orthosis, while reducing the FP/min during periods of rest or non-intentional control.

There are two main features of the hybrid BCI: (i) the reduction of false activations, and (ii) the online evaluation of a brain switch. First, we show that including the brain switch reduces the number of false activations by disabling the SSVEP-based BCI, during periods of non-intentional control. A slight decrease of the TP/min and FP/min (for SSVEP) in the hybrid BCI might have occurred because the participants needed more time to complete a run with the hybrid system. Longer duration of the runs could be a consequence of higher cognitive load due to the operation of the hybrid BCI, or it could reflect the time needed to correct errors from one of the two BCIs.

Second, the online self-paced paradigm can be seen as a benchmark application suitable to investigate, test, and develop different brain switch designs in real time applications with feedback [149]. Without explicit cues, the self-paced paradigm described above provides a guide for the expected behavior of the hybrid BCI; allowing the estimation of true an false activations for individual components of the system. To assess the performance of an asynchronous BCI, it is important to include periods of non-intentional control.

Chapter 7

Conclusion and further prospects

This thesis presented the design and evaluation of the asynchronous Graz Brain Switch. After providing an overview of the beta rebound (Chapter 2) and current brain switch designs (Chapter 3), we demonstrated the feasibility of realizing a brain switch based on the beta rebound after execution or imagination of brisk feet dorsiflexion (Chapter 4). Simulations of an asynchronous BCI revealed an average TPR of 0.74 for the detection of overt movement, and 0.59 for the detection of covert movement. In both cases, the FPR was below 0.10. The FPR limit was selected by design, and the brain switch could be tuned to a lower limit. However, there exist a trade-off between reducing the FPR and the highest TPR achievable. Although current brain switch designs aim at achieving an FPR equal to zero, there is no *online* system with such performance.

Taking advantage of the similarity of the beta rebound after execution of physical movement and after movement imagination, we proposed to set up the brain switch with data recorded during actual movement, for later operation through motor imagery (Chapter 5). In a training phase, we used motor execution data to set up a classifier with the best performance possible. In a calibration phase, we applied this classifier to motor imagery data and adjusted a set of post-processing parameters to limit the FPR ($\leq$0.10). Finally, we assessed the performance of this approach with a simulation of an asynchronous brain switch. The detection of the post-imagery beta rebound led to an average TPR of 0.46 and an FPR of 0.11.

In some cases, a brain switch trained to detect the peri-imagery ERD could outperform the original design of the Graz Brain Switch. Thus, the training and calibration phases may consider both alternatives to offer the best performance possible. This methodology presents a simple way to train a BCI for applications controlled by healthy users. Nonetheless, it would be possible to obtain data from attempted or passive movements. This would allow to use these methods in clinical applications for persons with stroke, spinal cord injury, or in a minimally conscious state.

Next, we evaluated the online performance of the Graz Brain Switch with a novel benchmark application (Chapter 6). Since online evaluation does not provide the number of false or true negatives, it is not possible to compute the TPR and FPR. Instead, we calculated the positive predictive value (PPV) to summarize the performance of the brain switch. The

average PPV was 0.74, with only 0.47 false positives per minute (FP/min). In comparison, current brain switch designs have reported 0.70 FP/min in offline simulations [156, 163] and 1.4 FP/min during online processing [162] for the detection of physical movement, and around 3.0 FP/min [162] for the online detection of motor imagery (healthy persons) and attempted movement (stroke patients). Additionally, we reported on the successful implementation of a *hybrid* BCI, in which the Graz Brain Switch is used to enable/disable a SSVEP-based BCI. In this case, the number of false activations during periods of non-intentional control could be reduced by the switch operation.

Besides giving an overview on the beta rebound, in Chapter 2 we reported for the first time on the beta rebound following the execution and withholding of physical movement, and on the differences between withholding of overt and covert movement. Investigating the response pattern, we observed a beta ERS (beta rebound) during the inhibition (withholding) of overt and covert movement. Comparing execution and inhibition of physical movement (feet dorsiflexion), we observed a beta rebound in the same frequency band and at the same electrode position, but with statistically significant differences in magnitude, namely, a larger beta rebound after execution as compared to during inhibition. Interestingly, withholding of motor execution and withholding of motor imagery present different response profiles in the EEG, composed by an early beta ERD terminated by the beta rebound (beta ERS, peaking around one second after cue onset). While the beta ERD was similar in both conditions, the beta rebound was significantly larger during withholding of motor execution. A possible interpretation for this difference is that motor execution demands a stronger active inhibition of neuronal networks in the motor cortex, as compared to motor imagery.

Future prospects for the Graz Brain Switch could be oriented towards enhancing its performance. For example, by including additional features besides the post-movement beta rebound. For the sake of practicality, the analyses presented in this thesis used a single Laplacian derivation around electrode position Cz, i.e. a set of five EEG channels. Although the beta rebound has a specific somatotopic organization, the localization of beta oscillations' sources in peri-Rolandic regions vary across persons [145]. It would be interesting to analyze the different bipolar derivations that can be computed from this set of electrodes, or from additional EEG channels to extract features that might be relevant for classification. For example, the *focal ERD/surround ERS* phenomenon [70] could be used to include information from the hand area (i.e. electrode position C3) to enhance the classification accuracy of imagination of foot movement.

Hybrid systems that include other types of biosignals, e.g. the electromyogram (EMG) or the electrocardiogram (ECG), could also benefit the Graz Brain Switch. Heart rate changes are of special interest, due to the close relation between the central nervous system and the cardiovascular system [196]. There exist a couple of reports on BCI control including heart rate [197, 198]. In this line, we have started by analyzing the heart rate during execution and inhibition of covert feet dorsiflexion (Go/NoGo experiment described in Chapter 2). Imagination of a brisk dorsiflexion not only produces the characteristic beta ERD/ERS pattern, but also a modulation of the heart rate (see Figure 7.1). The post-imagery beta rebound roughly coincides with a heart rate acceleration. Both phenomena,

i.e ERD/ERS and heart rate, display significant changes across sixteen naive participants. Although this is a preliminary observation, we expect that including heart rate information will boost the performance of the Graz Brain Switch at least in some participants.

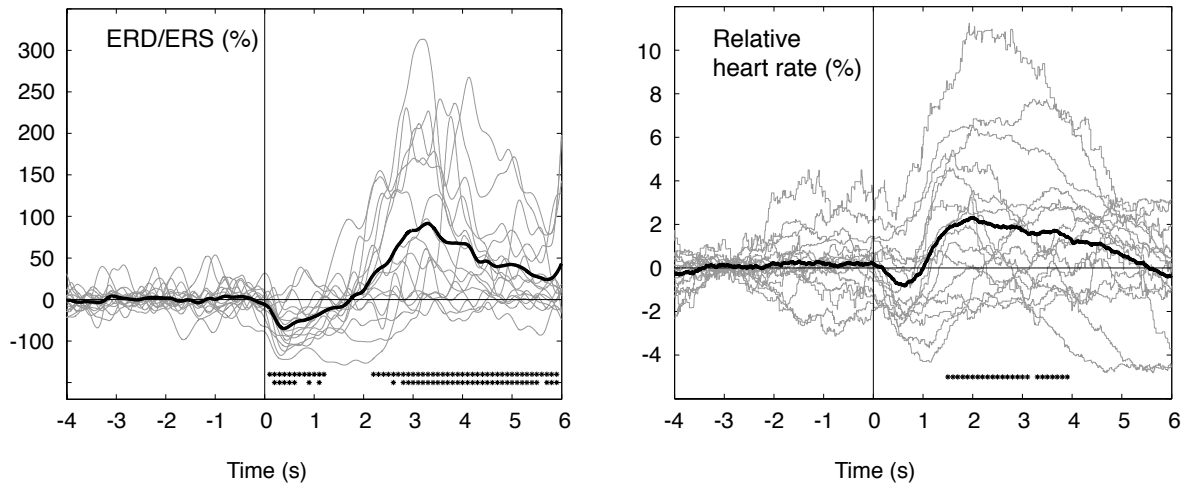

(a) (b)

Figure 7.1: Post-imagery beta ERS and HR acceleration. (a) Time course of the beta power after during imagination of brisk feet dorsiflexion. (b) Heart rate modulation during the same condition. Gray lines indicate the responses for individual participants. Grand average responses are plotted with black thick lines. A bootstrap algorithm was used to identify significant changes across all 16 participants (single asterisk indicates $p < 0.05$, and double vertical asterisks indicate $p < 0.01$.). Vertical lines indicate cue onset (Go). In comparison with Figure 2.10, the responses in this figure have been computed relative to cue onset, instead of motor offset.

From the investigation of the beta rebound after withholding of motor imagery, we conclude that post-processing could enhance the performance of the Graz Brain Switch, i.e. reduce the false activation rate. A beta rebound lasting longer than one second, should be clearly identified as a post-imagery beta rebound, while a shorter beta rebound can be considered as non-intentional control.

Appendix A

Inhibition of overt and covert foot movement—detailed information

The tables in this section provide detailed information on the comparisons between the post-movement beta rebound and the beta rebound during withholding of movement (ME-Go vs. ME-NoGo), and the beta rebound during withholding of overt foot movement (ME-NoGo vs. MI-NoGo); presented in Chapter 2.

Table A.1: Movement parameters and artifact free trials.

ID	Reaction time (ms)		Movement duration (s)		Artifact-free trials		
					ME		MI
	mean	s.d.	mean	s.d.	Go	NoGo	NoGo
s1	393	368	2.48	0.26	40	38	51
s2	240	54	1.87	0.15	40	39	20
s3	288	75	1.42	0.1	40	39	56
s4	482	87	1.56	0.2	40	38	45
s5	395	109	1.84	0.28	40	39	31
s6	497	246	1.67	0.37	40	40	34
s7	213	106	1.15	0.24	40	39	39
s8	356	79	1.54	0.11	40	40	50
s9	253	66	1.83	0.38	40	39	25
s10	671	113	1.31	0.17	40	39	47
s11	360	76	1.6	0.11	40	39	27
s12	426	163	1.54	0.2	40	39	53
s13	265	85	1.31	0.23	40	39	31
s14	227	85	1.45	0.17	40	37	11
s15	480	110	1.7	0.17	40	39	24
s16	326	85	1.7	0.11	40	37	49
mean	367.00		1.62		40.00	38.75	37.06
s.d.	124.15		0.31		0.00	0.86	13.55

Table A.2: Beta rebound characteristics: ME-Go, ME-NoGo, and MI-NoGo.

ID	Frequency band (Hz)		ME				MI	
			Go		NoGo		NoGo	
	f_1	f_2	amplitude (%)	latency (s)	amplitude (%)	latency (s)	amplitude (%)	latency (s)
s1	15	27	439	1.2	307	1	122	0.8
s2	13	20	98	0.5	323	0.9	159	1
s3	20	24	579	1.8	278	1	250	1.1
s4	14	28	341	0.9	166	1	53	1.2
s5	16	28	452	1.4	220	1.1	68	1.3
s6	13	25	513	1.2	318	0.9	217	0.8
s7	13	22	389	0.4	138	1.2	196	1.1
s8	16	24	385	0.3	194	1.4	–	–
s9	23	32	296	0.6	141	1.3	–	–
s10	26	37	271	0.6	55	0.6	–	–
s11	19	32	74	0.5	62	1.1	–	–
s12	25	34	436	0.9	89	0.9	–	–
s13	21	27	142	0.7	–	–	–	–
s14	21	28	128	1.1	–	–	–	–
s15	26	34	95	0.6	–	–	–	–
s16	20	32	517	1.5	–	–	–	–
mean	18.81	28.38	322.19	0.89	190.92	1.03	152.14	1.04
s.d.	4.67	4.77	169.21	0.44	98.58	0.21	74.80	0.19

Table A.3: Multichannel comparison between ME-Go and ME-NoGo.

TASK	ME-Go	ME-NoGo						
F(1,8) = 25.24 **	71.65 (101.84)^{a}	24.33 (48.38)^{a}						
CHANNEL	anterior	lateral left	Cz	lateral right	posterior			
F(4,32) = 26.91 ***	32.74 (44.70)^{a}	31.13 (46.66)^{a}	124.52 (140.15)$^{\boldsymbol{a}}$	21.62 (41.45)^{a}	29.94 (42.24)^{a}			
TIME	t = 0 s	t = 0.5 s	t = 1 s	t = 1.5 s	t = 2 s	t = 2.5 s		
F(5,40) = 11.02 **	7.98 (28.54)$^{\boldsymbol{a}}$	75.26 (81.78)^{a,b}	57.84 (81.9)^{a}	60.79 (104.09)^{a}	50.75 (95.76)^{a}	35.30 (69.28)^{a,b}		
TASK×CHANNEL		anterior	lateral left	Cz	lateral right	posterior		
F(4,32) = 12.41 **	ME-Go	48.01 (51.39)^{a}	40.88 (49.19)^{a}	197.5 (152.25)$^{\boldsymbol{a},b}$	27.69 (41.93)^{a}	44.17 (47.29)^{a}		
	ME-NoGo	17.46 (30.3)	21.37 (42.21)	51.55 (74.98)^{b}	15.55 (40.45)	15.70 (30.88)		
TASK×TIME		t = 0 s	t = 0.5 s	t = 1 s	t = 1.5 s	t = 2 s	t = 2.5 s	
F(5,40) = 8.11 **	ME-Go	7.49 (30.45)$^{\boldsymbol{a}}$	75.27 (86.78)^{a}	84.23 (100.79)^{a,c}	103.75 (130.99)^{a,d}	93.60 (119.10)^{a,e}	65.55 (86.5)^{a,f}	
	ME-NoGo	8.48 (26.84)^{b}	75.24 (77.45)$^{\boldsymbol{b}}$	31.45 (44.54)^{b,c}	17.83 (31.37)^{b,d}	7.90 (24.68)^{b,e}	5.05 (18.79)^{b,f}	
CHANNEL×TIME		t = 0 s	t = 0.5 s	t = 1 s	t = 1.5 s	t = 2 s	t = 2.5 s	
F(20,160) = 10.66 ***	anterior	11.81 (27.15)^{a}	61.13 (60.46)$^{\boldsymbol{a},h}$	32.4 (34.9)^{i}	37.01 (51.72)^{j}	31.70 (45.04)^{k}	22.35 (28.51)^{a,l}	
	lateral left	7.71 (39.09)^{b}	56.67 (61.84)$^{\boldsymbol{b},h}$	38.69 (38.13)^{i}	34.34 (45.57)^{j}	28.73 (40.32)^{k}	20.61 (41.58)^{b,l}	
	Cz	12.48 (14.38)$^{\boldsymbol{c}}$	160.61 (108.35)$^{c,d,\boldsymbol{h}}$	160.51 (127.32)$^{c,d,\boldsymbol{i}}$	172.29 (178.04)$^{c,d,e,\boldsymbol{j}}$	142.06 (170.16)$^{c,d,e,\boldsymbol{k}}$	99.18 (123.90)$^{c,\boldsymbol{d},\boldsymbol{l}}$	
	lateral right	-1.83 (28.28)^{f}	43.34 (58.52)^{f,h}	28.81 (29.96)^{i}	24.34 (35.44)^{j}	21.76 (49.58)^{k}	13.30 (27.61)^{l}	
	posterior	9.74 (29.18)^{g}	54.54 (50.46)$^{\boldsymbol{g},h}$	28.81 (36.24)^{i}	35.97 (49.59)^{j}	29.51 (43.01)^{k}	21.05 (31.86)^{g,l}	
TASK×CHANNEL×TIME			t = 0 s	t = 0.5 s	t = 1 s	t = 1.5 s	t = 2 s	t = 2.5 s
F(20,160) = 5.28 ***	ME-Go	anterior	11.56 (30.22)	66.46 (72.86)^{e}	51.93 (35.92)^{f}	62.32 (63.06)^{g}	58.78 (49.38)^{h}	37.00 (34.32)^{i}
		lateral left	8.38 (47.99)	47.38 (54.72)^{e}	47.71 (43.53)^{f}	53.7 (53.8)^{g}	50.1 (41.66)^{h}	38.00 (51.32)^{i}
		Cz	16.34 (11.23)$^{\boldsymbol{a},d}$	179.83 (109.57)$^{a,\boldsymbol{b},d,\boldsymbol{e},o}$	236.39 (131.20)$^{a,b,c,d,\boldsymbol{f},p}$	300.23 (166.75)$^{a,b,c,\boldsymbol{d},\boldsymbol{g},q}$	260.29 (169.70)$^{a,b,c,d,\boldsymbol{h},r}$	191.92 (110.86)$^{a,\boldsymbol{e},d,\boldsymbol{i},s}$
		lateral right	-7.90 (22.91)	27.51 (42.38)^{e}	39.15 (31.33)^{f}	41.52 (39.74)^{g}	43.55 (60.28)^{h}	22.30 (32.07)^{i}
		posterior	9.06 (29.23)	55.19 (55.04)^{e}	45.99 (42.82)^{f}	60.99 (59.34)^{g}	55.29 (46.82)^{h}	38.51 (36.91)^{i}
			t = 0 s	t = 0.5 s	t = 1 s	t = 1.5 s	t = 2 s	t = 2.5 s
	ME-NoGo	anterior	12.07 (25.55)	55.80 (48.93)^{m}	12.87 (20.97)^{n}	11.71 (16.36)	4.62 (14.88)	7.71 (8.17)
		lateral left	7.05 (30.71)	65.96 (70.27)^{j,m}	29.68 (31.82)^{n}	14.98 (25.99)	7.36 (26.3)	3.22 (18.99)^{j}
		Cz	8.62 (16.73)^{k,l}	141.39 (110.06)$^{\boldsymbol{k},\boldsymbol{m},o}$	84.62 (65.41)$^{k,\boldsymbol{l},\boldsymbol{n},p}$	44.36 (52.17)^{k,q}	23.84 (35.81)^{k,l,r}	6.45 (31.31)^{k,l,s}
		lateral right	4.25 (33.03)	59.18 (70.11)^{m}	18.46 (26.18)^{n}	7.16 (20.65)	-0.04 (22.81)	4.31 (20.24)
		posterior	10.43 (30.87)	53.9 (48.78)^{m}	11.64 (17.11)^{n}	10.95 (17.2)	3.73 (15.63)	3.58 (10.38)

Superscript letters within a factor or interaction section indicate significant differences.
Bold face superscript letters indicate greater/smaller than all others.
** indicates $p < 0.01$.
*** indicates $p < 0.001$.

Table A.4: Multichannel comparison between ME-Go and ME-NoGo.

TASK	ME-NoGo	MI-NoGo						
F(1,6) = 22.84 **	27.40 (59.79)^{a}	-3.89 (36.59)^{a}						
CHANNEL	anterior	lateral left	Cz	lateral right	posterior			
F(4,24) = 7.07 *	4.50 (32.99)^{a}	8.18 (46.46)^{a}	35.43 (82.38)$^{\boldsymbol{a}}$	6.43 (38.03)^{a}	4.23 (37.60)^{a}			
TIME	t = 0 s	t = 0.5 s	t = 1 s	t = 1.5 s	t = 2 s	t = 2.5 s		
F(5,30) = 28.65 ***	-7.44 (16.88)^{a,b}	-17.65 (24.25)^{a,b}	73.76 (78.98)$^{\boldsymbol{a}}$	21.96 (44.30)$^{a,\boldsymbol{b}}$	6.86 (30.26)^{a}	-6.70 (27.64)^{b}		
TASK×CHANNEL		anterior	lateral left	Cz	lateral right	posterior		
F(4,24) = 4.26 **	ME-NoGo	16.97 (37.40)^{a,c}	25.27 (52.08)^{a,d}	57.79 (96.70)$^{\boldsymbol{a},e}$	17.09 (42.04)^{a,f}	19.89 (42.06)^{a,g}		
	MI-NoGo	-7.97 (22.03)^{b,c}	-8.91 (32.55)^{b,d}	13.07 (58.04)$^{\boldsymbol{b},e}$	-4.24 (30.44)^{b,f}	-11.43 (24.29)^{b,g}		
TASK×TIME		t = 0 s	t = 0.5 s	t = 1 s	t = 1.5 s	t = 2 s	t = 2.5 s	
F(5,30) = 23.36 ***	ME-NoGo	-8.93 (16.41)^{a,b,c}	-14.14 (27.87)^{a,b,c}	115.48 (72.16)$^{\boldsymbol{a},e}$	45.67 (44.28)$^{a,\boldsymbol{b},f}$	21.12 (30.26)$^{a,b,\boldsymbol{c},g}$	5.21 (28.83)^{a,b,c,h}	
	MI-NoGo	-5.96 (17.44)^{d}	-21.17 (19.78)^{d}	32.04 (62.19)$^{\boldsymbol{d},e}$	-2.28 (28.94)^{d,f}	-7.39 (22.90)^{d,g}	-18.61 (20.67)^{d,h}	
CHANNEL×TIME		t = 0 s	t = 0.5 s	t = 1 s	t = 1.5 s	t = 2 s	t = 2.5 s	
F(20,120) = 12.39 ***	anterior	-1.31 (10.46)^{a}	-7.58 (21.05)^{a,i}	48.01 (48.28)$^{\boldsymbol{a},j}$	4.29 (25.73)^{a,k}	-6.19 (21.25)^{a,l}	-10.16 (19.02)^{a}	
	lateral left	-13.49 (16.77)^{b,c}	-17.78 (17.76)^{b,c,i}	60.33 (72.79)$^{\boldsymbol{b},j}$	20.41 (38.66)$^{b,\boldsymbol{c},k}$	7.81 (27.31)^{b,l}	-8.21 (32.19)^{b}	
	Cz	-13.94 (22.92)^{d,e}	-36.32 (29.06)^{d,e}	164.26 (92.15)$^{\boldsymbol{d},\boldsymbol{j}}$	60.72 (56.25)$^{d,\boldsymbol{e},\boldsymbol{k}}$	33.76 (36.93)$^{d,e,f,\boldsymbol{l}}$	4.11 (33.88)^{d,e,f}	
	lateral right	-6.99 (17.53)^{g}	-8.93 (25.96)^{g}	43.81 (51.13)$^{\boldsymbol{g},j}$	15.81 (43.31)^{g,k}	2.67 (24.72)^{g,l}	-7.80 (29.47)^{g}	
	posterior	-1.40 (11.17)^{h}	-17.66 (16.69)^{h}	52.51 (56.41)$^{\boldsymbol{h},j}$	7.23 (31.43)^{h,k}	-3.74 (24.19)^{h,l}	-11.44 (21.756)^{h}	
TASK×CHANNEL×TIME			t = 0 s	t = 0.5 s	t = 1 s	t = 1.5 s	t = 2 s	t = 2.5 s
F(20,120) = 1.78 *	ME-NoGo	anterior	-2.38 (12.85)^{a}	-4.99 (23.49)^{a}	82.76 (30.65)$^{\boldsymbol{a},l,s}$	20.87 (22.71)^{a,n}	5.64 (21.59)^{a,o}	-0.07 (19.04)^{a}
		lateral left	-11.20 (12.71)^{b,c}	-12.35 (20.97)^{b,c}	106.28 (55.13)$^{\boldsymbol{b},l,m,t}$	44.14 (32.17)^{b,c,n,v}	19.32 (25.38)^{b,o}	5.42 (37.94)^{b,c}
		Cz	-22.89 (21.88)^{d,e,f,g}	-35.04 (37.68)^{d,e,f,g}	221.59 (72.18)$^{\boldsymbol{d},\boldsymbol{l},w}$	103.07 (38.94)$^{d,\boldsymbol{e},\boldsymbol{n},x}$	61.39 (26.95)$^{d,e,\boldsymbol{f},\boldsymbol{o},y}$	18.63 (36.85)$^{d,e,f,\boldsymbol{g}}$
		lateral right	-8.12 (13.99)^{h,i}	-4.51 (30.04)^{h,i}	71.45 (44.24)$^{\boldsymbol{h},l,\boldsymbol{m},u}$	32.95 (47.77)$^{h,\boldsymbol{i},n}$	9.06 (19.70)^{h,o}	1.72 (31.24)^{h}
		posterior	-0.03 (12.15)^{j}	-13.79 (19.21)^{j,k}	95.32 (33.82)$^{\boldsymbol{j},l,m,z}$	27.31 (24.81)^{j,k,n,aa}	10.19 (21.92)^{j,o}	0.34 (17.01)^{j}
			t = 0 s	t = 0.5 s	t = 1 s	t = 1.5 s	t = 2 s	t = 2.5 s
	MI-NoGo	anterior	-0.38 (8.35)	-10.16 (19.80)	13.25 (35.97)^{r,s}	-12.29 (16.64)	-18.02 (13.63)	-20.25 (13.56)
		lateral left	-15.77 (20.88)	-23.21 (13.21)	14.37 (59.28)^{r,t}	-3.32 (29.83)^{v}	-3.69 (25.74)	-21.83 (19.31)
		Cz	-5.00 (21.73)^{p}	-37.60 (20.16)$^{p,\boldsymbol{q}}$	106.93 (74.30)$^{\boldsymbol{p},q,\boldsymbol{r},w}$	18.37 (33.95)^{p,q,x}	6.13 (21.17)^{p,q,y}	-10.40 (25.24)^{p}
		lateral right	-5.86 (21.62)	-13.35 (22.63)	16.16 (43.89)^{r,u}	-1.33 (33.12)	-3.72 (28.99)	-17.32 (26.36)
		posterior	-2.77 (10.88)	-21.53 (14.11)	9.51 (38.16)^{r,z}	-12.85 (24.16)^{aa}	-17.68 (18.29)	-23.23 (20.30)

Superscript letters within a factor or interaction section indicate significant differences.
Bold face superscript letters indicate greater/smaller than all others.
* indicates $p < 0.05$.
** indicates $p < 0.01$.
*** indicates $p < 0.001$.

Appendix B

A brain switch for the able-bodied—detailed information

The tables in this section provide detailed information on the individual TPR and FPR values of each participant, for the training (motor execution), calibration (motor imagery), and the simulation (evaluation) of an asynchronous brain switch operated through motor imagery of brisk dorsiflexion of both feet. According to Chapter 5, these tables represent the ERD-based classification, the ERS-based classification, and the classification focused on the detection of the beta rebound using a LDA as classifier.

Table B.1: Performance of the ERD-based classifier

ID	Training		Calibration	Evaluation	
	TPR	FPR	TPR	TPR	FPR
c1	0.58	0.12	0.17	0.25	0.11
c2	0.46	0.23	0.30	0.17	0.10
c3	0.52	0.14	0.13	0.05	0.06
c4	0.67	0.06	0.70	0.57	0.09
c5	0.92	0.04	0.60	0.55	0.15
c6*	0.29	0.18	0.13	0.12	0.08
c7*	0.36	0.18	0.23	0.23	0.11
c8	0.36	0.18	0.33	0.23	0.14
mean	0.52	0.14	0.32	0.27	0.11
s.d.	0.20	0.07	0.22	0.19	0.03

Naive participants marked with an asterisk (*).

Table B.2: Performance of the ERS-based classifier

ID	Training		Calibration	Evaluation	
	TPR	FPR	TPR	TPR	FPR
c1	0.76	0.03	0.97	0.88	0.02
c2	0.70	0.21	0.77	0.68	0.13
c3	0.73	0.07	0.70	0.63	0.09
c4	0.66	0.09	0.10	0.12	0.18
c5	0.37	0.15	0.37	0.37	0.10
c6*	0.52	0.09	0.33	0.50	0.10
c7*	0.43	0.13	0.43	0.25	0.09
c8	0.84	0.09	0.37	0.25	0.13
mean	0.63	0.11	0.51	0.46	0.11
s.d.	0.17	0.05	0.28	0.26	0.05

Naive participants marked with an asterisk (*).

Table B.3: Performance of the LDA-based classification.

ID	Training		Calibration		Evaluation	
	TPR	FPR	TPR	FPR	TPR	FPR
c1	0.96	0.05	0.97	0.07	0.92	0.05
c2	0.96	0.28	0.27	0.08	0.52	0.07
c3	0.93	0.11	0.63	0.07	0.53	0.05
c4	0.75	0.40	0.37	0.09	0.45	0.10
c5	0.97	0.33	0.27	0.06	0.50	0.07
c6*	0.93	0.20	0.33	0.09	0.53	0.12
c7*	0.93	0.27	0.67	0.07	0.38	0.07
c8	0.93	0.27	0.37	0.09	0.22	0.12
mean	0.92	0.24	0.49	0.08	0.51	0.08
s.d.	0.07	0.11	0.25	0.01	0.20	0.03

Naive participants marked with an asterisk (*).

Bibliography

[1] J. J. Vidal. Toward direct brain-computer communication. *Annual Review of Biophysics and Bioengineering*, 2:157–180, 1973.

[2] J. R. Wolpaw, N. Birbaumer, W. J. Heetderks, D. J. McFarland, P. Hunter Peckham, G. Schalk, E. Donchin, L. A. Quatrano, C. J. Robinson, and T. M. Vaughan. Brain-computer interface technology: a review of the first international meeting. *IEEE Transactions on Rehabilitation Engineering*, 8:164–173, 2000.

[3] L. A. Farwell and E. Donchin. Talking off the top of your head: toward a mental prosthesis utilizing event-related brain potentials. *Electroencephalography and Clinical Neurophysiology*, 70:510–523, 1988.

[4] N. Birbaumer, N. Ghanayim, T. Hinterberger, I. Iversen, B. Kotchoubey, A. Kübler, J. Perelmouter, E. Taub, and H. Flor. A spelling device for the paralysed. *Nature*, 398:297–298, 1999.

[5] G. Pfurtscheller, C. Guger, G. Müller, G. Krausz, and C. Neuper. Brain oscillations control hand orthosis in a tetraplegic. *Neuroscience Letters*, 292:211–214, 2000.

[6] C. Neuper, G. R. Müller, A. Kübler, N. Birbaumer, and G. Pfurtscheller. Clinical application of an EEG-based brain-computer interface: a case study in a patient with severe motor impairment. *Clinical Neurophysiology*, 114:399–409, 2003.

[7] G. Pfurtscheller, G. R. Müller, J. Pfurtscheller, H. J. Gerner, and R. Rupp. "Thought"-control of functional electrical stimulation to restore handgrasp in a patient with tetraplegia. *Neuroscience Letters*, 351:33–36, 2003.

[8] G. R. Müller-Putz, R. Scherer, G. Pfurtscheller, and R. Rupp. EEG-based neuroprosthesis control: a step towards clinical practice. *Neuroscience Letters*, 382:169–174, 2005.

[9] N. Birbaumer. Brain-computer interface research: coming of age. *Clinical Neurophysiology*, 117: 479–483, 2006.

[10] A. B. Schwartz, X. T. Cui, D. J. Weber, and D. W. Moran. Brain-controlled interfaces: movement restoration with neural prosthetics. *Neuron*, 52:205–220, 2006.

[11] J. R. Wolpaw. Brain-computer interfaces as new brain output pathways. *The Journal of Physiology*, 579:623–619, 2007.

[12] G. Pfurtscheller, G. Müller-Putz, R. Scherer, and C. Neuper. Rehabilitation with brain-computer interface systems. *IEEE Computer Magazine*, 41:58–65, 2008.

[13] N. Birbaumer, A. R. Murguialday, C. Weber, and P. Montoya. Neurofeedback and brain-computer interface: clinical applications. *International Review of Neurobiology*, 86:107–117, 2009.

[14] J. del R. Millán, R. Rupp, G. R. Müller-Putz, R. Murray-Smith, C. Giugliemma, M. Tangermann, C. Vidaurre, F. Cincotti, A. Kübler, R. Leeb, C. Neuper, K.-R. Müller, and D. Mattia. Combining brain-computer interfaces and assistive technologies: state-of-the-art and challenges. *Frontiers in Neuroscience*, 4:12, 2010.

[15] J. Münßinger, S. Halder, S. Kleih, A. Furdea, V. Raco, A. Hösle, and A. Kübler. Brain painting: first evaluation of a new brain-computer interface application with ALS-patients and healthy volunteers. *Frontiers in Neuroprosthetics*, 4:182, 2010.

[16] J. del R. Millán, F. Renkens, J. Mouri no, and W. Gerstner. Noninvasive brain-actuated control of a mobile robot by human EEG. *IEEE Transactions on Biomedical Engineering*, 51:1026–1033, 2004.

[17] E. C. Lalor, S. P. Kelly, C. Finucane, R. Burke, R. Smith, R. B. Reilly, and G. McDarby. Steady-state VEP-based brain-computer interface control in an immersive 3D gaming environment. *EURASIP Journal on Applied Signal Processing*, 19:3156–3164, 2005.

[18] R. Leeb, C. Keinrath, D. Friedman, C. Guger, R. Scherer, C. Neuper, M. Garau, A. Antley, A. Steed, M. Slater, and G. Pfurtscheller. Walking by thinking: the brainwaves are crucial, not the muscles! *Presence: Teleoperators and Virtual Environments*, 15:500–514, 2006.

[19] G. Pfurtscheller, R. Leeb, C. Keinrath, D. Friedman, C. Neuper, C. Guger, and M. Slater. Walking from thought. *Brain Research*, 1071:145–152, 2006.

[20] A. Lécuyer, F. Lotte, R. B. Reilly, R. Leeb, M. Hirose, and M. Slater. Brain-computer interfaces, virtual reality and videogames. *Computer*, 41:66–72, 2008.

[21] A. Nijholt. BCI for games: a 'state of the art' survey. In S. Stevens and S. Saldamarco, editors, *Entertainment Computing - ICEC 2008*, pages 225–228. Springer Berlin/Heidelberg, 2009.

[22] J. J. Daly and J. R. Wolpaw. Brain-computer interfaces in neurological rehabilitation. *The Lancet Neurology*, 7:1032–1043, 2008. Review of BCIs in neurological rehabilitation.

[23] G. Prasad, P. Herman, D. Coyle, S. McDonough, and J. Crosbie. Applying a brain-computer interface to support motor imagery practice in people with stroke for upper limb recovery: a feasibility study. *Journal of Neuroengineering and Rehabilitation*, 7:60, 2010.

[24] W. Wang, J. L. Collinger, M. A. Perez, E. C. Tyler-Kabara, L. G. Cohen, N. Birbaumer, S. W. Brose, A. B. Schwartz, M. L. Boninger, and D. J. Weber. Neural interface technology for rehabilitation exploiting and promoting neuroplasticity. *Physical Medicine and Rehabilitation Clinics of North America*, 21:157–178, 2010.

[25] J.-M. Belda-Lois, Mena-del Horno S, Bermejo-Bosch I, C. Moreno J, J. L. Pons, D. Farina, M. Iosa, M. Molinari, F. Tamburella, A. Ramos, A. Caria, T. Solis-Escalante, C. Brunner, and M. Rea. Rehabilitation of gait after stroke: a review towards a top-down approach. *Journal of NeuroEngineering and Rehabilitation*, 8:66, 2011.

[26] D. Cruse, S. Chennu, C. Chatelle, T. A. Bekinschtein, D. Fernández-Espejo, J. D. Pickard, S. Laureys, and A. M. Owen. Bedside detection of awareness in the vegetative state: a cohort study. *Lancet*, 378:2088–2094, 2011.

[27] F. Pichiorri, F. D. V. Fallani, F. Cincotti, F. Babiloni, M. Molinari, S. C. Kleih, C. Neuper A. Kübler, and D. Mattia. Sensorimotor rhythm-based brain-computer interface training: the impact on motor cortical responsiveness. *Journal of Neural Engineering*, 8:025020, 2011.

[28] B. Z. Allison, C. Brunner, V. Kaiser, G. R. Müller-Putz, C. Neuper, and G. Pfurtscheller. Toward a hybrid brain-computer interface based on imagined movement and visual attention. *Journal of Neural Engineering*, 7:026007, 2010.

[29] G. Pfurtscheller, B. Z. Allison, C. Brunner, G. Bauernfeind, T. Solis-Escalante, R. Scherer, T. O. Zander, G. Müller-Putz, C. Neuper, and N. Birbaumer. The hybrid BCI. *Frontiers in Neuroscience*, 4:30, 2010.

[30] R. Leeb, H. Sagha, R. Chavarriaga, and J. del R. Millán. A hybrid brain-computer interface based on the fusion of electroencephalographic and electromyographic activities. *Journal of Neural Engineering*, 8:025011, 2011.

[31] G. R. Müller-Putz, C. Breitwieser, F. Cincotti, R. Leeb, M. Schreuder, F. Leotta, M. Tavella, L. Bianchi, A. Kreillinger, A. Ramsay, M. Rohm, M. Sagebaum, L. Tonin, C. Neuper, and J. del R. Millán. Tools for brain-computer interaction: a general concept for a hybrid BCI. *Frontiers in Neuroinformatics*, 5:30, 2011.

[32] B. Allison, R. Leeb, C. Brunner, G. R. Müller-Putz, G. Bauernfeind, J. W. Kelly, and C. Neuper. Toward smarter BCIs: extending BCIs through hybridization and intelligent control. *Journal of Neural Engineering*, 9:013301, 2012.

[33] B. Graimann. *Movement-related patterns in ECoG and EEG: visualization and detection.* PhD thesis, Graz University of Technology, 2002.

[34] G. Pfurtscheller and C. Neuper. Motor imagery and direct brain-computer communication. *Proceedings of the IEEE*, 89:1123–1134, 2001.

[35] C. Guger, G. Edlinger, W. Harkam, I. Niedermayer, and G. Pfurtscheller. How many people are able to operate an EEG-based brain-computer interface (BCI)? *IEEE Transactions on Neural Systems and Rehabilitation Engineering*, 11:145–147, 2003.

[36] T. Dickhaus, C. Sanelli, K-R. Müller, G. Curio, and B. Blankertz. Predicting BCI performance to study BCI illiteracy. *BMC Neuroscience*, 10(Suppl 1):P84, 2009.

[37] C. Guger, S. Daban, E. Sellers, C. Holzner, G. Krausz, R. Carabalona, F. Gramatica, and G. Edlinger. How many people are able to control a P300-based brain-computer interface (BCI)? *Neuroscience Letters*, 462:94–98, 2009.

[38] B. Allison, T. Lüth, D. Valbuena, A. Teymourian, I. Volosyak, and A. Gräser. BCI demographics: how many (and what kinds of) people can use an SSVEP BCI? *IEEE Transactions on Neural Systems Rehabilitation Engineering*, 18:107–113, 2010.

[39] C. Vidaurre, A. Schlögl, R. Cabeza, R. Scherer, and G. Pfurtscheller. A fully on-line adaptive BCI. *IEEE Transactions on Biomedical Engineering*, 53:1214–1219, 2006.

[40] C. Vidaurre and B. Blankertz. Towards a cure for BCI illiteracy. *Brain Topography*, 23:194–198, 2010.

[41] J. Faller, C. Vidaurre, T. Solis-Escalante, C. Neuper, and R. Scherer. Autocalibration and recurrent adaptation: Towards a plug and play online ERD-BCI. *IEEE Transactions on Neural Systems Rehabilitation Engineering*, In Press, 2012.

[42] S. G. Mason, A. Bashashati, M. Fatourechi, K. F. Navarro, and G. E. Birch. A comprehensive survey of brain interface technology designs. *Annals of Biomedical Engineering*, 35:137–169, 2007.

[43] Future BNCI (EU-Project number ICT 2010-248320). Future BNCI: A roadmap for future directions in brain/neuronal computer interaction reseach, 2011. URL `http://future-bnci.org/images/stories/Future_BNCI_Roadmap.pdf`.

[44] J. D. Simeral, S-P. Kim, M. J. Black, J. P. Donoghue, and L. R. Hochberg. Neural control of cursor trajectory and click by a human with tetraplegia 1000 days after implant of an intracortical microelectrode array. *Journal of Neural Engineering*, 8:1–24, 2011.

[45] J. R. Wolpaw. Brain-computer interface research comes of age: traditional assumptions meet emerging realities. *Journal of Motor Behaviour*, 42:351–353, 2010.

[46] D. J. McFarland, W. A. Sarnacki, and J. R. Wolpaw. Electroencephalographic (EEG) control of three-dimensional movement. *Journal of Neural Engineering*, 7:036007, 2010.

[47] A. J. Doud, J. P. Lucas, M. T. Pisansky, and B. He. Continuous three-dimensional control of a virtual helicopter using a motor imagery based brain-computer interface. *PLoS ONE*, 6:e26322, 2011.

[48] S. M. Laconte. Decoding fMRI brain states in real-time. *Neuroimage*, 56:440–454, 2011.

[49] A. Owen, M. Coleman, M. Boly, M. Davis, S. Laureys, and J. Pickard. Detecting awareness in the vegetative state. *Science*, 313:1402, 2006.

[50] R. Sitaram, A. Caria, R. Veit, T. Gaber, G. Rota, A. Kübler, and N. Birbaumer. fMRI brain-computer interface: a tool for neuroscientific research and treatment. *Computational Intelligence and Neuroscience*, 2007:25487, 2007.

[51] R. Sitaram, N. Weiskopf, A. Caria, R. Veit, M. Erb, and N. Birbaumer. fMRI brain-computer interfaces. *IEEE Signal Processing Magazine*, 25:95–106, 2008.

[52] X. Cui, S. Bray, D. M. Bryant, G. H. Glover, and A. L. Reiss. A quantitative comparison of NIRS and fMRI across multiple cognitive tasks. *Neuroimage*, 54:2808–2821, 2010.

[53] S. Coyle, T. Ward, C. Markham, and G. McDarby. On the suitability of near-infrared (NIR) systems for next-generation brain-computer interfaces. *Physiological Measurement*, 25:815–822, 2004.

[54] S. M. Coyle, T. E. Ward, and C. M. Markham. Brain-computer interface using a simplified functional near-infrared spectroscopy system. *Journal of Neural Engineering*, 4:219–226, 2007.

[55] R. Sitaram, H. Zhang, C. Guan, M. Thulasidas, Y. Hoshi, A. Ishikawa, K. Shimizu, and N. Birbaumer. Temporal classification of multichannel near-infrared spectroscopy signals of motor imagery for developing a brain-computer interface. *Neuroimage*, 34:1416–1427, 2007.

[56] G. Bauernfeind, R. Leeb, S. Wriessnegger, and G. Pfurtscheller. Development, set-up and first results of a one-channel near-infrared spectroscopy system. *Biomedizinische Technik*, 53:36–43, 2008.

[57] G. Bauernfeind, R. Scherer, G. Pfurtscheller, and C. Neuper. Single-trial classification of antagonistic oxyhemoglobin responses during mental arithmetic. *Medical and Biological Engineering and Computing*, 49:979–984, 2011.

[58] F. H. Lopes da Silva. Event-related potentials: methodology and quantification. In E. Niedermayer and F. H. Lopes da Silva, editors, *Electroencephalography: basic principles, clinical applications and related fields*, pages 991–1001. Williams & Wilkins, 2005.

[59] D. Regan. *Human brain electrophysiology: evoked potentials and evoked magnetic fields in science and medicine*. Elsevier, 1989.

[60] G. Pfurtscheller and A. Aranibar. Evaluation of event-related desynchronization (ERD) preceding and following voluntary self-paced movements. *Electroencephalography and Clinical Neurophysiology*, 46:138–146, 1979.

[61] J. Kalcher and G. Pfurtscheller. Discrimination between phase-locked and non-phase-locked event-related EEG activity. *Electroencephalography and Clinical Neurophysiology*, 94:381–384, 1995.

[62] G. Pfurtscheller and F. H. Lopes da Silva. Event-related EEG/MEG synchronization and desynchronization: basic principles. *Clinical Neurophysiology*, 110:1842–1857, 1999.

[63] G. Dornhege, J. del R. Millán, T. Hinterberger, D. McFarland, and K.-R. Müller, editors. *Toward Brain-Computer Interfacing*. MIT Press, 2007.

[64] G. Pfurtscheller. Central beta rhythm during sensorimotor activities in man. *Electroencephalography and Clinical Neurophysiology*, 51:253–264, 1981.

[65] R. Salmelin, M. Hamalainen, M. Kajola, and R. Hari. Functional segregation of movement related rhythmic activity in the human brain. *Neuroimage*, 2:237–243, 1995.

[66] C. Neuper and G. Pfurtscheller. Post movement synchronization of beta rhythms in the EEG over the cortical foot area in man. *Neuroscience Letters*, 216:17–20, 1996.

[67] G. Pfurtscheller, K. Zalaudek, and C. Neuper. Event-related beta synchronization after wrist, finger and thumb movement. *Electroencephalography and Clinical Neurophysiology*, 9:154–160, 1998.

[68] G. Pfurtscheller, C. Neuper, and J. Kalcher. 40 Hz oscillations during motor behavior in man. *Neuroscience Letters*, 162:179–182, 1993.

[69] S. Salenius, R. Salmelin, C. Neuper, G. Pfurtscheller, and R. Hari. Human cortical 40 Hz rhythm is closely related to EMG rhythmicity. *Neuroscience Letters*, 213:75–78, 1996.

[70] G. Pfurtscheller and C. Neuper. Event-related synchronization of mu rhythm in the EEG over the cortical hand area in man. *Neuroscience Letters*, 174:93–96, 1994.

[71] P. Suffczynski, P. J. M. Pijn, G. Pfurtscheller, and F. H. Lopes da Silva. Event-related dynamics of alpha band rhythms: a neuronal network model of focal ERD/surround ERS. In G. Pfurtscheller and F.H. Lopes da Silva, editors, *Event-Related Desynchronization*, volume 6 of *Handbook of Electroencephalography and Clinical Neurophysiology*, chapter 5, pages 67–85. Elsevier Science, 1999.

[72] G. Pfurtscheller and F. H. Lopes da Silva. Event-related desynchronization (ERD) and event-related synchronization (ERS). In *Electroencephalography: basic principles, clinical applications and related fields*. Williams & Wilkins, 2005.

[73] G. Pfurtscheller, G. Bauernfeind, S. C. Wriessnegger, and C. Neuper. Focal frontal (de)oxyhemoglobin responses during simple arithmetic. *International Journal of Psychophysiology*, 76:186–192, 2010.

[74] H. H. Ehrsson, S. Geyer, and E. Naito. Imagery of voluntary movement of fingers, toes, and tongue activates corresponding body-part-specific motor representations. *Journal of Neurophysiology*, 90: 3304–3316, 2003.

[75] S. G. Mason and G. E. Birch. A brain-controlled switch for asynchronous control applications. *IEEE Transactions on Biomedical Engineering*, 47:1297–1307, 2000.

[76] C. Neuper and G. Pfurtscheller. Evidence for distinct beta resonance frequencies in human EEG related to specific sensorimotor cortical areas. *Clinical Neurophysiology*, 112:2084–2097, 2001.

[77] G. Pfurtscheller, C. Neuper, K. Pichler-Zalaudek, G. Edlinger, and F. H. Lopes da Silva. Do brain oscillations of different frequencies indicate interaction between cortical areas in humans? *Neuroscience Letters*, 286:66–68, 2000.

[78] R. Chen, Z. Yassen, L. G. Cohen, and M. Hallett. The time course of corticospinal excitability in reaction time and self-paced movements. *Annals of Neurology*, 44:317–325, 1998.

[79] R. Salmelin and R. Hari. Spatiotemporal characteristics of sensorimotor neuromagnetic rhythms related to thumb movement. *Neuroscience*, 60:537–550, 1994.

[80] G. Pfurtscheller, A. Stancák Jr., and G. Edlinger. On the existence of different types of central beta rhythms below 30 Hz. *Electroencephalography and Clinical Neurophysiology*, 102:316–325, 1997.

[81] R. Hari and R. Salmelin. Human cortical oscillations: a neuromagnetic view through the skull. *Trends in Neurosciences*, 20:44–49, 1997.

[82] M. van Burik and G. Pfurtscheller. Functional imaging of postmovement beta event-related synchronization. *Journal of Clinical Neurophysiology*, 16:383–390, 1999.

[83] S. Ohara, A. Ikeda, T. Kunieda, S. Yazawa, K. Baba, T. Nagamine, W. Taki, N. Hashimoto, T. Mihara, and H. Shibasaki. Movement-related change of electrocorticographic activity in human supplementary motor area proper. *Brain*, 123:1203–1215, 2000.

[84] G. Pfurtscheller, M. Wörtz, G. Supp, and F. H. Lopes da Silva. Early onset of post-movement beta electroencephalogram synchronization in the supplementary motor area during self-paced finger movement in man. *Neuroscience Letters*, 339:111–114, 2003.

[85] M. T. Jurkiewicz, W. C. Gaetz, A. C. Bostan, and D. Cheyene. Post-movement beta rebound is generated in motor cortex: evidence from neuromagnetic recordings. *Neuroimage*, 32:1281–1289, 2006.

[86] M. Alegre, I. G. Gurtubay, A. Labarga, J. Iriarte, M. Valencia, and J. Artieda. Frontal and central oscillatory changes related to different aspects of the motor process: a study in go/no-go paradigms. *Experimental Brain Research*, 159:14–22, 2004.

[87] T. Koelewijn, H. T. van Schie, H. Bekkering, R. Oostenveld, and O. Jensen. Motor-cortical beta oscillations are modulated by correctnes of observed action. *Neuroimage*, 40:767–775, 2008.

[88] M. Alegre, A. Labarga, I. G. Gurtubay, J. Iriarte, A. Malanda, and J. Artieda. Beta electroencephalograph changes during passive movements: sensory afferences contribute to beta event-related desynchronization in humans. *Neuroscience Letters*, 331:29–32, 2002.

[89] R. Chen, B. Corwell, and M. Hallett. Modulation of motor cortex excitability by median nerve and digit stimulation. *Expert Review of Brain Research*, 129:77–86, 1999.

[90] S. Salenius, Schnitzler A, R. Salmelin, V. Jousmäki, and R. Hari. Modulation of human cortical rolandic rhythms during natural sensorimotor tasks. *Neuroimage*, 5:221–228, 1997.

[91] A. Schnitzler, S. Salenius, R. Salmelin, V. Jousmäki, and R. Hari. Involvement of primary motor cortex in motor imagery: a neuromagnetic study. *Neuroimage*, 6:201–208, 1997.

[92] R. Hari, N. Forss, S. Avikainen, E. Kirveskari, S. Salenius, and G. Rizzolatti. Activation of human primary motor cortex during action observation: a neuromagnetic study. *Proceedings of the National Academy of Sciences*, 95:15061–15065, 1998.

[93] G. Pfurtscheller, M. Wörtz, G. R. Müller, S. Wriessnegger, and K. Pfurtscheller. Contrasting behavior of beta event-related synchronization and somatosensory evoked potential after median nerve stimulation during finger manipulation in man. *Neuroscience Letters*, 323:113–116, 2002.

[94] J. Järveläinen, M. Schürmann, and R. Hari. Activation of the human primary motor cortex during observation of tool use. *Neuroimage*, 23:187–192, 2004.

[95] L. M. Parkes, M. C. M. Bastiaansen, and D. G. Norris. Combining EEG and fMRI to investigate the post-movement beta rebound. *Neuroimage*, 29:685–696, 2006.

[96] P. Ritter, M. Moosmann, and A. Villringer. Rolandic alpha and beta EEG rythms' strengths are inversely related to fMRI-BOLD signal in primary somatosensory and motor cortex. *Human Brain Mapping*, 30:1168–1187, 2009.

[97] H. Yuan, T. Liu, R. Szarkowski, C. Rios, J. Ashe, and B. He. Negative covariation between task-related responses in alpha/beta-band activiry and BOLD in human sensorimotor cortex: an EEG and fMRI study of motor imagery and movements. *Neuroimage*, 49:2596–2606, 2010.

[98] O. Jensen, P. Goel, N. Kopell, M. Pohja, R. Hari, and B. Ermentrout. On the human sensorimotor-cortex beta rhythm: sources and modeling. *Neuroimage*, 26:347–355, 2005.

[99] W. Gaetz, J.C. Edgar, D.J. Wang, and T.P.L. Roberts. Relating MEG measured motor cortocal oscillations to resting γ-Aminobutyric acid (GABA) concentration. *Neuroimage*, 55:616–621, 2011.

[100] S. D. Hall, I. M. Stanford, N. Yamawaki, C. J. McAllister, K. C. Rönnqvist, G. L. Woodhall, and P. L. Furlong. The role of GABAergic modulation in motor function related neuronal network activity. *Neuroimage*, 56:506–1510, 2011.

[101] T. Silén, N. Forss, O. Jensen, and R. Hari. Abnormal reactivity of the $\sim$20-Hz motor cortex rhythm in Unverricht Lundborg type progressive myoclonus epilepsy. *Neuroimage*, 12:707–712, 2000.

[102] E. Visani, L. Minati, L. Canafoglia, L. Gilioli, A. Granvillano, G. Varotto, D. Aquino, P. Fazio, M. G. Bruzzone, and S. Franceschetti. Abnormal ERD/ERS but unnaffected BOLD response in patients with Unverricht-Lundborg disease during index extension: a simultaneous EEG-fMRI study. *Brain Topography*, 24:65–77, 2011.

[103] F. Cassim, W. Szurhaj, H. Sediri, D. Devos, J.-L. Bourriez, I. Poirot, P. Derambure, L Defebvre, and J.-D. Guieu. Brief and sustained movement: differences in event-related (de)syncrhonization (ERD/ERS) patterns. *Clinical Neurophysiology*, 111:2032–2039, 2000.

[104] F. Cassim, C. Monaca, W. Szurhaj, J.-L. Bourriez, L. Defebvre, P. Derambure, and J.-D. Guieu. Does post-movement beta synchronization reflect an idling motor cortex? *Neuroreport*, 12:3859–3863, 2001.

[105] G. Pfurtscheller, G. Krausz, and C. Neuper. Mechanical stimulation of the fingertip can induce bursts of beta oscillations in sensorimotor areas. *Journal of Clinical Neurophysiology*, 18:559–564, 2001.

[106] E. Houdayer, E. Labyt, F. Cassim, J. L. Boussiez, and Ph. Derambure. Relationship between event-related beta synchronization and afferent inputs: analysis of finger movement and peripheral nerve stimulations. *Clinical Neurophysiology*, 117:628–636, 2006.

[107] G. Caetano, V. Jousmäki, and R. Hari. Actor's and observer's primary motor cortices stabilize similarly after seen or heard motor actions. *Proceedings of the National Academy of Sciences*, 104: 9058–9062, 2007.

[108] N. Reyns, E. Houdayer, J.L. Bourriez, S. Blond, and P. Derambure. Post-movemement beta synchronization in subjects presenting with sensory deafferentiation. *Clinical Neurophysiology*, 119: 1335–1345, 2008.

[109] A. Degardin, E. Houdayer, J-L. Bourriez, A. Destée, L. Defebvre, P. Derambure, and D. Devos. Deficient "sensory" beta synchronization in Parkinson's disease. *Clinical Neurophysiology*, 120:636–642, 2009.

[110] K. Gourab and B. D. Schmit. Changes in movement-related beta-band EEG signals in human spinal cord injury. *Clinical Neurophysiology*, 121:2017–2023, 2010.

[111] W. Gaetz, M. MacDonald, D. Cheyne, and O. C. Sinead. Neuromagnetic imaging of movement-related cortical oscillations in children and adults: age predicts post-movement beta rebound. *Neuroimage*, 51:792–807, 2010.

[112] G. Pfurtscheller, C. Neuper, C. Brunner, and F. H. Lopes da Silva. Beta rebound after different types of motor imagery in man. *Neuroscience Letters*, 378:156–159, 2005.

[113] T. Shibata, I. Shimoyama, T. Ito, D. Abla, H. Iwasa, K. Koseki, N. Yamanouchi, T. Sato, and Y. Nakajima. Event-related dynamics of the gamma-band oscillation in the human brain: information processing during a GO/NOGO hand movement tasks. *Neuroscience reseach*, 33:215–222, 1999.

[114] L. Leocani, C. Toro, P. Zhuang, C. Gerloff, and M. Hallet. Event-related desynchronization in reaction time paradigms: a comparison with event-related potentials and corticospinal excitability. *Clinical Neurophysiology*, 112:923–930, 2001.

[115] A. K. Engel and P. Fries. Beta-band oscillations – signaling the status quo? *Current Opinion in Neurobiology*, 20:156–165, 2010.

[116] A. Stancák and G. Pfurtscheller. Desynchronization and recovery of β rhythms during brisk and slow self-paced finger movements in man. *Neuroscience Letters*, 196:21–24, 1995.

[117] M. Alegre, A. Labarga, I. García de Gurtubay, J. Iriarte, A. Malanda, and J. Artieda. Movement-related changes in cortical oscillatory activity in ballistic, sustained and negative movements. *Experimental Brain Research*, 148:17–25, 2003.

[118] N. Erbil and P. Ungan. Changes in the alpha and beta amplitudes of the central EEG during the onset, continuation, and offset of long-duration repetitive hand movements. *Brain Research*, 1169: 44–56, 2007.

[119] K. Blinowska, R. Kus, M. Kaminski, and J. Janiszewska. Transmission of brain activity during cognitive task. *Brain Topography*, 23:205–213, 2010.

[120] Y. Zhang, Y. Chen, L. Bressler, and M. Ding. Response preparation and inhibition: the role of the cortical sensorimotor beta rhythms. *Neuroscience*, 156:238–246, 2008.

[121] A. Stancák Jr., A. Rimi, and G. Pfurtscheller. The effects of external load on movement-related changes of the sensorimotor EEG rhythms. *Electroencephalography and Clinical Neurophysiology*, 102:495–504, 1997.

[122] A. Stancák Jr. and G. Pfurtscheller. Event-related desynchronization of central beta-rhythms during brisk and slow self-paced finger movements of dominant and nondominant hand. *Cognitive Brain Research*, 4:171–183, 1996.

[123] C. Keinrath, S. Wriessnegger, G. R. Müller-Putz, and G. Pfurtscheller. Post-movement beta synchronization after kinesthetic illusion, active and passive movements. *International Journal of Psychophysiology*, 62:321–327, 2006.

[124] G. R. Müller-Putz, D. Zimmermann, B. Graimann, K. Nestinger, G. Korisek, and G. Pfurtscheller. Event-related beta EEG-changes during passive and attempted foot movements in paraplegic patients. *Brain Research*, 1137:84–91, 2007.

[125] G. R. Müller, C. Neuper, R. Rupp, C. Keinrath, H. J. Gerner, and G. Pfurtscheller. Event-related beta EEG changes during wrist movements induced by functional electrical stimulation of forearm muscles in man. *Neuroscience Letters*, 340:143–147, 2003.

[126] W. Gaetz and D. Cheyene. Localization of sensorimotor cortical rhythms induced by tactile stimulation using spatially filtered MEG. *Neuroimage*, 30:899–908, 2006.

[127] G. Rizzolatti, L. Fadiga, V. Gallese, and L. Fogassi. Premotor cortex and the recognition of motor actions. *Cognitive Brain Research*, 3:131–141, 1996.

[128] G. Rizzolatti, L. Fogassi, and V. Gallese. Neurophysiological mechanisms underlying the understanding and imitation of action. *Nature Reviews Neuroscience*, 2:661–670, 2001.

[129] S. D. Muthukumaraswamy and B. W. Johnson. Primary motor cortex activation during action observation revealed by wavelet analysis of the EEG. *Clinical Neurophysiology*, 115:1760–1766, 2004.

[130] C. Babiloni, F. Babiloni, F. Carducci, F. Cincotti, G. Cocozza, C. Del Percio, D. V. Moretti, and P. M. Rossini. Human cortical electroencephalography (EEG) rhythms during the observation of simple aimless movements: a high-resolution EEG study. *Neuroimage*, 17:559–572, 2002.

[131] E. Honaga, R. Ishii, R. Kurimoto, L. Canuet, K. Ikezawa, H. Takahashi, T. Nakahachi, M. Iwase, I. Mizuta, T. Yoshimine, and M. Takeda. Post-movement beta rebound abnormality as indicator of mirror neuron system dysfunction in autistic spectrum disorder: an MEG study. *Neuroscience Letters*, 478:141–145, 2010.

[132] M. U. Trenner, H. R. Heekeren, M. Bauer, K. Rössner, R. Wenzel, A. Villringer, and M. Fahle. What happens in between? human oscillatory brain activity related to crossmodal spatial cueing. *PLoS ONE*, 1:e1467, 2008.

[133] J. Decety. The neurophysiological basis of motor imagery. *Behavioural Brain Research*, 77:45–52, 1996.

[134] G. Pfurtscheller. EEG event-related desynchronization (ERD) and synchronization (ERS). *Electroencephalography and Clinical Neurophysiology*, 103:26, 1997.

[135] C. Neuper and G. Pfurtscheller. Event-related dynamics of cortical rhythms: frequency-specific features and functional correlates. *International Journal of Psychophysiology*, 43:41–58, 2001.

[136] G. Pfurtscheller, G. R. Müller-Putz, J . Pfurtscheller, and R. Rupp. EEG-based asynchronous BCI controls functional electrical stimulation in a tetraplegic patient. *EURASIP Journal on Applied Signal Processing*, 19:3152–3155, 2005.

[137] A. Ikeda, H. O. Lüders, R. C. Burgess, and H. Shibasaki. Movement-related potentials recorded from supplementary motor area and primary motor area – role of supplementary motor area in voluntary movements. *Brain*, 115:1017–1043, 1992.

[138] E. Walsh, S. Kühn, M. Brass, D. Wenke, and P. Haggard. EEG activations during intentional inhibition of voluntary action: an electrophysiological correlate of self-control? *Neuropsychologia*, 48:619–626, 2010.

[139] T. Solis-Escalante, G. R. Müller-Putz, G. Pfurtscheller, and C. Neuper. Cue-induced beta rebound during withholding of overt and covert foot movement. *Clinical Neurophysiology*, 123:1182–1190, 2012.

[140] B. Hjorth. An on-line transformation of EEG scalp potentials into orthogonal source derivations. *Electroencephalography and Clinical Neurophysiology*, 39:526–530, 1975.

[141] A. Guillot, F. Lebon, D. Rouffet, S. Champely, J. Doyon, and C. Collet. Muscular responses during motor imagery as a function of muscle contraction types. *International Journal of Psychophysiology*, 66:18–27, 2007.

[142] B. Graimann, J. E. Huggins, S. P. Levine, and G. Pfurtscheller. Visualization of significant ERD/ERS patterns in multichannel EEG and ECoG data. *Clinical Neurophysiology*, 113:43–47, 2002.

[143] A. Schlögl and C. Brunner. BioSig: a free and open source software library for BCI research. *IEEE Computer Magazine*, 41:44–50, 2008.

[144] M. Alegre, I. García de Gurtubay, A. Labarga, J. Iriarte, A. Malanda, and J. Artieda. Alpha and beta oscillatory changes during stimulus-induced movement paradigms: effect of stimulus predictability. *Neuroreport*, 14:381–385, 2003.

[145] C. Tzagarakis, N. F. Ince, A. C. Leuthold, and G. Pellizzer. Beta-band activity during motor planning reflects response uncertainty. *The Journal of Neuroscience*, 30(34):11270–11277, Aug 2010. doi: 10.1523/JNEUROSCI.6026-09.2010. URL `http://dx.doi.org/10.1523/JNEUROSCI.6026-09.2010`.

[146] S. P. Levine, J. E. Huggins, S. L. BeMent, R. K. Kushwaha, L. A. Schuh, M. M. Rohde, E. A. Passaro, D. A. Ross, K. V. Elisevich, and B. J. Smith. A direct brain interface based on event-related potentials. *IEEE Transactions on Rehabilitation Engineering*, 8:180–185, 2000.

[147] J. Kaiser, J. Perelmouter, I. H. Iversen, N. Neumann, N. Ghanayim, T. Hinterberger, A. Kübler, B. Kotchoubey, and N. Birbaumer. Self-initiation of EEG-based communication in paralized patients. *Clinical Neurophysiology*, 112:551–554, 2001.

[148] M. Cheng, X. Gao, S. Gao, and D. Xu. Design and implementation of a brain-computer interface with high transfer rates. *IEEE Transactions on Neural Systems and Rehabilitation Engineering*, 49: 1181–1186, 2002.

[149] G. Bauernfeind, R. Ortner, P. Linortner, C. Neuper, and G. Pfurtscheller. Self-activation of an SSVEP-based orthosis control using near-infrared spectroscopy (NIRS). In *Proceedings of the BBCI Workshop 2009*, 2009.

[150] L. Deecke, B. Grözinger, and H. H. Kornhuber. Voluntary finger movement in man: cerebral potentials and theory. *Biological Cybernetics*, 23:99–119, 1976.

[151] G. Barrett, H. Shibasaki, and R. Neshige. Cortical potentials preceding voluntary movement: evidence for three periods of preparation in man. *Electroencephalography and Clinical Neurophysiology*, 63:327–339, 1986.

[152] G. E. Birch, Z. Bozorgzadeh, and S. G. Mason. Initial on-line evaluations of the LF-ASD brain-computer interface with able-bodied and spinal-cord subjects using imagined voluntary motor potentials. *IEEE Transactions on Neural Systems and Rehabilitation Engineering*, 10:219–224, 2002.

[153] J. Borisoff, S. G. Mason, A. Bashashati, and G. E. Birch. Brain-computer interface design for asynchronous control applications: improvements to the LF-ASD asynchronous brain switch. *IEEE Transactions on Biomedical Engineering*, 51:985–992, 2004.

[154] A. Bashashati, S. Mason, R. K. Ward, and G. E. Birch. An improved asynchronous brain interface: making use of the temporal history of the LF-ASD feature vectors. *Journal of Neural Engineering*, 3:87–94, 2006.

[155] M. Fatourechi, S. Mason, G. Birch, and R. Ward. Is information transfer rate a suitable performance measure for self-paced Brain interface systems? In *IEEE International symposium on Signal Processing and Information Technology*, 2006.

[156] M. Fatourechi, R. K. Ward, and G. E. Birch. A self-paced brain-computer interface system with a low false positive rate. *Journal of Neural Engineering*, 5:9–23, 2008.

[157] M. Fatourechi, R. K. Ward, and G. E. Birch. Performance of a self-paced brain computer interface on data contaminated with eye-movement artifacts and on data recorded in a subsequent session. *Computational Intelligence in Neuroscience*, 2008 ID 749204:1–13, 2008.

[158] F. Faradji, R. K. Ward, and G. E. Birch. Plausibility assessment of a 2-state self-paced mental task-based BCI using the no-control performance analysis. *Journal of Neuroscience Methods*, 180: 330–339, 2009.

[159] F. Faradji, R. K. Ward, and G. E. Birch. Toward development of a two-state brain–computer interface based on mental tasks. *Journal of Neural Engineering*, 8:046014, 2011.

[160] E. Yom-Tov and G. F. Inbar. Detection of movement-related potentials from the electroencephalogram for possible use in a brain-computer interface. *Medical and Biological Engineering and Computing*, 41:85–93, 2003.

[161] A. T. Boye, U. Q. Kristiansen, M. Billinger, O. Feix do Nascimento, and D. Farina. Identification of movement-related cortical potentials with optimized spatial filtering and principal component analysis. *Biomedical Signal Processing and Control*, 3:300–304, 2008.

[162] I. K. Niazi, N. Jiang, O. Tiberghien, J. F. Nielsen, K. Dremstrup, and D. Farina. Detection of movement intention from single-trial movement-related cortical potentials. *Journal of Neural Engineering*, 8:066009, 2011.

[163] B. A. S. Hasan and J. Q. Gan. Unsupervised movement onset detection from EEG recorded during self-paced real hand movement. *Medical and Biological Engineering and Computing*, 48:245–253, 2010.

[164] B. Graimann, J. E. Huggins abd A. Schlögl, S. P. Levine, and G. Pfurtscheller. Detection of movement-related desynchronization patterns in ongoing single-channel electrocorticogram. *IEEE Transactions on Neural Systems and Rehabilitation Engineering*, 11:276–281, 2003.

[165] G. Townsend, B. Graimann, and G. Pfurtscheller. Continuous EEG classification during motor imagery – simulation of an asynchronous BCI. *IEEE Transactions on Neural Systems and Rehabilitation Engineering*, 12:258–265, 2004.

[166] M. W. Keith, P. H. Peckham, G. B. Thorpe, K. C. Stroh, B. Smith, J. R. Buckett, K. L. Kilgore, and J. W. Jatich. Implantable functional neuro-muscular stimulation in the tetraplegic hand. *The Journal of Hand Surgery*, 14:524–530, 1989.

[167] G. R. Müller-Putz, R. Scherer, G. Pfurtscheller, and R. Rupp. Brain-computer interfaces for control of neuroprostheses: from synchronous to asynchronous mode of operation. *Biomedizinische Technik*, 51:57–63, 2006.

[168] R. Scherer, G. R. Müller, C. Neuper, B. Graimann, and G. Pfurtscheller. An asynchronously controlled EEG-based virtual keyboard: improvement of the spelling rates. *IEEE Transactions on Neural Systems and Rehabilitation Engineering*, 51:979–984, 2004.

[169] R. Leeb, V. Settgast, D. W. Fellner, and G. Pfurtscheller. Self-paced exploring of the Austrian National Library through thoughts. *International Journal of Bioelectromagnetism*, 9:237–244, 2007.

[170] R. Scherer, F. Lee, A. Schlögl, R. Leeb, H. Bischof, and G. Pfurtscheller. Toward self-paced brain-computer communication: navigation through virtual worlds. *IEEE Transactions on Biomedical Engineering*, 55:675–682, 2008.

[171] G. R Müller-Putz, R. Scherer, G. Pfurtscheller, and C. Neuper. Temporal coding of brain patterns for direct limb control in humans. *Frontiers in Neuroscience*, 4:34, 2010.

[172] R. T. Lauer, P. H. Peckham, and K. L. Kilgore. EEG-based control of a hand grasp neuroprosthesis. *Neuroreport*, 10:1767–1771, 1999.

[173] J. M. Heasman, T. R. D. Scott, L. Kirkup, R. Y. Flynn, V. A. Vare, and C. R. Gschwind. Control of a hand grasp neuroprosthesis using an electroencephalogram-triggered switch: demonstration of improvements in performance using wavepacket analysis. *Medical and Biological Engineering and Computing*, 40:588–593, 2002.

[174] O. Bai, V. Rathi, P. Lin, D. Huang, H. Battapady, D. Y. Fei, L. Schneider, E. Houdayer, X. Chen, and M. Hallett. Prediction of human voluntary movement before it occurs. *Clinical Neurophysiology*, 122(2):364–72, 2011.

[175] O. Bai, P. Lin, S. Vorbach, J. Li, S. Furlani, and M. Hallett. Exploration of computational methods for classification of movement intention during human voluntary movement from single trial EEG. *Clinical Neurophysiology*, 118:2637–2655, 2007.

[176] K. Qian, P. Nikolov, D. Huang, D-Y. Fei, X. Chen, and O. Bai. A motor imagery-based online interactive brain-controlled switch: paradigm development and preliminary test. *Clinical Neurophysiology*, 121:1303–1313, 2010.

[177] A. Kübler, B. Kotchoubey, T. Hinterberger, N. Ghanayim, J. Perelmouter, M. Schauer, C. Fritsch, E. Taub, and N. Birbaumer. The thought translation device: a nerurophysiological approach to communication in total motor paralysis. *Experimental Brain Research*, 124:223–232, 1999.

[178] G. Pfurtscheller, T. Solis-Escalante, R. Ortner, P. Linortner, and G. R. Müller-Putz. Self-paced operation of an SSVEP-based orthosis with and without an imagery-based "brain switch": a feasibility study towards a hybrid BCIs. *IEEE Transactions on Neural Systems and Rehabilitation Engineering*, 18:409–414, 2010.

[179] R. O. Duda, P. E. Hart, and D. G. Stork. *Pattern Classification (2nd Edition)*. Wiley-Interscience, 2001. ISBN 0471056693.

[180] A. Schlögl, J. Kronegg, J. E. Huggins, and S. G. Mason. Evaluation criteria for BCI research. In *Toward brain-computer interfacing*. MIT Press, 2007.

[181] G. R. Müller-Putz, R. Scherer, C. Brunner, R. Leeb, and G. Pfurtscheller. Better than random? A closer look on BCI results. *International Journal of Bioelectromagnetism*, 10:52–55, 2008.

[182] G. R. Müller-Putz, V. Kaiser, T. Solis-Escalante, and G. Pfurtscheller. Fast set-up asynchronous brain-switch based on detection of foot motor imagery in 1-channel EEG. *Medical and Biological Engineering and Computing*, 48:229–233, 2010.

[183] C.-C. Chang and C.-J. Lin. *LIBSVM: a library for support vector machines*, 2001. Software available at `http://www.csie.ntu.edu.tw/~cjlin/libsvm`.

[184] A. Schlögl, C. Brunner, R. Scherer, and A. Glatz. BioSig: an open-source software library for BCI research. In G. Dornhege, J. del R. Millán, T. Hinterberger, D. J. McFarland, and K.-R. Müller, editors, *Toward brain-computer interfacing*, chapter 20, pages 347–358. MIT Press, 2007.

[185] T. Wu, C. Lin, and R. Weng. Probability estimates for multi-class classification by pairwise coupling. *Journal of Machine Learning Research*, 5:975 – 1005, 2004.

[186] S. Keerthi and C.-J. Lin. Asymptotic behaviors of support vector machines with Gaussian kernel. *Neural Computation*, 15:1667–1689, 2003. ISSN 0899-7667.

[187] G. Pfurtscheller and C. Neuper. Motor imagery activates primary sensorimotor area in humans. *Neuroscience Letters*, 239:65–68, 1997.

[188] E. Gerardin, A. Sirigu, S. Lehŕicy, J.-B. Poline, B. Gaymard, C. Marsault, Y. Agid, and D. Le Bihan. Partially overlapping neural networks for real and imagined hand movements. *Cerebral Cortex*, 10: 1093–1104, 2000.

[189] T. Solis-Escalante, G. R. Müller-Putz, and G. Pfurtscheller. Overt foot movement detection in one single Laplacian EEG derivation. *Journal of Neuroscience Methods*, 175:148–153, 2008.

[190] T. Solis-Escalante, G. R. Müller-Putz, C. Brunner, V. Kaiser, and G. Pfurtscheller. Analysis of sensorimotor rhythms for the implementation of a brain switch for healthy subjects. *Biomedical Signal Processing and Control*, 5:15–20, 2010.

[191] M. Pregenzer, G. Pfurtscheller, and D. Flotzinger. Automated feature selection with a distinction sensitive learning vector quantizer. *Neurocomputing*, 11:19–29, 1996.

[192] G. R. Müller-Putz, R. Scherer, and G. Pfurtscheller. Game-like training to learn single switch operated neuroprosthetic control. In *Workshop of the International Conference on Advances in Computer Entertainment Technology ACE 2007*, volume BrainPlay'07: Playing with your brain (Brain-Computer Interfaces and Games), pages 49–51, 2007.

[193] G. Bauernfeind. *Using functional near-infrared spectroscopy (fNIRS) for optical brain-computer interface (oBCI) applications*. PhD thesis, Graz University of Technology, 2012.

[194] P. Linortner, R. Ortner, G. R. Müller-Putz, C. Neuper, and G. Pfurtscheller. Self -paced control of a hand orthosis using SSVEP-based BCI. In *Proceedings of the 13th International Conference on Human-Computer Interaction*, 2009.

[195] G. R. Müller-Putz and G. Pfurtscheller. Control of an electrical prosthesis with an SSVEP-based BCI. *IEEE Transactions on Biomedical Engineering*, 55:361–364, 2008.

[196] J. F. Thayer and R. D. Lane. Claude Bernard and the heart-brain connection: further elaboration of a model of neurovisceral integration. *Neuroscience & Biobehavioral Reviews*, 33:81–88, 2009.

[197] R. Scherer, G. R. Müller-Putz, and G. Pfurtscheller. Self-initiation of EEG-based brain-computer communication using the heart rate responses. *Journal of Neural Engineering*, 4:L23–L29, 2007.

[198] G. Pfurtscheller, R. Leeb, D. Friedman, and M. Slater. Centrally controlled heart rate changes during mental practice in immersive virtual environment: a case study with a tetraplegics. *International Journal of Psychophysiology*, 68:1–5, 2008.